

ผลของการเติมโลหะต่ออนุภาคสังกะสีออกไซด์ขนาดนาโนเมตร

ที่สังเคราะห์โดยวิธีโซลโวเทอร์มอล



นาย ชีราวุธ เรืองสนาม

สถาบันวิทยบริการ

วิทยานิพนธ์นี้เป็นส่วนหนึ่งของการศึกษาตามหลักสูตรปริญญาวิศวกรรมศาสตรมหาบัณฑิต

สาขาวิชาวิศวกรรมเคมี ภาควิชาวิศวกรรมเคมี

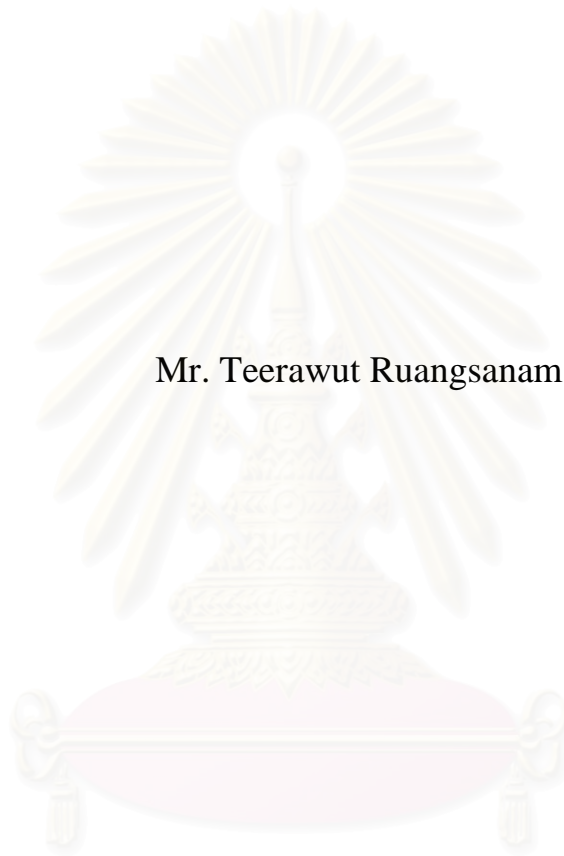
คณะวิศวกรรมศาสตร์ จุฬาลงกรณ์มหาวิทยาลัย

ปีการศึกษา 2548

ISBN 974-17-5294-6

ลิขสิทธิ์ของจุฬาลงกรณ์มหาวิทยาลัย

EFFECTS OF METAL-DOPING ON ZINC OXIDE NANOPARTICLES
SYNTHESIZED VIA SOLVOTHERMAL METHOD



Mr. Teerawut Ruangsanam

A Thesis Submitted in Partial Fulfillment of the Requirements
for the Degree of Master of Engineering Program in Chemical Engineering

Department of Chemical Engineering

Faculty of Engineering


Chulalongkorn University

Academic Year 2005


ISBN 974-17-5294-6

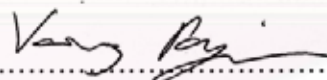
Thesis Title EFFECTS OF METAL-DOPING ON ZINC OXIDE
 NANOPARTICLES SYNTHESIZED VIA
 SOLVOTHERMAL METHOD
By Mr. Teerawut Ruangsanam
Field of Study Chemical Engineering
Thesis Advisor Assistant Professor Varong Pavarajarn, Ph.D.
Thesis Co-advisor Okorn Mekasuwandumrong, Ph.D.

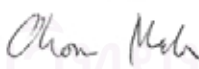
Accepted by the Faculty of Engineering, Chulalongkorn University in Partial
Fulfillment of the Requirements for the Master's Degree


..... Dean of the Faculty of Engineering
(Professor Direk Lavansiri, Ph.D.)

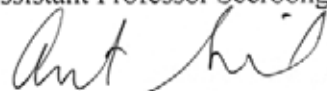
THESIS COMMITTEE


..... Chairman
(Associate Professor Suttichai Assabumrungrat, Ph.D.)


..... Thesis Advisor
(Assistant Professor Varong Pavarajarn, Ph.D.)


..... Thesis Co-advisor
(Okorn Mekasuwandumrong, Ph.D.)


..... Member
(Assistant Professor Seeroong Prichanont, Ph.D.)


..... Member
(Akawat Sirisuk, Ph.D.)

ธีรารุท เรื่องสนาม: ผลของการเติมโลหะต่ออนุภาคสังกะสีออกไซด์ขนาดนาโนเมตร ที่สังเคราะห์โดยวิธีโซลโวเทอร์มอล (EFFECTS OF METAL-DOPING ON ZINC OXIDE NANOPARTICLES SYNTHESIZED VIA SOLVOTHERMAL METHOD) อ. ที่ปรึกษา : ผศ. ดร. วรงค์ ปวราจารย์, อ. ที่ปรึกษาร่วม : ดร. โกรธ เมฆาสุวรรณดำรง, 98 หน้า. ISBN 974-47-5294-6.

งานวิจัยนี้ศึกษาสมบัติของอนุภาคนาโนเมตรของสังกะสีออกไซด์ที่ถูกเติมด้วยโลหะ ซึ่งถูกสังเคราะห์ด้วยวิธีโซลโวเทอร์มอล ซึ่งเป็นการแตกตัวด้วยความร้อนของสังกะสีอะซิเตทใน 1, 4 บิวเทนไดออล ที่อุณหภูมิ 220 องศาเซลเซียส เป็นเวลา 2 ชั่วโมง ได้ทำการศึกษาสมบัติทางกายภาพของผลิตภัณฑ์โดยเครื่องมือ XRD, SEM, XPS และ UV/Vis การเติมแกเลียม ทองแดง อลูมิเนียมและแมกนีเซียมอันเป็นโลหะตัวที่สองในปริมาณ ร้อยละ 0 – 12.5 อะตอมเข้าไปในผลึกของสังกะสีออกไซด์ในระหว่างการสังเคราะห์ด้วยวิธีโซลโวเทอร์มอลและการให้ความร้อนที่อุณหภูมิ 300 – 900 องศาเซลเซียสได้ถูกศึกษา พบว่าเมื่อแกเลียมและอลูมิเนียมซึ่งถูกรวมเข้าไปในโครงสร้างของสังกะสีออกไซด์มีผลต่อสมบัติของอนุภาคนาโนเมตรของสังกะสีออกไซด์ การเลื่อนไปทางสีน้ำเงินของเส้นสเปกตรัมการดูดซับแสงอัลตราไวโอเล็ตของการเติมแกเลียมและอลูมิเนียมแสดงให้เห็นถึงการเปลี่ยนแปลงในระดับชั้นอิเล็กทรอนิกส์ของผลิตภัณฑ์การเพิ่มปริมาณของแกเลียมและอลูมิเนียมทำให้เกิดการเลื่อนออกไปมากยิ่งขึ้น การเติมโลหะตัวที่สองยังมีผลต่อรูปร่างของอนุภาคที่สังเคราะห์ได้ การให้ความร้อนมีผลให้เกิดการเลื่อนไปทางสีแดงของเส้นสเปกตรัมการดูดซับแสงอัลตราไวโอเล็ตของสังกะสีออกไซด์ที่เติมแกเลียมและอลูมิเนียม สำหรับการเติมทองแดงและแมกนีเซียมนั้นสมบัติของตัวอย่างที่สังเคราะห์มีลักษณะเหมือนกับสังกะสีออกไซด์ที่ไม่เติมโลหะ แต่เมื่อให้ความร้อนพบว่าเกิดการเลื่อนไปทางสีน้ำเงินของเส้นสเปกตรัมการดูดซับแสงอัลตราไวโอเล็ตในตัวอย่างที่เติมแมกนีเซียม เนื่องจากสังกะสีออกไซด์และแมกนีเซียมเกิดการกลายเป็นโลหะผสมที่อุณหภูมิสูงกว่า 700 องศาเซลเซียส การสลายตัวของเมทิลีนบลูด้วยการเร่งด้วยแสงและเส้นสเปกตรัมของโฟโตลูมิเนสเซนส์ได้ถูกใช้ในการศึกษาสมบัติของสังกะสีออกไซด์ที่เติมโลหะด้วยเช่นกัน

ภาควิชา.....วิศวกรรมเคมี.....
สาขาวิชา.....วิศวกรรมเคมี.....
ปีการศึกษา..... 2548.....

ลายมือชื่อนิสิต.....ธีรารุท เรืองสนาม.....
ลายมือชื่ออาจารย์ที่ปรึกษา.....
ลายมือชื่ออาจารย์ที่ปรึกษาร่วม.....

4770581521 : MAJOR CHEMICAL ENGINEERING

KEY WORD : ZINC OXIDE; NANOPARTICLE; METAL DOPING; DOPING;
SOLVOTHERMAL METHOD.

TEERAWUT RUANGSANAM : (EFFECTS OF METAL-DOPING ON ZINC
OXIDE NANOPARTICLES SYNTHESIZED VIA SOLVOTHERMAL
METHOD) THESIS ADVISOR: ASST. PROF. VARONG PAVARAJARN,
Ph.D., THESIS COADVISOR: OKORN MEKASUWANDUMRONG, Ph.D.,
98 pp. ISBN 974-17-5294-6.

This research studies properties of metal-doped ZnO nanoparticles synthesized via solvothermal method, i.e. thermal decomposition of zinc acetate in 1,4-butanediol, at 220°C for 2 h. The physical properties of the product were investigated by XRD, SEM, XPS and UV/Vis. Doping of Ga, Cu, Al and Mg as the secondary metal at metal content 0 - 12.5 at.% into ZnO crystals during solvothermal synthesis and calcinations at temperature 300 – 900 °C were also investigated. It was found that Ga and Al incorporated in ZnO crystal structure affected properties of ZnO nanoparticles. Blue-shift in UV absorption spectrum from Ga and Al doping indicated a change in electronic states of the product. An increase in the content of Ga and Al doping resulted in further shift in the UV absorption spectrum. Addition of the secondary metal also affected morphology of the synthesized particles. Calcination resulted in red-shift in UV absorption spectrum of Ga- and Al-doped zinc oxide. For Cu and Mg doping, the properties of as-synthesized samples were the same as undoped ZnO, but calcination caused blue-shift in UV absorption spectrum of Mg-doped ZnO because ZnO was alloyed with Mg by calcination at temperature higher than 700°C. The photocatalytic degradation of methylene blue and the photoluminescence spectra were also employed to investigate properties of metal-doped ZnO.

DepartmentChemical Engineering.....

Field of Study ..Chemical Engineering.....

Academic year2005.....

Student's signatureTeerawut R.....

Advisor's signatureVarong Pavarajarn.....

Co-advisor's signatureOkorn Mekasuwandumrong.....

ACKNOWLEDGEMENTS

The author wishes to express his sincere gratitude and appreciation to his advisor, Assistant Professor Dr. Varong Pavarajarn, and co advisor, Dr. Okorn Mekasuwandumrong for their valuable suggestions, stimulating, useful discussions throughout this research and devotion to revise this thesis otherwise it can not be completed in a short time. In addition, the author would also be grateful to Associate Professor Dr. Suttichai Assabumrungrat, as the chairman, and Dr. Akawat Sirisuk, Assistant Professor Dr. Seeroong Prichanont, as the members of the thesis committee. The supports from TRF and Graduate school of Chulalongkorn University are also gratefully acknowledged.

Most of all, the author would like to express his highest gratitude to his parents who always pay attention to his all the times for suggestions and their wills. The most success of graduation is devoted to his parents.

Finally, the author wishes to thank the members of the Center of Excellence on Catalysis and Catalytic Reaction Engineering, Department of Chemical Engineering, Faculty of Engineering, Chulalongkorn University for their assistance.

สถาบันวิทยบริการ
จุฬาลงกรณ์มหาวิทยาลัย

TABLE OF CONTENTS

	page
ABSTRACT (IN THAI)	iv
ABSTRACT (IN ENGLISH)	v
ACKNOWLEDGEMENTS	vi
TABLE OF CONTENTS	vii
LIST OF TABLES	x
LIST OF FIGURES	xi
CHAPTER	
I INTRODUCTION	1
II THEORY	4
2.1 Properties of Zinc Oxide	4
2.2 Doping of Zinc Oxide.....	6
2.3 Methods for Synthesizing Zinc Oxide	9
2.3.1 Thermal decomposition method	9
2.3.2 Sol-gel method	11
2.3.3 Precipitation method.....	11
2.4 Electronic Structure of Semiconductor	12
2.4.1 Direct and indirect band gap semiconductors....	13
2.4.2 The fundamental absorption process	14
2.5 Photoluminescence	17
2.5.1 Principle of photoluminescence spectroscopy....	17
2.5.2 Practical uses of photoluminescence.....	18
2.6 Photocatalytic Process	19
III EXPERIMENTAL.....	22
3.1 Chemicals.....	22
3.2 Equipment.....	22
3.3 Experimental Procedures.....	24

	page
CHAPTER	
3.3.1 Preparation of zinc oxide	24
3.3.2 Calcination of the metal-doped zinc oxide.....	24
3.3.3 Photocatalytic activity evaluation.....	24
3.4 Characterizations of Samples.....	25
3.4.1 X-ray diffraction analysis.....	25
3.4.2 Surface area measurement.....	25
3.4.3 Scanning electron microscopy.....	26
3.4.4 UV-Visible absorption.....	26
3.4.5 X-ray photoelectron spectroscopy.....	26
3.4.6 Photoluminescence.....	26
IV RESULTS AND DISCUSSION	
4.1 Properties of Undoped and Metal-Doped Zinc Oxide.....	27
4.1.1 XRD analysis.....	27
4.1.2 Lattice parameters of metal-doped zinc oxide.....	31
4.1.3 Morphology of metal-doped zinc oxide.....	33
4.1.4 XPS analysis.....	40
4.1.5 Optical properties of metal-doped zinc oxide.....	42
4.2 Effect of Calcination Temperature.....	48
4.2.1 XRD analysis.....	48
4.2.2 Lattice parameters of calcined product.....	53
4.2.3 Morphology of calcined product.....	54
4.2.4 Optical properties of calcined product.....	59
4.3 Photocatalytic Activity.....	64
4.4 Photoluminescence Analysis.....	71
V CONCLUSIONS AND RECOMMENDATIONS.....	74
5.1 Conclusions.....	74
5.2 Recommendations for Future Studies.....	75
REFERENCES	76

APPENDICES

APPENDIX A	CALCULATION OF LATTICE PARAMETERS	85
APPENDIX B	CALCULATION OF BAND GAP ENERGY	87
APPENDIX C	ANALYSIS OF SOLVENT AFTER SOLVOHERMAL SYNTHESIS BY INDUCTIVELY COUPLE PLASMA OPTICAL EMISSION	90
APPENDIX D	LIST OF PUBLICATION.....	91
VITA		98



สถาบันวิทยบริการ
จุฬาลงกรณ์มหาวิทยาลัย

LIST OF TABLES

Table	Page
2.1 Properties of wurtzite ZnO	5
2.2 The literature review of effect of metal content on metal doped ZnO film	8
4.1 Composition of metal-doped zinc oxide characterized by XPS analysis	40
4.2 Properties of photocatalysts employed in the photocatalytic degradation experiments	66
4.3 The band gap energy of zinc oxide samples determined from the UV-Vis spectroscopy and from photoluminescence.....	73
A-1 Lattice parameters of metal-doped zinc oxide at various metal contents.....	86
A-2 Lattice parameters of metal-doped zinc oxide calcined at various temperatures	86
B-1 The band gap energy of metal-doped zinc oxide at various metal content.....	88
B-2 The band gap energy of metal-doped zinc oxide at various calcine temperature.....	89

LIST OF FIGURES

Figure	page
2.1 Stick and ball representation of ZnO crystal structures.....	4
2.2 Compressional strain induced by the incorporation of a large impurity...	7
2.3 Energy banding of allowed levels in diamond as a function of spacing between atoms	7
2.4 Band structure of a semiconductor showing a full valence band and an empty conduction band. The Fermi level lies within the forbidden bandgap.....	13
2.5 Determination of $\lambda_{1/2}$ from the optical absorbance spectra	15
2.6 (a) Optical absorbance spectra of samples (b) The band gap energy are determined by extrapolation of the linear part of the plot of α^2 versus $h\nu$ on x-axis.....	16
3.1 Diagram of the reaction equipment for the catalyst preparation.....	23
3.2 Autoclave reactor	23
4.1 The XRD pattern of undoped zinc oxide (a) and gallium-doped zinc oxide at dopant contents of (b) 0.5, (c) 2.5, (d) 5, (e) 7.5, (f) 10 and (g) 12.5 at.%.....	28
4.2 The XRD pattern of undoped zinc oxide (a) and aluminium-doped zinc oxide at dopant contents of (b) 0.5, (c) 2.5, (d) 5, (e) 7.5, (f) 10 and (g) 12.5 at.%.....	28
4.3 The XRD pattern of undoped zinc oxide (a) and copper-doped zinc oxide at dopant contents of (b) 0.5, (c) 2.5, (d) 5, (e) 7.5, (f) 10 and (g) 12.5 at.%.....	29
4.4 The XRD pattern of undoped zinc oxide (a) and magnesium-doped zinc oxide at dopant contents of (b) 0.5, (c) 2.5, (d) 5, (e) 7.5, (f) 10 and (g) 12.5 at.%.....	29

Figure	page
4.5 Shifting in XRD pattern of (a) gallium-, (b) aluminium-, (c) copper- and (d) magnesium-doped zinc oxide at various doping contents.....	30
4.6 The lattice constants of (a) gallium-, (b), aluminium- (c) copper- and magnesium-doped zinc oxide at metal content in the range of 0 to 12.5 at.%.....	32
4.7 SEM micrographs of undoped zinc oxide.....	34
4.8 SEM micrographs of gallium-doped zinc oxide (a) 0.5, (b) 2.5, (c) 5, (d) 7.5, (e) 10, (f) 12.5 percent atom.....	34
4.9 SEM micrographs of aluminium-doped zinc oxide (a) 0.5, (b) 2.5, (c) 5, (d) 7.5, (e) 10, (f) 12.5 percent atom.....	35
4.10 SEM micrographs of copper-doped zinc oxide (a) 0.5, (b) 2.5, (c) 5, (d) 7.5, (e) 10, (f) 12.5 percent atom.....	36
4.11 SEM micrographs of magnesium-doped zinc oxide (a) 0.5, (b) 2.5, (c) 5, (d) 7.5, (e) 10, (f) 12.5 percent atom.....	37
4.12 Average diameter and length of gallium-doped zinc oxide at doping content of 0 to 12.5 at.%.....	38
4.13 Average diameter and length of aluminium-doped zinc oxide at doping content of 0 to 12.5 at.%.....	38
4.14 Average diameter and length of copper-doped zinc oxide at doping content of 0 to 12.5 at.%.....	38
4.15 Average diameter and length of magnesium-doped zinc oxide at doping content of 0 to 12.5 at.%.....	39
4.16 Aspect ratio of zinc oxide powder doped with: gallium, aluminium, copper and magnesium at various metal content.	39
4.17 The Zn 2p binding energy of metal-doped zinc oxide at various metal contents (at.%).	41
4.18 The O 1s binding energy of metal-doped zinc oxide at various metal contents (at.%).	41

Figure	page
4.19 The absorption spectra of gallium-doped zinc oxide at metal content 0 to 12.5 at.%.....	43
4.20 The absorption spectra of aluminium-doped zinc oxide at metal content 0 to 12.5 at.%.....	44
4.21 The absorption spectra of copper-doped zinc oxide at metal content 0 to 12.5 at.%.....	44
4.22 The absorption spectra of magnesium-doped zinc oxide at metal content 0 to 12.5 at.%.....	45
4.23 The band gap energy of (a) gallium, (b) copper, (c) aluminium and (d) magnesium-doped zinc oxide at metal content 0 to 12.5 at.%.....	46
4.24 The XRD patterns of 5 at.% gallium-doped zinc oxide: (i) pre-calcined and calcined at (ii) 300°C, (iii) 500°C and (iv) 900°C. (b) The enlarged XRD pattern of gallium-doped zinc oxide.....	50
4.25 The XRD patterns of 7.5 at.% aluminium-doped zinc oxide: (i) pre-calcined and calcined at (ii) 300°C, (iii) 500°C and (iv) 900°C. (b) The enlarged XRD pattern of aluminium-doped zinc oxide.....	51
4.26 The XRD patterns of 7.5 at.% copper-doped zinc oxide: (i) pre-calcined and calcined at (ii) 300°C, (iii) 500°C and (iv) 900°C. (b) The enlarged XRD pattern of copper-doped zinc oxide.....	52
4.27 The XRD patterns of 7.5 at.% magnesium-doped zinc oxide: (i) pre-calcined and calcined at (ii) 300°C, (iii) 500°C and (iv) 900°C. ...	53
4.28 The lattice constants of (a) 5 at.% gallium-, (b) 7.5 at.% aluminium, (c) 7.5 at.% copper- and (d) 7.5 at.% magnesium-doped zinc oxide after calcination at various temperatures.....	54
4.29 SEM micrographs of 5 at.% gallium-doped zinc oxide : (a) pre-calcined and calcined at (b) 300°C, (c) 500 °C and (d) 900 °C.....	55
4.30 SEM micrographs of 7.5 at.% aluminium-doped zinc oxide : (a) pre-calcined and calcined at (b) 300°C, (c) 500 °C and (d) 900 °C.....	56

Figure	page
4.31 SEM micrographs of 7.5 at.% copper-doped zinc oxide : (a) pre-calcined and calcined at (b) 300°C, (c) 500 °C and (d) 900 °C.....	57
4.32 SEM micrographs of 7.5 at.% magnesium-doped zinc oxide : (a) pre-calcined and calcined at (b) 300°C, (c) 500 °C and (d) 900 °C.....	58
4.33 The absorption spectra of 5 at.% of gallium-doped zinc oxide after calcination at various temperatures	59
4.34 The absorption spectra of 7.5 at.% of aluminium-doped zinc oxide after calcination at various temperatures	60
4.35 The absorption spectra of 7.5 at.% of copper-doped zinc oxide after calcination at various temperatures	60
4.36 The absorption spectra of 7.5 at.% of magnesium-doped zinc oxide after calcination at various temperatures	61
4.37 The band gap energy of (a) 5 at.% gallium-, (b) 7.5 at.% aluminium-, (c) 7.5 at.% copper-and (d) 7.5 at.% magnesium-doped zinc oxide, calcined at various temperatures.....	63
4.38 Photocatalytic degradation of methylene blue solution, using metal-doped zinc oxide particles under UV irradiation	65
4.39 Photocatalytic degradation of methylene blue solution, using metal-doped zinc oxide particles under solar irradiation	65
4.40 Spectral power distribution of the UV lamps employed in this research and absorption spectra of: (a) 5 at.% gallium-doped zinc oxide, (b) 7.5 at.% aluminium-doped zinc oxide and (c) undoped, 7.5 at.% copper-doped and 7.5 at.% magnesium-doped zinc oxide.....	67
4.41 Photocatalytic degradation of methylene blue solution on zinc oxide doped with various contents of gallium under UV irradiation.....	68
4.42 Photocatalytic degradation of methylene blue solution on zinc oxide doped with various contents of gallium under solar irradiation.....	69

Figure	page
4.43 Photocatalytic degradation of methylene blue solution under UV irradiation on undoped and gallium-doped zinc oxide that has been calcined at various temperatures	70
4.44 Photocatalytic degradation of methylene blue solution under solar irradiation on undoped and gallium-doped zinc oxide that has been calcined at various temperatures	70
4.45 Photoluminescence of undoped and metal-doped zinc oxide in form of wavelength: (a) undoped zinc oxide, (b) 5 at.% gallium-, (c) 7.5 at.% copper, (d) 7.5 at.% aluminium- and (e) 7.5 at.% magnesium-doped zinc oxide.....	72
4.46 Photoluminescence of undoped and metal-doped zinc oxide in form of energy: (a) undoped zinc oxide, (b) 5 at.% gallium-, (c) 7.5 at.% copper, (d) 7.5 at.% aluminium- and (e) 7.5 at.% magnesium-doped zinc oxide.....	72
B-1 The UV-Vis absorption spectra of 0.5 at.% gallium-doped zinc oxide. The wavelength at half-absorption intensity ($\lambda_{1/2}$) is the band-gap energy of the material.....	88
C-1 zinc and cu content into solvent after synthesis of 12.5 at.% copper-doped zinc oxide are prepared.....	90

CHAPTER I

INTRODUCTION

Nanosized materials have been attractive in their potential uses for both interconnect and functional units in fabricating electronic, optoelectronic, electrochemical and electromechanical nanodevices. In the past few years, many efforts have been devoted to develop various nanoscaled materials. The changing in electrical and optical properties are targeted for wide varieties of potential applications.

Zinc oxide (ZnO) has been recognized as one of the most promising oxide semiconductor materials because of its good optical, electrical and piezoelectrical properties. It has received a considerable amount of attention over the last few years to be used in many applications. Zinc oxide can be used in various fields and also has good potential for high temperature electronic applications, including short-wavelength display diode and laser. In particular, nanostructured ZnO is expected to have properties suitable for applications in shock resistance, sound insulation, varistor, gas-sensor, catalyst, light emitting diode (LED), photodetector, solar cell, ultraviolet nanolaser, flat panel display as well as lotion for diaper rash and sunburn. Composition of ZnO in polymer matrix can absorb and shield electromagnetic wave and eliminate static charge deposition in some electronic devices.

Semiconductors such as TiO_2 , ZnO, Fe_2O_3 , CdS, and ZnS, can act as sensitizers for light-induced redox-processes due to the electronic structure of the metal atoms in chemical combination, which is characterized by a filled valence band, and an empty conduction band [Hoffmann et al., 1995]. Upon irradiation, valence band electrons are promoted to the conduction band leaving a hole behind. These electron-hole pairs can either recombine or can interact separately with other molecules. The holes may react either with electron donors in the solution, or with hydroxide ions to produce powerful oxidizing species like hydroxyl (oxidation potential 2.8 V) or super oxide radicals. Although TiO_2 in anatase form (band gap energy of 3.2 eV) has been used for many environmental applications, ZnO (band gap energy of 3.2 eV) is a suitable alternative to TiO_2 so far as band gap energy is

concerned. The quantum efficiency of ZnO powder is also significantly larger than that of TiO₂ powder, and higher catalytic efficiencies have been reported for ZnO [Sakthivel et al., 1999].

In the last decade, ZnO have been prepared by various methods such as solvothermal synthesis [Inoue, 1992], hydrothermal synthesis [Sue et al., 2004], thermal decomposition [Yang et al., 2004], spray pyrolysis [Wang, 2004], sol-gel synthesis [Kamalasanan et al., 1996], wet chemical techniques [Wu et al., 2004], chemical vapor deposition (CVD) [Kim et al., 2003] and precipitation method [Rodriguez-Paez et al., 2001]. It is commonly acknowledged that morphology and properties of ZnO particles depend upon how the particles are synthesized.

Solvothermal synthesis is an interesting method. It is improved from the hydrothermal synthesis by using organic solvent instead of water at elevated temperature (200-300°C) under autogeneous pressure. This technique is based on thermal decomposition of organometallic compound in organic solvent and the technique has been successfully applied for the synthesis of various types of nanosized metal oxide with large surface area, high crystallinity and high thermal stability [Inoue et al., 1995; Iwamoto et al., 2001; Mekasuwandumrong et al., 2004]. Single crystal ZnO with small diameter and high crystallization has been successfully prepared, in one step, by this method as well.

Doping is a technique to alter electrical properties by adding foreign of element to change intrinsic defects, i.e., oxygen vacancies and/or zinc interstitials [Jeong et al., 2005]. it can tune the band gap energy. For instance, Cd doping can decrease the band gap, which consequently resulting in a low [John et al., 2005]. On the contrary, the increased band gap, which can be achieved by Mg doping, can give high breakdown voltage and lower noise to the material. Moreover, semiconductor with relatively wide band gap can be operated at higher temperatures with higher power [Shan et al., 2004]. Doped zinc oxides have attracted much attention as an alternative for high quality optoelectronic materials such as indium tin oxide (ITO), due to their inexpensive, abundance in nature, and non-toxic features [Ren et al., 2004]. For the photocatalyst application, doping can improve efficiency of the reaction by altering zinc oxide to absorb not only UV but also visible light visible

light accounts for 45% of energy in the solar radiation while UV light accounts for less than 10% [Lin et al., 2005].

Doping of ZnO film has been reported by many authors. Aluminum-, copper-, gallium- or magnesium-doped ZnO films show changes in both optical and electrical properties [Paraguay, 2000; Cheong et al., 2002; Shan et al., 2004]. Nevertheless, it is equally challenging to synthesize metal-doped ZnO powder for various applications, such as electronic devices and photocatalysis.

Objectives of the research:

1. Study of the effects of metal dopants (i.e. aluminum, copper, gallium and magnesium), doping content and calcination temperature on physical, chemical and electronic properties of zinc oxide nanoparticles synthesized by solvothermal method.
2. Study the activity of the resulting metal-doped zinc oxide by using photocatalytic decomposition of methylene blue.

The present thesis is arranged as follows:

Chapter I is the introduction of this work.

Chapter II presents theory and literature reviews of the preparation method and properties metal doped ZnO in previous works relating to this research.

Chapter III describes preparation method of ZnO powder by solvothermal method and characterization techniques.

Chapter IV exhibits the experimental results and discussion of the research.

In the last chapter, Chapter V, the overall conclusions and recommendations for the future studies of this research are given.

CHAPTER II

THEORY AND LITERATURE REVIEWS

2.1 Properties of Zinc Oxide

Zinc oxide is a II-VI compound semiconductor of which the ionicity resides at the borderline between covalent and ionic semiconductor. The crystal structures shared by zinc oxide are wurtzite, zinc blende, and rocksalt, as schematically shown in Figure 2.1. At ambient conditions, the thermodynamically stable phase is wurtzite. The zinc-blende structure can be formed only by the growth of ZnO on cubic substrate. The rocksalt structure may be obtained at relatively high pressure.

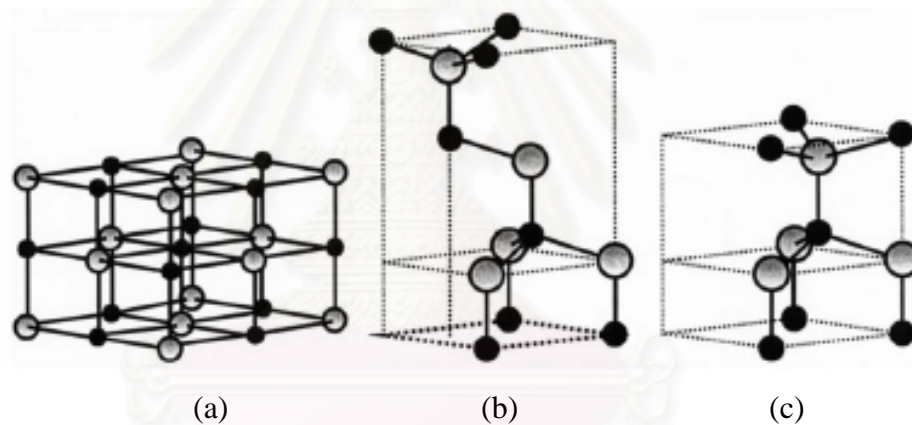


Figure 2.1 Stick and ball representation of zinc oxide crystal structures:
(a) cubic rocksalt, (b) cubic zinc blende, and (c) hexagonal wurtzite.
The shaded gray and black spheres denote Zn and O atoms, respectively.

Zinc oxide is an n-type semiconductor with a band gap of 3.20 eV and the free exciton energy of 60 meV, which makes it very high potential for room temperature light emission. This also gives zinc oxide strong resistance to high temperature electronic degradation during operation. Therefore, it is attractive for many optoelectronic applications in the range of blue and violet light as well as UV devices for wide range of technological applications. Zinc oxide also exhibits dual

semiconducting and piezoelectric properties. The other properties are given in Table 2.1.

Table 2.1 Properties of wurtzite zinc oxide

<i>Property</i>	<i>Value</i>
Lattice parameters at 300 K	
<i>a</i>	0.32495 nm
<i>c</i>	0.52069 nm
<i>a/c</i>	1.602 (ideal hexagonal structure is 1.633)
Density	5.606 g/cm ³
Melting point	1975 °C
Thermal conductivity	130 W/m.K
Linear expansion coefficient (/°C)	<i>a</i> : 6.5 x 10 ⁻⁶ <i>c</i> : 3.0 x 10 ⁻⁶
Static dielectric constant	8.656
Energy gap	3.2 eV, direct
Exciton binding energy	60 meV

Zinc oxide occurs in nature as mineral. Zinc oxide is prepared in industrial scale by vaporizing zinc metal and oxidizing the generated zinc vapor with preheated air. Zinc oxide has numerous industrial applications. It is a common white pigment in paints. It is used to make enamel, white printing ink, white glue, opaque glasses, and floor tiles. It is also used in cosmetics, pharmaceutical applications such as antiseptic and astringent, dental cements, batteries, electrical equipments, and piezoelectric devices. Other applications are the use as flame retardant, and UV absorber in plastics. Nevertheless, the current major application of zinc oxide is in the preparation of most zinc salts.

2.2 Doping of Zinc Oxide

Doping is a technique employed to control electrical properties of semiconductors by addition of element to change intrinsic defects, i.e., oxygen vacancies and/or zinc interstitials in the crystal [Jeong et al., 2005]. When an impurity atom is introduced in a lattice, it produces several types of interactions. If the impurity atom replaces one of the constituent atoms of the crystal and provides the crystal with one or more additional electrons than the atom it replaced, the impurity is a donor. Examples of donor are doping of As to Ge-site of a germanium crystal, doping of Te to As-site of GaAs, and doping of Si to Ga-site of GaAs. On the other hand, if the impurity atom has less electron than the atom it replaces, it is called an acceptor (e.g., Zn doped on a Ga-site in GaAs, or Si doped on an As-site in GaAs).

In a semiconductor, a deviation from stoichiometry can also generate the state of electron donor or acceptor. For instance, it has been shown that vacancy in PbTe, which results in imbalance ratio between Pb and Te, can determine whether the material is *n*-type or *p*-type [Parada et al., 1969]. Since each Pb atom is associated with 4 electrons, Pb-vacancy leaves two holes in the valence band. Therefore, a Pb-vacancy in the Te-rich PbTe transfers two states from the valence band to the conduction band, which makes it a *p*-type semiconductor. On the other hand, a Te-vacancy in Pb-rich material transfers 8 levels from the valence band to the conduction band, which removes 6 electrons from Te atom. Hence, two electrons, which can no longer be accommodated in the valence band, occupy the lowest two states of the conduction band, making the Pb-rich PbTe an *n*-type semiconductor.

There is still another type of interaction between impurities and the surrounding crystals: the deformation potential [Shockley et al., 1950]. Since the impurity is usually either larger or smaller than an atom of the host lattice, the presence of the impurity causes a local mechanical strain in crystal (e.g. a compressional strain as shown in Figure 2.2.) As evidenced from Figure 2.3, in some materials, compressional strain can increase the energy gap, while dilation can decrease it. This type of interaction will, therefore, also perturb the band edges. An interstitial atom evidently induces a deformation potential corresponding to compressional strain, whereas a vacancy will have the opposite effect, since it

produces dilational strain. Usually, both interstitials and vacancies are present in addition to substitutional impurities [Pankove, 1971].

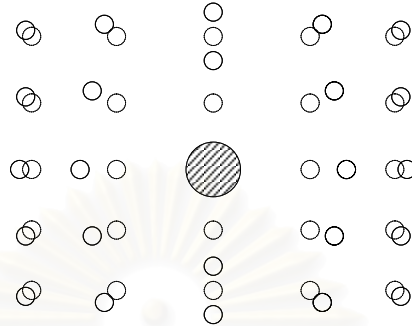


Figure 2.2 Compressional strain induced by the incorporation of a large impurity.

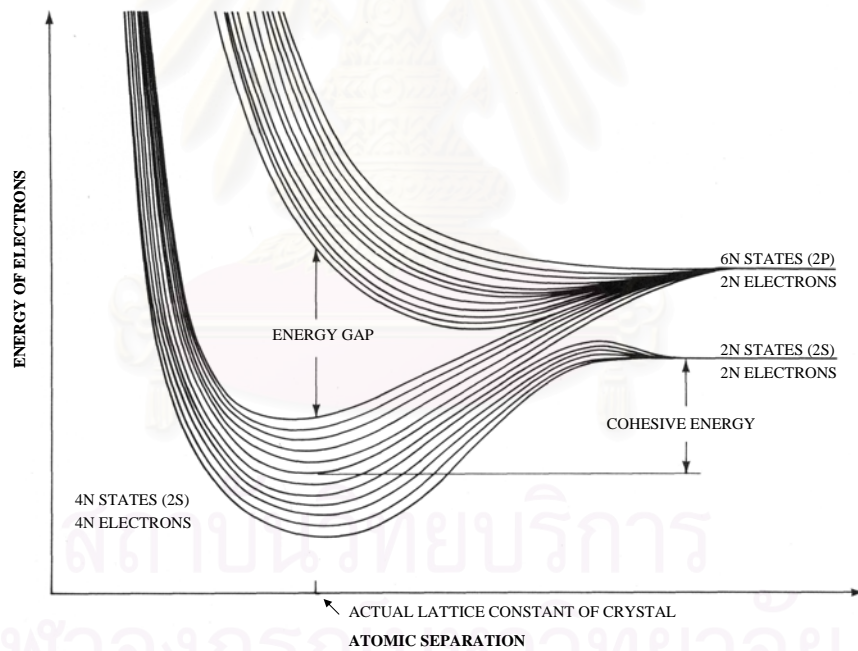


Figure 2.3 Energy banding of allowed levels in diamond as a function of spacing between atoms [Kimball, 1935].

Gallium-, copper-, aluminum- and magnesium-doped zinc oxide films show changes in both optical and electrical properties. Examples of report for zinc oxide doping are given in Table 2.2.

Table 2.2 The literature review of effect of metal content on metal-doped zinc oxide film.

<i>Dopant</i>	<i>Authors</i>	<i>Content of dopant</i>	<i>Band Gap Energy (eV)</i>
Ga	Khramovskyy et al, 2006	0 – 10 wt.%	3.26 – 3.56
	Aghamalyan et al, 2005	0 – 2 at.%	3.30 – 3.83
Cu	Bahsi et al, 2006	0 – 1 at.%	3.28 – 3.26
Al	Kuo et al, 2006	0 – 5 mol.%	3.30 – 3.305
	Xu et al et al, 2006	0 – 2 mol.%	3.34 – 3.46
Mg	Shan et al, 2004	0 – 5 at.%	3.28 – 3.39
	Ohtomo et al, 1998	0 – 33 at.%	3.36 – 3.99

In 2004, Shan and coworkers (2004) synthesized pure and Mg-doped ZnO thin films on glass substrates by pulsed laser deposition. It was found that all films had a preferred (002) orientation. The XRD peak position of (002) orientation was found shifting from 34.39° to 34.55° , after magnesium was incorporated into the film. An increase in the dopant concentration resulted in the decrease in lattice parameters, i.e. a from 3.25 to 3.23 Å, and c from 5.20 to 5.16 Å. The optical band gap energies determined from the obtained absorption spectra are 3.274, 3.285, 3.304, 3.317, 3.324, 3.334, and 3.430 eV for zinc oxide thin films doped with 0, 0.5, 1.0, 1.5, 2.5, 3 and 5 at.% of Mg, respectively. Interestingly, the band gap energy of Mg-doped ZnO thin film increases linearly with increasing dopant concentration [Shan et al., 2004].

In 2006, Xu and coworkers (2006) studied Al-doped ZnO thin films prepared by the sol-gel method. They observed that zinc oxide thin film doped with 1.5 mol.% aluminum resulted in XRD peaks with the highest intensity. The peak intensity of film decreased with increased doping concentration. This result indicates that an increase in doping concentration deteriorates crystallinity of the film, which may be due to stress caused by the difference in size between zinc ion and the dopant, as well as the segregation of dopant in grain boundaries at high doping concentration. Moreover, optical band-gap of the sample also depends on the concentration of Al doped, varying from 3.34 eV for undoped zinc oxide film to 3.46 eV for zinc oxide film doped with 2.0 mol.% Al [Xu et al., 2006].

In 2006, Khranovskyy and coworkers (2006) synthesized Ga-doped ZnO thin films by plasma enhanced metalorganic chemical vapor deposition (PEMOCVD). The doping content was between 0 - 10 wt.% of gallium precursor content in the deposition mixture. They observed that the band gap energy was 3.26, 3.40, 3.33, 3.385 and 3.56 eV for zinc oxide thin films doped with 0, 1, 3, 5 and 10 wt.%, respectively. Gallium was introduced into the film during film growth. Gallium was ionized into Ga^{3+} and replaced Zn^{2+} . Parts of the doped gallium become active donors and contribute free electron density to the zinc oxide film. The electron density increases with the concentration of electrically active Ga atoms. It is also evident that the optical band gap is enlarged. AFM analysis showed that all deposited films were polycrystalline and consisted of hexagonal grains with average grain size varying from 115.3 nm (for 1% of Ga content) to 74.9 nm (for 10% of Ga content) [Khranovskyy et al., 2006].

In 2006, Bahsi and coworkers synthesized Cu-doped ZnO on glass substrates by a sol-gel technique. XRD analyses showed that all samples were polycrystalline and consisted of single zinc oxide phase with zincite structure. The lattice parameters of the undoped film were very close to the parameters obtained from zincite structure (JCPDS 36-1451). Cu doping increased a and decreased c parameter. Moreover, Cu doping increased the average grain size and decreased band gap energy [Bahsi et al., 2006].

2.3 Methods for Synthesizing Zinc Oxide

Zinc oxide particles have been prepared by several methods. In general, the methods which have been reported for zinc oxide include: thermal decomposition method, sol-gel method and precipitation method.

2.3.1 Thermal decomposition method

This method has been called differently, e.g. hydrothermal method, glycothermal method and solvothermal method, when different reaction medium is used. Nevertheless, the methods mentioned have been used to successfully synthesize

various types of nanosized metal oxides with large surface area, high crystallinity and high thermal stability [Chen et al., 2003; Payakgul et al., 2005; Yang, 2005].

Solvothermal method has been developed to synthesize metal oxide and binary metal oxide via the decomposition of metal-alkoxide precursor in organic solvent. They are principally similar to hydrothermal method which employs water as the reaction medium. The use of solvent instead of water produces different form of intermediates, of which the stability is not so strong. Instability of the intermediate gives large driving force for the formation of product. Therefore, the synthesis can be accomplished at a relatively low temperature and pressure in a closed system and can be easily controlled. Moreover, it has been applied to successfully synthesize nanocrystalline zinc oxide with high crystallinity in one step. In 2004, Tonto and coworkers (2004) synthesized zinc oxide nanorods with narrow particle-size distribution by solvothermal reaction of zinc acetate in various organic solvents (1,3 propanediol, 1,4 butanediol, 1,5 pentanediol, 1,6 hexanediol, 1-butanol, 1-hexanol, 1-octanol, 1-decanol, benzene, toluene and xylene) at 200-300°C for 2 hours. All products are the hexagonal wurtzite structure. No impurity or secondary phase was observed. The linear relationship between boiling points of organic solvent and aspect ratios (length/diameter of zinc oxide particles) was reported [Tonto, 2004]. According to advantages of the solvothermal reaction mentioned above, this method was selected to prepare zinc oxide in this work.

Doping of metal oxide can also be done during solvothermal synthesis by mixing dopant to the precursor. Dovolos and coworkers (2003) synthesized europium-doped yttrium oxide by solvothermal method. In the experiment, yttrium oxide as well as the yttrium oxide/ europium oxide mixture were treated in isopropanol under supercritical condition in a hermetically closed autoclave with controlled pressure, at temperature of 500°C for 20 hours. The size of europium-doped yttrium oxide particles is smaller than 5 µm. The grains of the product are irregular aggregated and independent of the presence of doping ion [Davalos et al., 2003]. Masayuki and coworkers (2005) synthesized Er³⁺-doped YAG (Er:YAG) nanocrystals by glycothermal synthesis. Sample was prepared from a mixture of aluminium isopropoxide, yttrium acetate tetrahydrate, and erbium acetate tetrahydrate suspending

in 1, 4-butanediol in an autoclave. The autoclave was completely purged with nitrogen, heated to the 300°C at a rate of 2.3°C min⁻¹, and kept for 2 h. The products obtained were nanocrystals with high surface area [Nishi et al., 2005].

2.3.2 Sol-gel method

Sol-gel chemistry is based on inorganic polymerization reaction. When ultrafine colloidal dispersions lose fluid, they can turn into a highly viscous mass. Such mass is called a gel. When chemical methods are used to turn solution of metal compounds into gels, it is called sol-gel process. Highly reactive and pure ceramic powders can be prepared from such gels. Two routes are usually described in the literature depending on whether the precursor is aqueous solution of inorganic salt or an alkoxide in organic solvent. Kamalasanan and coworkers (1996) synthesized zinc oxide thin films by the sol-gel technique. The XRD pattern showed that the sample was crystallized in hexagonal wurtzite structure. The product was highly transparent without any crack or void. The films showed interference colors depending on its thickness [Kamalasanan et al., 1996].

2.3.3 Precipitation method

Precipitation method involves the growth of crystals from a solvent of different composition to the crystal. The reactants may or may not be in the same phase before the precipitation take place. If the reactants are in the same phase, the precipitation is homogeneous, otherwise, it is heterogeneous. The homogeneous precipitation is often preferred because its behavior is more controllable [Chen et al., 1993].

Basically, all process parameters influence quality of the final product of the precipitation. It is usually desired to get the precipitates with specific properties. These properties may involved physical properties of particle such the nature of the phase formed, chemical composition, purity, particle size, surface area, pore size, pore volumes, and separability from the mother liquor. On the other hand, it may include the demands which are imposed by the requirement of downstream processes, such as drying, palletizing or calcinations. It is therefore necessary to optimize the parameters

in order to produce the desired material. A variety of particle sizes and shapes can be produced, depending on the reaction conditions. Moreover, the particles can be agglomerates of much finer primary particles. Rodriguez-Paez and coworkers (2001) synthesized zinc oxide nanoparticles by precipitation method, using zinc acetate dihydrate aqueous solutions and nitric acid as reagents. The XRD pattern showed that sample was zinc oxides in hexagonal wurtzite form with crystal size about 50 nm [Rodriguez-Paez et al., 2001].

2.4 Electronic Structure of Semiconductor

In solid-state physics, semiconductors (and insulators) are defined as solids in which the uppermost band of *occupied* electron energy states, known as the valence band, is completely full at absolute zero temperature (0 K). In the other words, the Fermi energy of the electrons lies within the forbidden bandgap. The Fermi energy, or Fermi level can be thought of as the energy up to which available electron states are occupied at absolute zero temperature.

At room temperature, there is the smearing of the energy distribution of electrons, such that a small, but not insignificant number of electrons have enough energy to cross the energy band gap into the conduction band. These electrons break loose from the covalent bonding among neighbouring atoms in the solid, and they are free to move around, hence conducting charges. The covalent bonds from which these excited electrons had previously occupied now have missing electrons, or *holes*, which are free to move around as well. It should be noted that the hole itself does not actually move, but a neighbouring electron can move to fill the hole, leaving a hole where it originally come from. By this way, the holes appear to move.

It is an important distinction between conductors and semiconductors such that, in semiconductors, movement of charge (current) is facilitated by both electrons and holes. For the conductors where the Fermi level lies within the conduction band, the band is only half filled with electrons. Therefore, only small amount of energy is needed for the electrons to find other unoccupied states in the conductor. On the contrary, the Fermi level in semiconductors lies in the valence band. The excitation of

electrons from the valence band to the conduction band in semiconductors depends on the band gap.

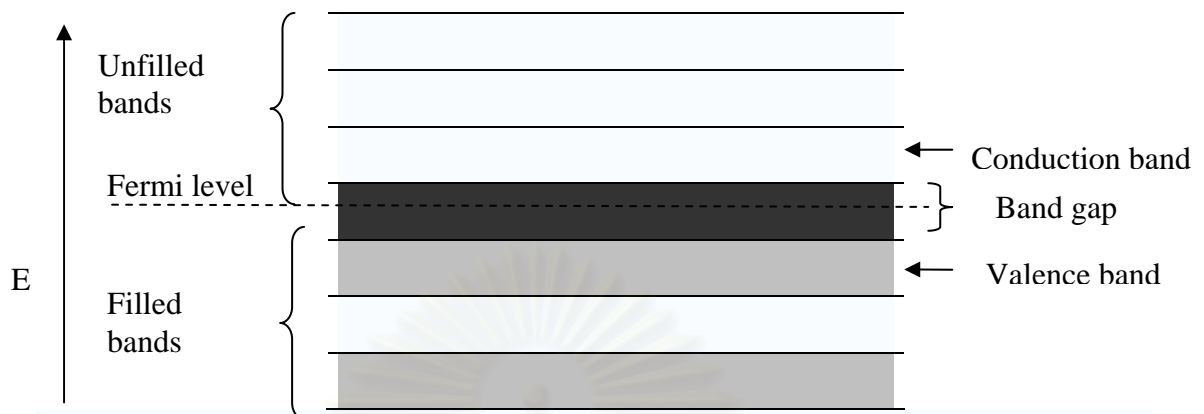


Figure 2.4 Band structure of a semiconductor showing a full valence band and an empty conduction band. The Fermi level lies within the forbidden bandgap.

The current-carrying electrons in the conduction band are known as "free electrons" although they are often simply called "electrons" if context allows this usage to be clear. The holes in the valence band behave very much like positively-charged counterparts of electrons, and they are usually treated as if they are real charged particles.

2.4.1 Direct and indirect band gap semiconductors

The band gap energy of semiconductor can be classified into direct and indirect band gap energy.

Direct band gap means that the conduction band lies directly above the valence band. A semiconductor with direct band gap can be used to emit light. The prime example of a direct band gap semiconductor is gallium arsenide, a material commonly used in laser diodes.

Indirect band gap semiconductors are inefficient in emitting light. This is because any electrons present in the conduction band quickly settle into the minimum energy of that band. Electrons in this minimum require source of momentum to

overcome the offset and fall into the valence band. Momentum of photons is very small comparing to this energy offset. Since the electron cannot rejoin the valence band by radiative recombination, conduction band electrons typically last quite some time before recombining through less efficient means. Silicon is an indirect bandgap semiconductor, and hence is not generally useful for light-emitting diodes or laser diodes. Indirect bandgap semiconductors can absorb light, however this only occurs for photons with significantly more energy than the band gap. This is why pure silicon appears dark grey and opaque, rather than clear.

2.4.2 The fundamental absorption process

The most important light absorption process in semiconductors involves the transition of electrons from the valence band to the conduction band. Because of its importance, the process is referred to as *fundamental absorption*.

In fundamental absorption, an electron absorbs an incident photon and jump from the valence band to the conduction band. Therefore, the energy of photon must be equal to or greater than the band gap energy (E_g), or the frequency of the incident photon (ν) must be;

$$\nu \geq E_g/h \quad (2.1)$$

where, h is Planck constant (4.135×10^{-15} eV.s)

The frequency of photon which corresponding exactly to the band gap energy is referred to as the absorption edge (ν_0), where $\nu_0 = E_g/h$.

The absorption edge is useful for determining band gap energy in semiconductors. It has replaced the earlier method that based on conductivity and has been a standard procedure for band gap determination, because of its accuracy and convenience. The optical method also reveals many more details about the band structure than the conductivity method.

To fine the absorption edge, the optical absorbance spectra of the sample, as shown in Figure 2.5, must be obtained (e.g. form UV-Visible spectrophotometer). The wavelength where the absorbance becomes 50% of the maximum absorbance (i.e. excitonic peak) is called $\lambda_{1/2}$. Meulenkamp and coworkers (1998) have reported that the frequency calculated from $\lambda_{1/2}$ is analogous to the absorption edge [Meulenkamp, 1998]. This method gives the result comparable to other studies and can reduce errors from the spectra with broad absorption edge [Madler et al., 2002].

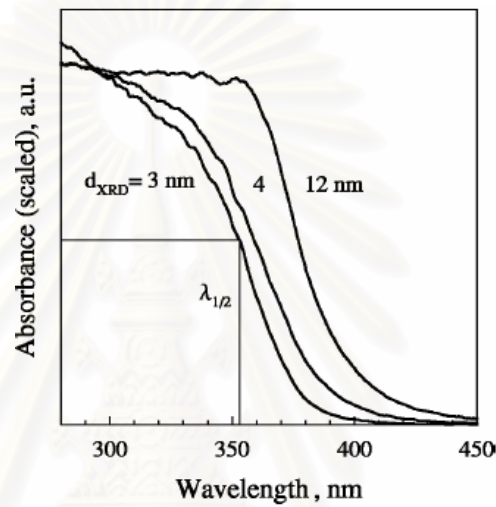


Figure 2.5 Determination of $\lambda_{1/2}$ from the optical absorbance spectra [Madler et al., 2002].

For semiconductor film, band gap can be calculated by other equations, depending on characteristic of the semiconductors.

For a *direct band gap semiconductor*:

$$\alpha_d = A(h\nu - E_g)^{1/2} \quad (2.2)$$

where α_d = Absorption coefficient, which can be calculated by using the formula of Pankove [Pankove, 1971; Mott et al., 1979].

$$\alpha_d = \frac{1}{d} \ln \left[\frac{(1-R)^2}{2T} + \left\{ \frac{(1-R)^4}{4T^2} - R^2 \right\}^{0.5} \right] \quad (2.3)$$

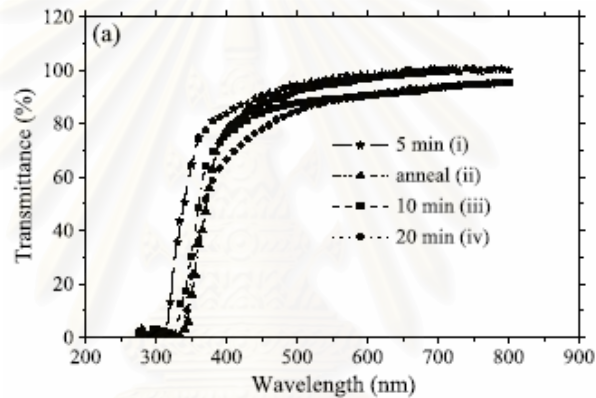
A = Constant involving the properties of the bands

R = Reflectance data

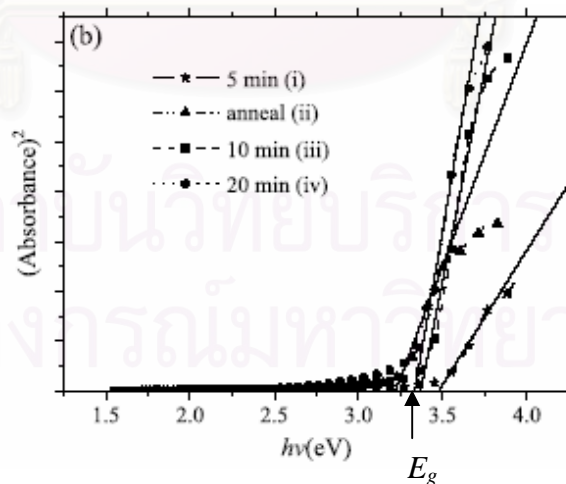
T = Transmittance data

d = film thickness (nm)

In 2005, Weng and coworkers synthesised zinc oxide thin film by electrochemical deposition. The band gap energy of samples were determined from relationship in equation (2.2) by extrapolation of the linear part in the plot of $(\text{absorbance})^2$ versus the excitation energy, $h\nu$ [Weng et al., 2005]. It should be noted that the use of $(\text{absorbance})^2$ is in accordance with $(\alpha_d)^2$ in equation (2.2). The methods are given in Figure 2.6.



(a)



(b)

Figure 2.6 (a) Optical absorbance spectra of samples
 (b) The band gap energy are determined by extrapolation of the linear part of the plot of α^2 versus $h\nu$ on x-axis [Weng et al., 2005].

For an *indirect band gap semiconductor*:

$$\alpha_i = A'(T) (h\nu - E_g)^2 \quad (2.4)$$

where $A'(T)$ = Constant containing parameters pertaining to the bands and the temperature [Blatt, 1968].

2.5 Photoluminescence

2.5.1 Principle of photoluminescence spectroscopy

Various processes whereby electrons may be excited by the absorption of radiation. Once electrons have been excited, the distribution of electrons is no longer in equilibrium, and they eventually decay into lower states, emitting radiation in the process. This emission is referred to as *luminescence*.

The study and characterization of luminescence property in different materials form one of the main fields of research in semiconductors. A very common luminescent device, for example, is a television screen. The images seen are formed by the luminescent coating on the screen, which is excited by an electron beam within the instrument.

Photoluminescence (PL) spectroscopy is used to characterize luminescence of the sample. Photoluminescence spectroscopy is a contactless, nondestructive method of probing the electronic structure of materials. Light is directed onto a sample, where it is absorbed and imparts excess energy into the material in a process called photo-excitation. One way this excess energy can be dissipated by the sample is through the emission of light, or luminescence. In the case of photo-excitation, this luminescence is called photoluminescence. The intensity and spectral content of this photoluminescence is a direct measure of various important material properties.

2.5.2 Practical uses of photoluminescence

Band gap determination

The most common radiative transition in semiconductors is between states in the conduction and valence bands, with the energy difference being known as the band gap. Band gap determination is particularly useful when working with new compound semiconductors. For zinc oxide, the main peak of UV emission is attributed to the radiative annihilation of excitons, which is corresponding to band gap energy.

Impurity levels and defect detections

Radiative transitions in semiconductors also involve localized defect levels. The photoluminescence energy associated with these levels can be used to identify specific defects, and the amount of photoluminescence can be used to determine their concentration.

Recombination mechanisms

The return of the excited electrons to equilibrium, also known as "recombination," can involve both radiative and nonradiative processes. The amount of photoluminescence and its dependence on the level of photo-excitation and temperature are directly related to the dominant recombination process. Analysis of photoluminescence helps to understand the underlying physics of the recombination mechanism.

Material quality

In general, nonradiative processes are associated with localized defect levels, whose presence is detrimental to material quality and subsequent device performance. Thus, material quality can be measured by quantifying the amount of radiative recombination.

2.6 Photocatalytic Process

The photocatalytic reaction starts with the exposure of photocatalyst to light. After light is absorbed by photocatalyst, two types of carriers, i.e. electron (e^-) and holes (h^+), are generated. A semiconductor oxide is good photocatalyst because of the long life for both of these carriers. For this reason, semiconductor oxides such as TiO_2 , ZnO , $SrTiO_3$, K_4NbO_2 , Fe_2O_3 and SnO_2 are used in photocatalytic process.

In photocatalytic process, the minimum energy required to actuate the reaction is corresponding to the band gap of the photocatalyst. When a photon of energy higher or equal to the band gap energy is absorbed by a semiconductor, an electron from the valence band is promoted to the conduction band with simultaneous generation of an electronic vacancy or hole in the valence band. These holes can react with water to produce the highly reactivity hydroxyl radical (OH^\cdot). Both the holes and the hydroxyl radicals are very powerful oxidants, which can be used to oxidize most organic materials. For zinc oxide, the band gap energy is 3.20 eV, which corresponds to ultraviolet radiation with wavelength of 387.5 nanometers. Therefore, ultraviolet radiation with wavelength shorter than 387.5 nm is required to initiate the photocatalytic reaction using zinc oxide as photocatalyst.

Methylene blue (MB) decomposition and anti-microbial testings have been carried out to study photocatalytic ability of zinc oxide. Photocatalytic decomposition of the MB solutions was characterized by a UV-vis spectrometer. The wavelengths that are prevailingly absorbed by MB are 665, 292, and 246 nm whereas the maximum peak occurs at 665 nm. The mechanism of MB decomposition by photocatalytic process can be explained in 5 steps.

1. Conduction band electrons (e^-) and valence band holes (h^+) are generated on the surface of zinc oxide particles upon the illumination by light with energy greater than the band gap energy, as demonstrated in (2.5).



2. Holes can react with water adhering to the surface of zinc oxide particles to form highly reactive hydroxyl radicals ($\text{OH}\cdot$), as shown in (2.6).



3. Oxygen dissolved in the solution acts as an electron acceptor by forming a super-oxide radical anion ($\text{O}_2^{\cdot-}$), as shown in (2.7).



4. The suspension of super-oxide radical anions may act as oxidizing agents or as an additional source of hydroxyl radicals via the subsequent formation of hydrogen peroxide as shown in (2.8)–(2.10).



5. The powerful oxidants associated with hydroxyl radicals react with the methylene blue (MB^+), and make the blue solution colorless, as shown in (2.11).



For anti-microbial testings, under illumination, the powdered photocatalyst produces super-oxide ions and hydroxyl radicals that are very powerful oxidants in the same manner as previously described for photocatalytic process. These highly reactive particles are able to oxidize organic materials and are effective against

bacteria as well. When the cell membrane of bacteria is in contact with the powerful oxidants, it is decomposed and consequently the bacteria will die. Photocatalyst not only kill the bacteria, but also clean their bodies. The body of a bacterium cell will be decomposed into carbon dioxide and water [Lin et al., 2005].

Although TiO_2 has been used for many photocatalytic applications, ZnO show higher capability than TiO_2 in many applications. Mrowetz and coworkers compared catalytic activity of TiO_2 and ZnO in the degradation of formic acid and benzoic acid. They observed that ZnO appeared to be more effective photocatalyst than TiO_2 for benzoic acid degradation [Mrowetz et al., 2005]. Sakthivel and coworkers compare photocatalytic efficiency of ZnO, TiO_2 , SnO_2 , ZrO_2 , $\alpha\text{-Fe}_2\text{O}_3$, WO_3 and CdS using solar photocatalytic degradation of Acid Brown 14. They observed that ZnO is the most active photocatalyst for the degradation of Acid Brown 14 using sunlight as a energy source. The main reason for this greater activity of ZnO is that ZnO absorbs large fraction of the solar spectrum. In the catalysts with smaller band gap, the excited electron in conduction band rapidly fall into the hole and consequently results in reduced catalytic activity. Many investigators have reported that low band gap semiconductors suffer from limited photoactivity and lack of reproducibility. For catalysts with wide band gap energy which usually are stable and non-corrosive, they exhibit less activity because the light energy is not sufficient for excitation [Sakthivel et al., 2003].

CHAPTER III

EXPERIMENTAL

The synthesis of undoped and metal-doped zinc oxide using solvothermal process in organic solvent is explained in this chapter. The chemicals, samples preparation and characterization are also explained.

3.1 Chemicals

ZnO synthesis are prepared with the following reagents:

1. Zinc acetate ($\text{Zn}(\text{CH}_3\text{COO})_2$), 99.99%, available from Sigma-Aldrich.
2. 1, 4 Butanediol (1,4-BG, $\text{HO}(\text{CH}_2)_4\text{OH}$), 99%, available from Aldrich.
3. Gallium acetylacetonate ($\text{Ga}(\text{C}_5\text{H}_8\text{O}_2)_3$), 99%, available from Aldrich.
4. Copper acetylacetonate ($\text{Cu}(\text{C}_5\text{H}_7\text{O}_2)$), 97%, available from Aldrich.
5. Aluminium acetylacetonate ($\text{Al}(\text{C}_5\text{H}_7\text{O}_2)$), 99%, available from Aldrich.
6. Magnesium acetylacetonate dihydrate ($\text{Mg}(\text{C}_5\text{H}_8\text{O}_2)_2 \cdot \text{H}_2\text{O}$), 98%, available from Aldrich.

3.2 Equipment

The detailed schematic diagram of the equipment used for ZnO synthesis is mainly consisted of an autoclave reactor, as shown in Figure 4.1. The autoclave reactor is shown in Figure 4.2. The reactor has the following features.

- Made from stainless steel
- Volume of 1000 cm^3
- 10 cm inside diameter
- Maximum temperature of 350°C
- Pressure gauge in the range of 0-140 bar
- Relief valve used to prevent runaway reaction
- Iron jacket was used to reduce the volume of autoclave to be 300 cm^3
- Test tube was used to contain the reagent and glycol

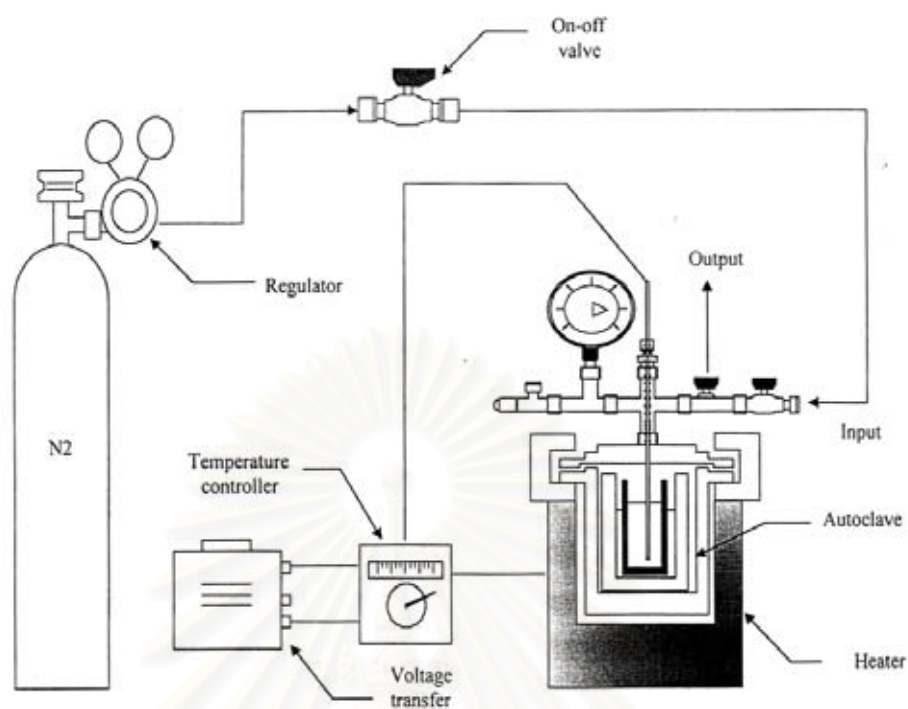


Figure 3.1 Diagram of the reaction equipment for the catalyst preparation.

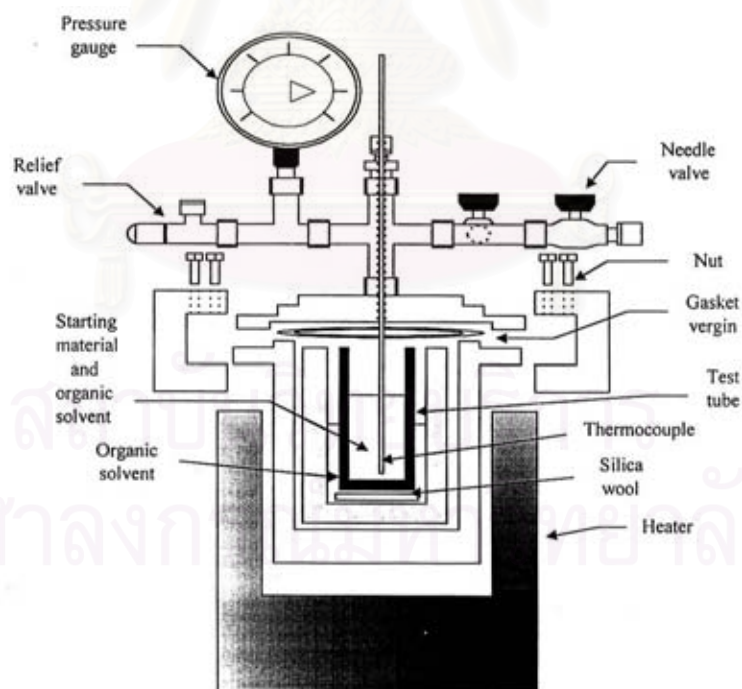


Figure 3.2 Autoclave reactor.

3.3 Experimental Procedures

3.3.1 Preparation of zinc oxide

Zinc oxide was prepared by solvothermal method using zinc acetate as starting material. Gallium acetylacetonate, copper acetylacetonate, aluminium acetylacetonate and magnesium acetylacetonate dihydrate was used as precursors for metal doping. About 15 g of the mixture of zinc acetate and metal precursor at predetermined ratio was suspended in 100 ml of solvent, i.e. 1, 4-butanediol, contained in a test tube. The test tube was then placed in an autoclave. In the gap between the test tube and autoclave wall, 30 ml of the same solvent was added. After the autoclave was completely purged with nitrogen, the autoclave was heated to 220°C at the rate of 2.5°C min⁻¹ and held at that temperature for 2 hours. Pressure in the autoclave reactor gradually increased autogeneously as the temperature was raised and the reaction proceeded. After the holding period, the autoclave was cooled to room temperature. The resulting powder was collected after repeatedly washed with methanol. The content of metal in zinc oxide powder was varied from 0 to 12.5 at.%.

3.3.2 Calcination of the metal-doped zinc oxide

The metal-doped ZnO was subjected to heat treatment at temperature ranging between 300 and 900°C in air for 1 hour at the heating rate of 10°C/min by using a box furnace.

3.3.3 Photocatalytic activity evaluation

Photocatalytic activity was evaluated from the decomposition of methylene blue (MB), C₁₆H₁₈N₃S, aqueous solution at the concentration of 10 ppm. The undoped and metal-doped zinc oxide were used as photocatalysts. A total of 0.012 g of sample was added into 50 ml of the above methylene blue solution under vigorous agitation. The photoreactor employed was a 50-ml beaker surrounded by 6 low-pressure mercury lamps. The distance between the lamps and the beaker was fixed at 10 cm. Two electric fans were used to cool the reaction solution. Complete mixing was

achieved by magnetic stirring. The average power of the mercury lamp, with wavelengths ranging from 300 to 400 nm, was 1.4 mW/cm^2 . Samples were periodically removed from the reactor and the Ultraviolet-Visible spectrometer (UV-Vis Lambda 650, Perkin Elmer) was used to monitor the change in MB concentration of the samples. In order to study the effect of intensity of UV rays, solar radiation was used instead of UV irradiation. It should be noted that the catalyst was kept in methylene blue solution in darkness for 1 h before UV light illumination, in order to eliminate the effect of methylene blue absorption onto the catalyst.

3.4 Characterizations of Samples

3.4.1 X-ray diffraction analysis (XRD)

X-ray diffraction (XRD) analysis of zinc oxide was performed by a SIEMENS D5000 X-ray diffractometer connected with a personal computer with Diffract AT version 3.3 program at the Center of Excellence on Catalysis and Catalytic Reaction Engineering, Chulalongkorn University. The measurement was carried out by using $\text{CuK}\alpha$ radiation with Ni filter. The condition of the measurement is shown as followed:

2 θ range of detection	:	10 – 80 °
Resolution	:	0.02 °
Number of Scan	:	10

3.4.2 Surface area measurement

The specific surface area of zinc oxide particles was measured according to the single point BET method, by using nitrogen as the adsorbate. The operating conditions are as follows:

Sample weight	~ 0.2 g
Degas temperature	200°C

3.4.3 Scanning electron microscopy (SEM)

Morphology and size of the secondary particles of the prepared zinc oxide were observed by using JEOL JSM6400 Scanning Electron Microscope (SEM) at the Scientific and Technological Research Equipment Centre, Chulalongkorn University (STREC).

3.4.4 UV-visible absorption

UV-visible absorption spectroscopy measurement was carried out in a UV/VIS spectrophotometer (PerkinElmer Lambda 650, wavelength between 220 and 800 nm and step size 1 nm.). In this work, concentration of methylene blue solution in photodegradation experiments was also monitored by the absorption at wavelength of 665 nm.

3.4.5 X-ray photoelectron spectroscopy

The elemental content on the surface of the synthesized zinc oxide was determined by using X-ray photoelectron spectroscopy (Amicus, using $MgK\alpha$ radiation) at the Center of Excellences on Catalysis and Catalytic Reaction Engineering, Chulalongkorn University.

3.4.6 Photoluminescence

The emission energy of zinc oxide was determined by photoluminescence (Perkin elmer – Luminescence spectrometer LS50) at Mahidol university. The operating condition of measurement is shown as followings:

Range of detection	:	373 – 720 nm
Excited energy	:	366 nm
Excited slit	:	4.0 nm
Emission slit	:	4.0 nm
Scan speed	:	100 nm/min

CHAPTER IV

RESULTS AND DISCUSSION

4.1 Properties of Undoped and Metal-Doped Zinc Oxide

4.1.1 XRD analysis

The results from XRD analysis of gallium-, copper-, aluminum- and magnesium-doped zinc oxide with the metal content in the range of 0 to 12.5 at.% are shown in Figure 4.1 – 4.4. The diffraction peaks of all products can be indexed to hexagonal wurtzite structure of zinc oxide (JCPDS 36-1451). Therefore, the presence of impurity in the amount investigated does not affect the wurtzite structure of zinc oxide. The strong intensity of diffraction peaks indicates that the resulting products have high crystallinity. It should be noted that no other crystalline phase is detected, except when copper is doped into zinc oxide. At copper metal content higher than 2.5 at.%, the XRD pattern shows the diffraction peaks of impurity, which can be indexed to metallic copper (JCPDS 04-0836) [Zhu et al., 2004]. It indicates that copper acetylacetonate, the precursor of copper, is decomposed but not fully incorporated into zinc oxide structure. The solid solubility of copper into zinc oxide structure is limited to 2.5 at.%. For other metals, the solid solubility limit has been previously reported elsewhere [Bhattacharya et al., 2004; Yu et al., 2004].

Detailed investigation indicates that the XRD patterns of the all samples are slightly shifted from the pattern of pure zinc oxide as shown in Figure 4.5. This observation indicates the change in crystal structure and lattice parameters of the samples. In the previous work, Park et al. reported that the substitution of small Al ions (radius of 53 pm) into the Zn^{2+} (radius of 74 pm) site in the aluminium-doped zinc oxide crystal resulted in an increase in the 2θ value of the (002) reflection plane in XRD pattern of zinc oxide because crystal size was decreased [Park et al., 1997]. Shan et al. reported that the doping of magnesium changed the peak position of (002) reflection from 34.39° to 34.55° [Liu et al., 2003].

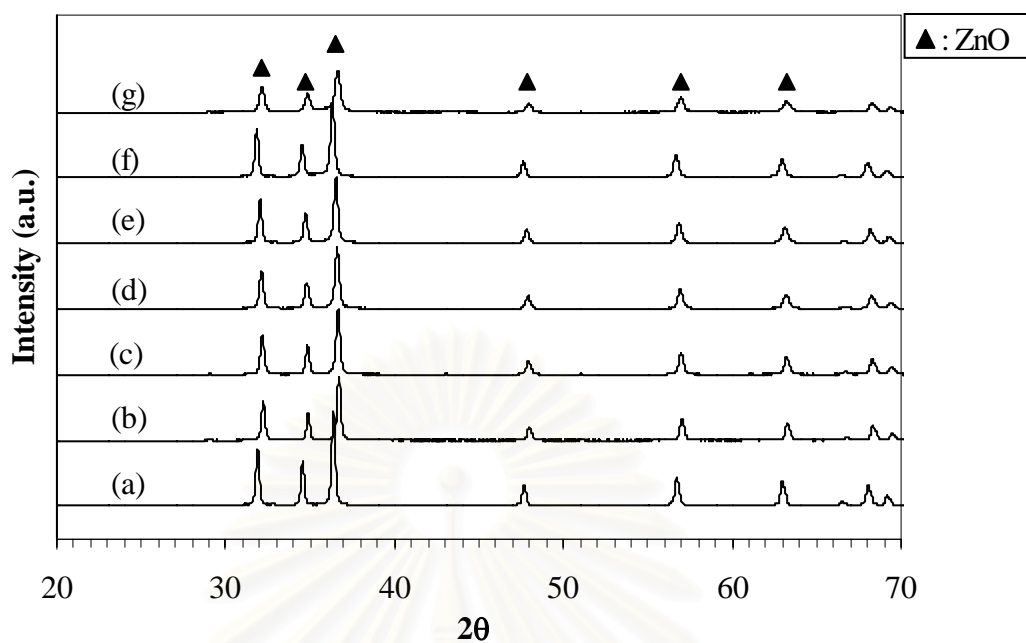


Figure 4.1 The XRD patterns of undoped zinc oxide (a) and gallium-doped zinc oxide at dopant contents of (b) 0.5, (c) 2.5, (d) 5, (e) 7.5, (f) 10 and (g) 12.5 at.%.

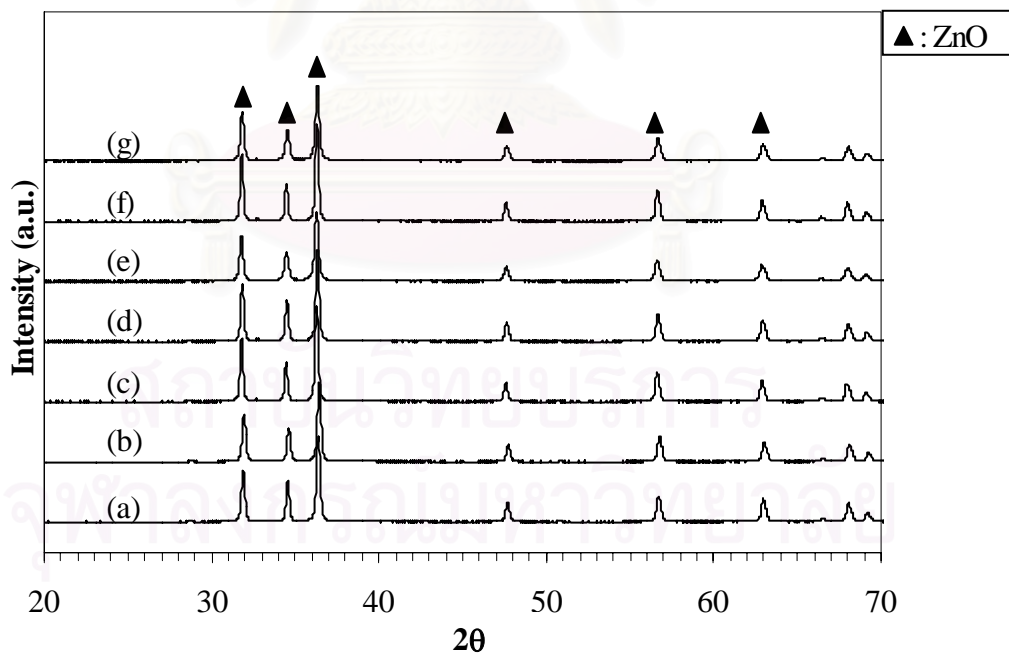


Figure 4.2 The XRD patterns of undoped zinc oxide (a) and aluminium-doped zinc oxide at dopant contents of (b) 0.5, (c) 2.5, (d) 5, (e) 7.5, (f) 10 and (g) 12.5 at.%.

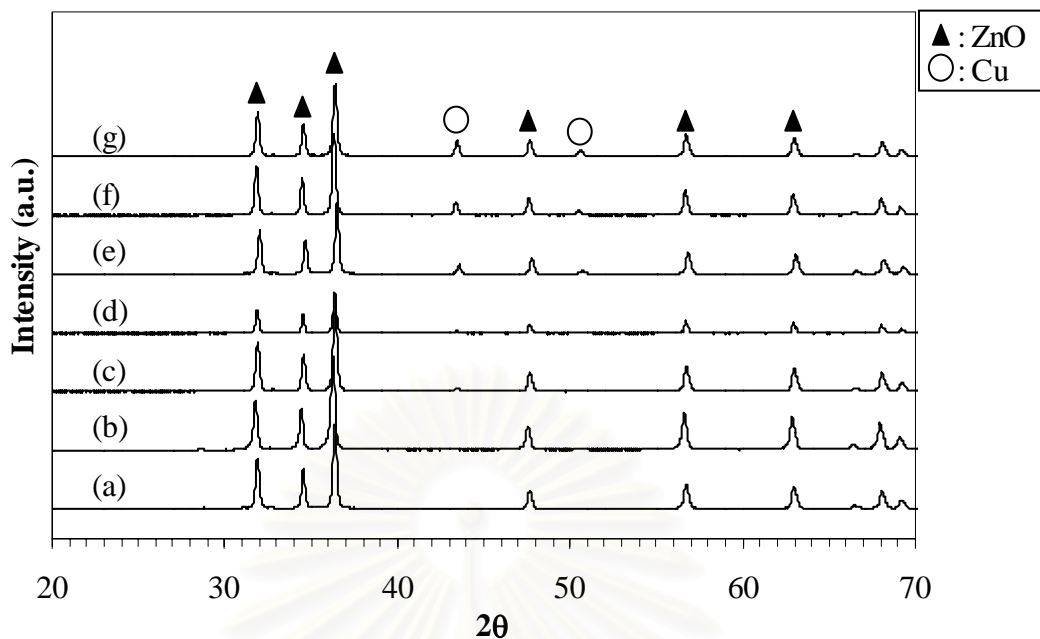


Figure 4.3 The XRD patterns of undoped zinc oxide (a) and copper-doped zinc oxide at dopant contents of (b) 0.5, (c) 2.5, (d) 5, (e) 7.5, (f) 10 and (g) 12.5 at.%.

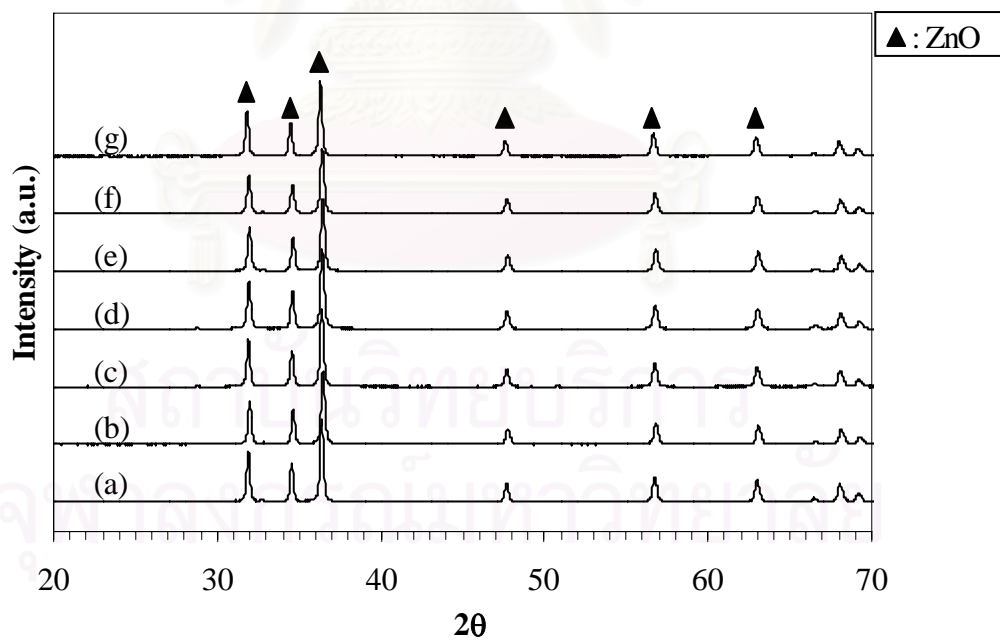


Figure 4.4 The XRD patterns of undoped zinc oxide (a) and magnesium-doped zinc oxide at dopant contents of (b) 0.5, (c) 2.5, (d) 5, (e) 7.5, (f) 10 and (g) 12.5 at.%.

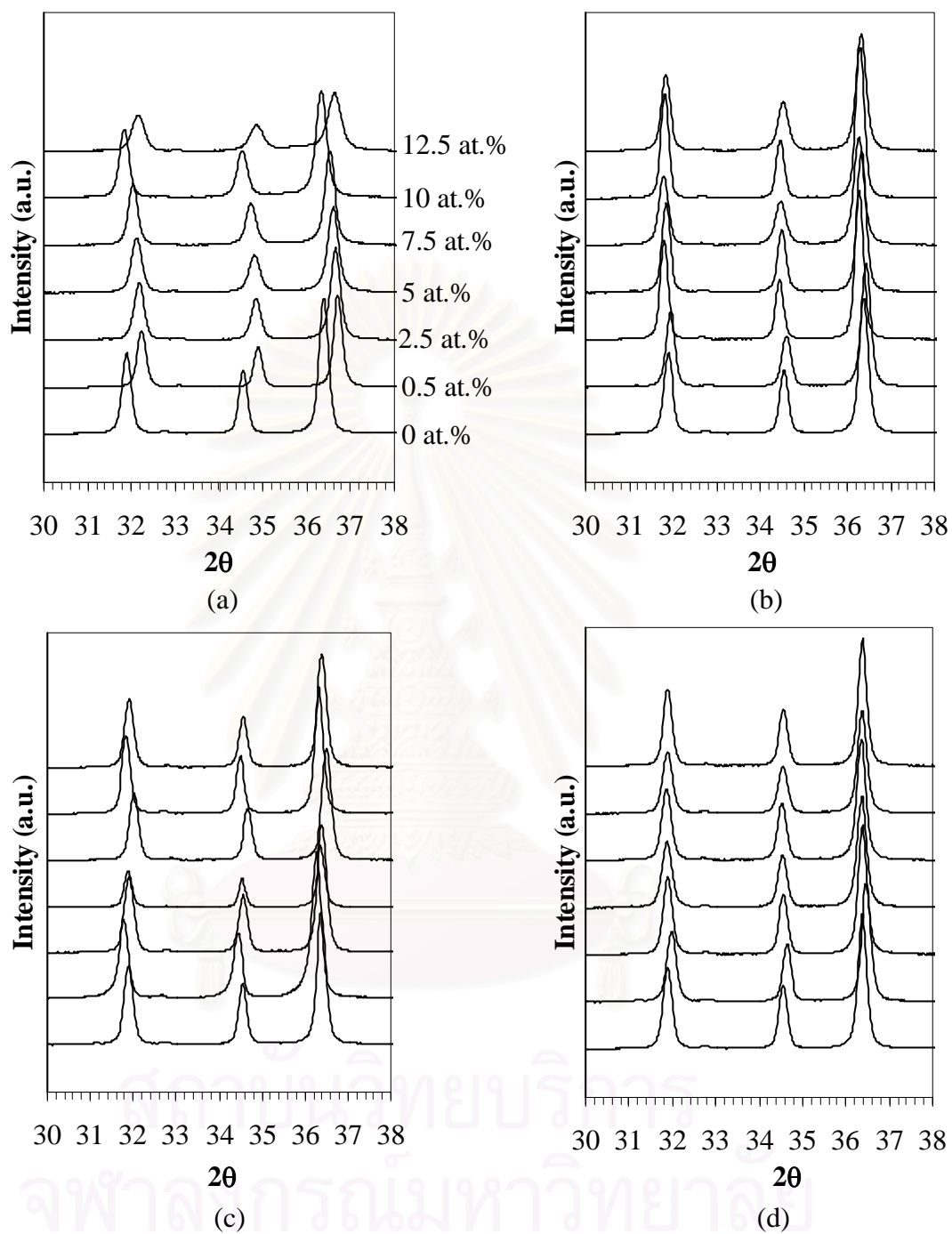
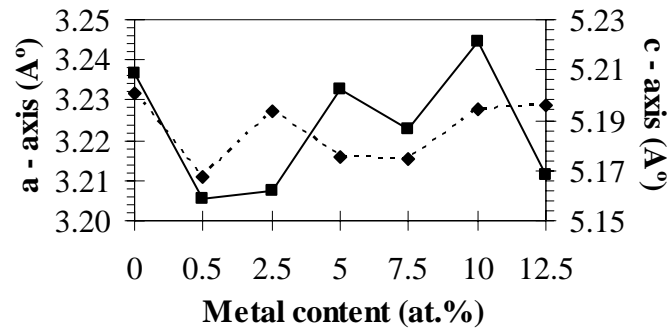


Figure 4.5 Shifting in XRD pattern of (a) gallium- (b) aluminium- (c) copper- and (d) magnesium-doped zinc oxide at various doping contents.

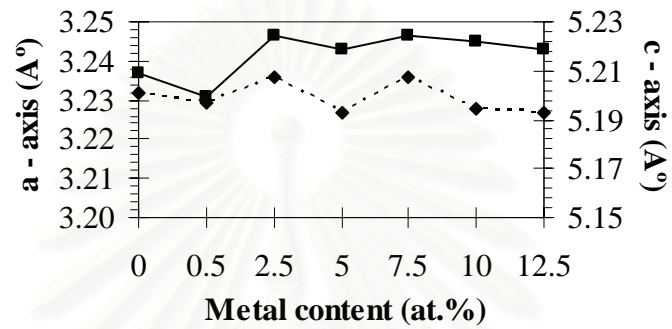
4.1.2 Lattice parameters of metal-doped zinc oxide

Ozgur and coworkers (2005) reported that the lattice parameters of a semiconductor usually depend on the following factors: (i) concentration of foreign atoms and defects as well as their difference in ionic radii with respect to the substituted matrix ion, (ii) external strains (for example, those induced by substrate), and (iii) temperature [Özgül et al., 2005]. Figure 4.6 shows lattice parameters that are calculated from the XRD patterns of undoped and metal-doped zinc oxide. The lattice [Liu et al., 2003] constants a and c of the wurtzite structure zinc oxide were calculated, according to Bragg's law [Liu et al., 2003]. Detailed calculation are shown in the Appendix A.

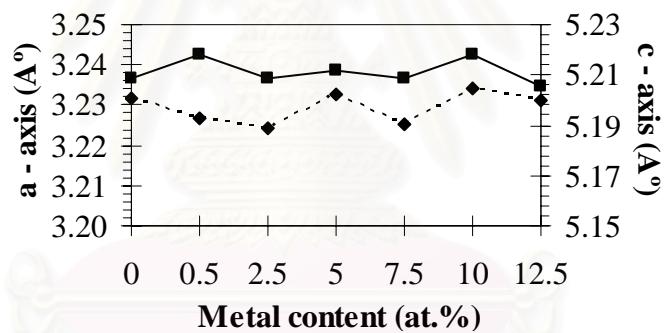
Results in this work evidently present that the lattice constants are altered by the presence of dopant in zinc oxide structure. Furthermore, the change in lattice constants a and c of are the generally related. At the doping content of 0.5 at.%, both a and c of gallium-, aluminium- and magnesium-doped zinc oxide are decreased, comparing to those of undoped zinc oxide. Because ionic radius of gallium, aluminium and magnesium is smaller than zinc ion, it causes a decrease in size of the crystal lattice of metal-doped zinc oxide. The effect of ionic radius on crystal size have been previously reported [Park et al., 1997; Posada et al., 2003; Cao et al., 2004; Yu et al., 2004; Pei et al., 2005; Bahsi et al., 2006]. For copper-doped zinc oxide, the ionic radius of Cu^{2+} (74 pm) and Cu^{1+} (71 pm) are relatively the same as ionic radius of Zn^{2+} (74 pm). Therefore, the deviation in lattice parameters can not be explained solely by ionic radius difference [Bahsi et al., 2006]. For the doping content higher than 0.5 at.%, the change in lattice parameter may be affected by both of (i) dopant ionic radius and (ii) the rearrangement of atoms due to the coulombic interaction between Zn^{2+} and O^{2-} ions [Yu et al., 2004].



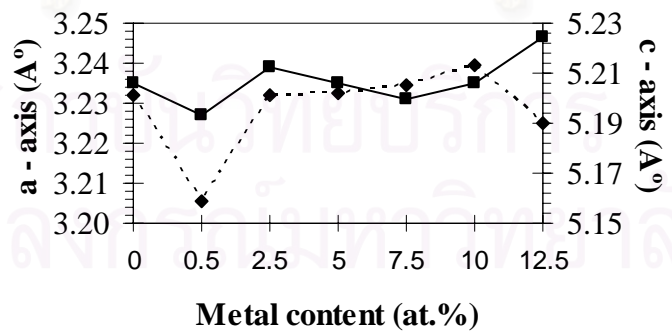
(a)



(b)



(c)



(d)

Figure 4.6 The lattice constants of (a) gallium-, (b) aluminium-, (c) copper- and (d) magnesium-doped zinc oxide at metal content in the range of 0 to 12.5 at.%.: (—) a - axis, (---) c - axis.

4.1.3 Morphology of metal-doped zinc oxide

The SEM micrographs of undoped and metal-doped zinc oxide are shown in Figure 4.7 – 4.11. For undoped zinc oxide (Figure 4.7), it is obvious that the particles shown are ellipsoidal with uniform size. On the contrary, most metal-doped zinc oxide powder is not uniform in size and shape [Paraguay, 2000; Cheong et al., 2002; Gomeza, 2005; Jeong et al., 2005]. The nonuniform sample usually consists of two types of particles, i.e. ellipsoidal as observed in the undoped zinc oxide and the rod morphology which is longer and bigger in diameter than the former type.

Figure 4.12 - 4.15 shows the relationship of the average diameter and length of the metal-doped zinc oxide with respect to metal content. The average diameter and length of the sample were determined from 50 randomly selected particles, using image analyzer program (SemAfore 4.0). It should be noted that the error bars in the figure represent standard deviation of the data. It is clearly indicated that morphology of zinc oxide is affected by metal content. At low metal content, the error bars of gallium- and aluminium-doped samples show very large size distribution, especially in length of particles. This effect seems to level-off after the doping content is higher than 2.5 at.%, except for 10 at.%. The error bar of gallium- and aluminium-doped samples is shortest at 5 and 7.5 at.%, respectively. For copper- and magnesium-doped zinc oxide, the particle size of almost all samples are the uniform, except for 10 at.-%-copper and 12.5 at.-%-magnesium doping. The aspect ratio of the particles is also affected by type of metal doped and the content of metal, as shown in Figure 4.16. Only magnesium has almost no effect on the aspect ratio. The report in literature has shown that, for solvothermal synthesis, concentration of starting material does not preferentially affect the growth of zinc oxide crystal in different orientation [Tonto, 2004]. However, in this research, it was observed that both size and aspect ratio of zinc oxide particle can be altered by doping metal at different concentration.

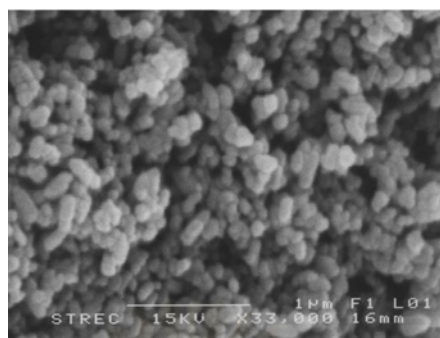


Figure 4.7 SEM micrographs of undoped zinc oxide

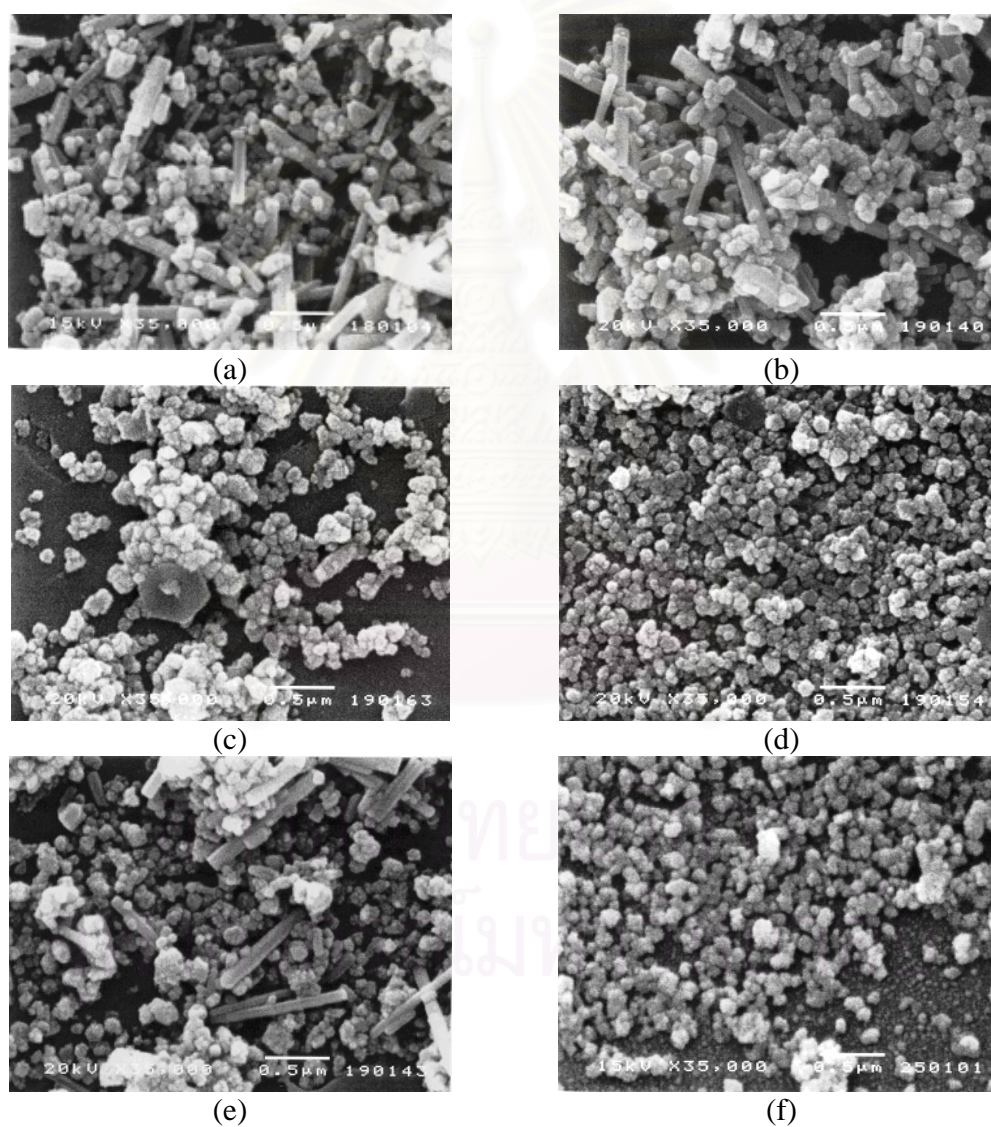


Figure 4.8 SEM micrographs of gallium-doped zinc oxide at: (a) 0.5, (b) 2.5, (c) 5, (d) 7.5, (e) 10, (f) 12.5 at.%.

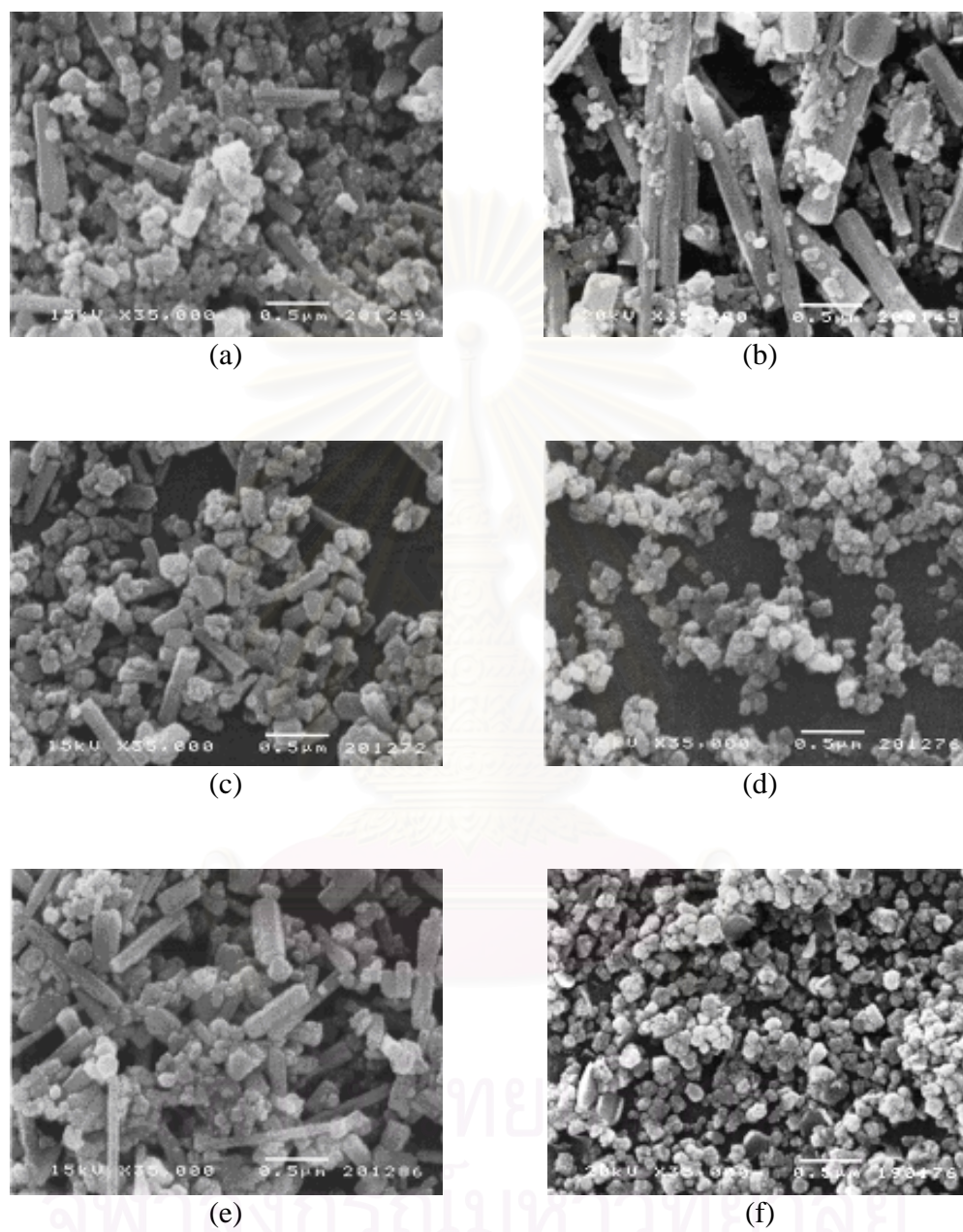


Figure 4.9 SEM micrographs of aluminium-doped zinc oxide at: (a) 0.5, (b) 2.5, (c) 5, (d) 7.5, (e) 10, (f) 12.5 at.%.

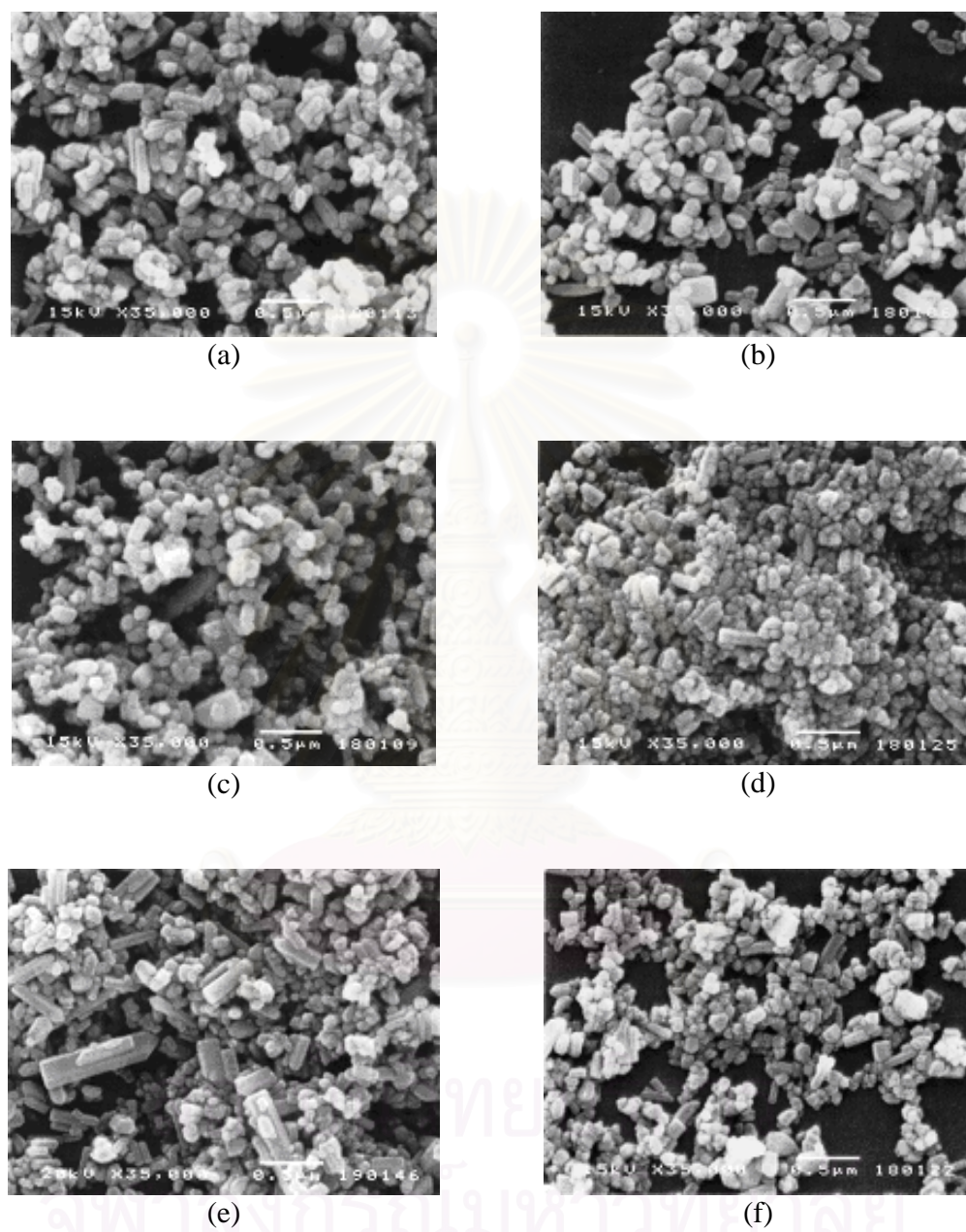


Figure 4.10 SEM micrographs of copper-doped zinc oxide at: (a) 0.5, (b) 2.5, (c) 5, (d) 7.5, (e) 10, (f) 12.5 at.%.

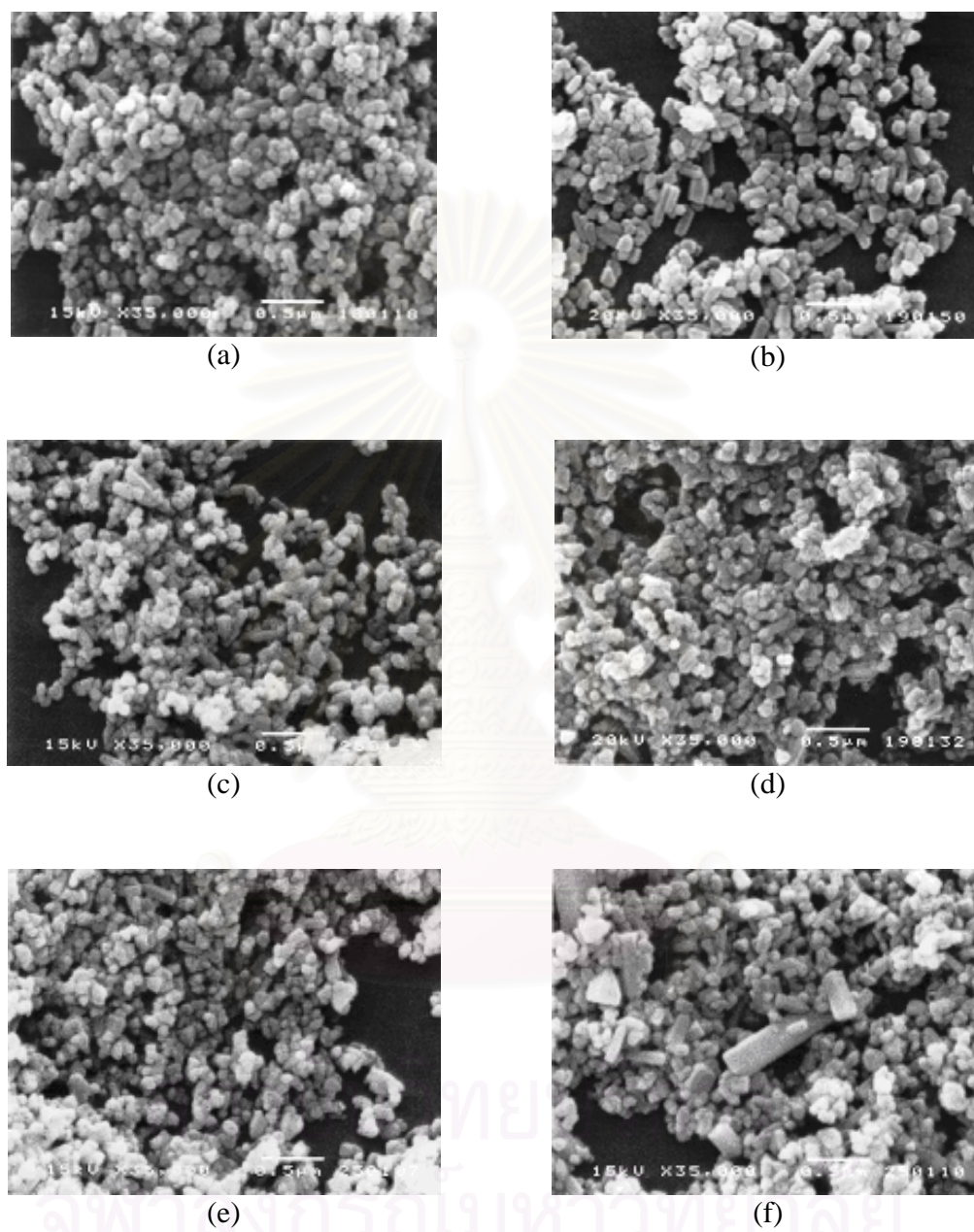


Figure 4.11 SEM micrographs of magnesium-doped zinc oxide at: (a) 0.5, (b) 2.5, (c) 5, (d) 7.5, (e) 10, (f) 12.5 at.%.
จุฬาลงกรณ์มหาวิทยาลัย

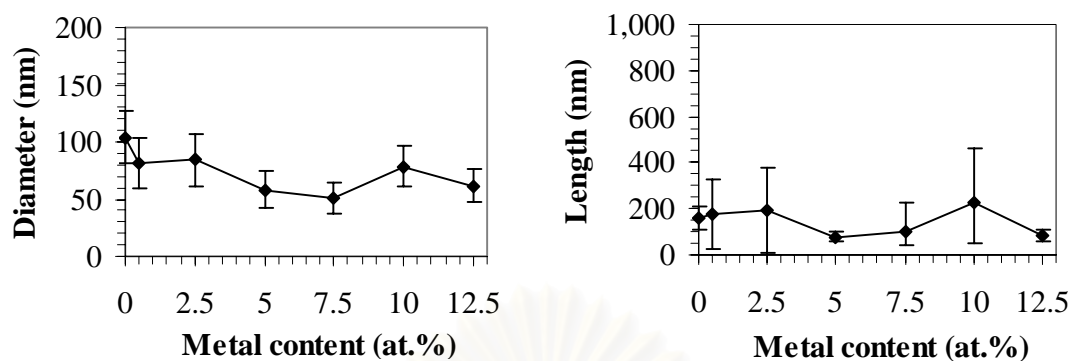


Figure 4.12 Average diameter and length of gallium-doped zinc oxide at doping content of 0 to 12.5 at.%.

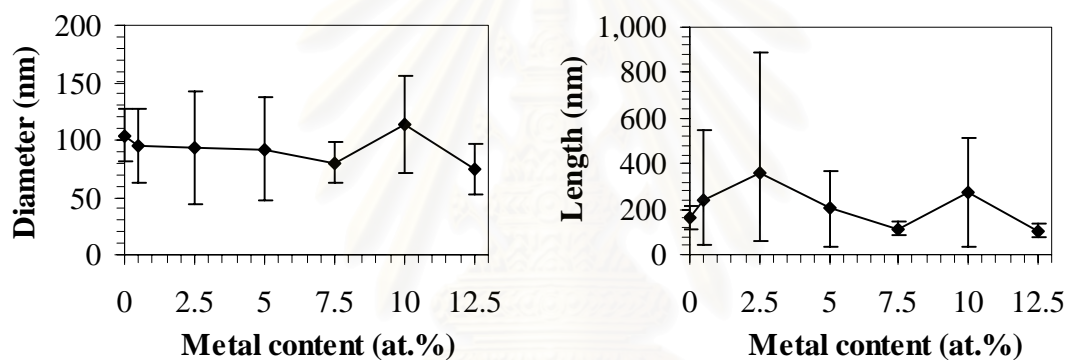


Figure 4.13 Average diameter and length of aluminium-doped zinc oxide at doping content of 0 to 12.5 at.%.

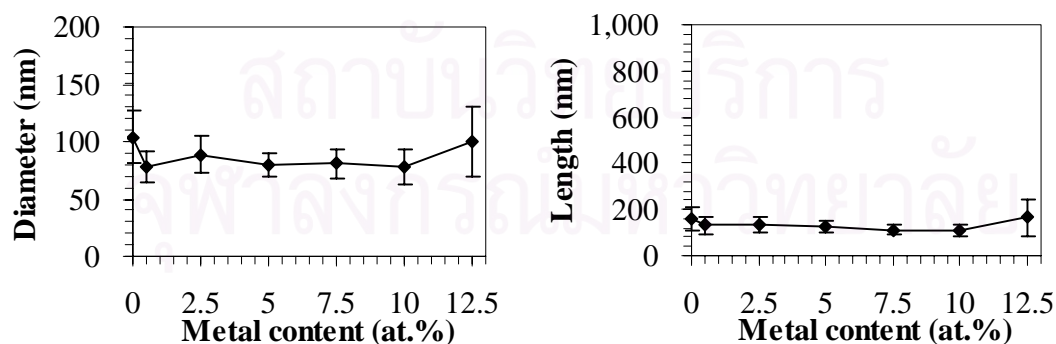


Figure 4.14 Average diameter and length of copper-doped zinc oxide at doping content of 0 to 12.5 at.%.

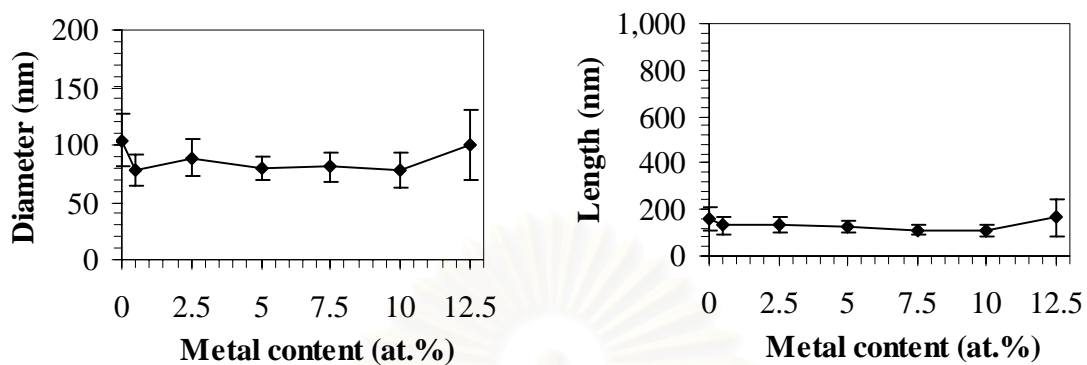


Figure 4.15 Average diameter and length of magnesium-doped zinc oxide at doping content of 0 to 12.5 at.%.

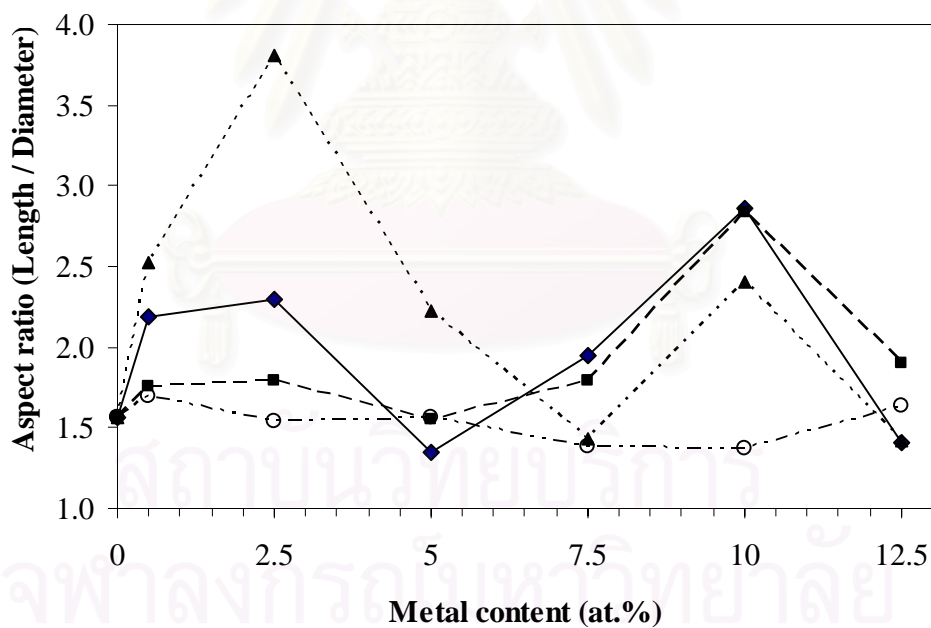


Figure 4.16 Aspect ratio of zinc oxide powder doped with: (◆) gallium, (▲) aluminium, (■) copper and (○) magnesium at various metal contents.

4.1.4 XPS analysis

Table 4.1 shows the composition of metal-doped zinc oxide characterized by XPS analysis. The XPS spectra of Zn 2p, O 1s, Ga 2p, Cu 2p, Al 2p and Mg 2s were chosen to present the signal of element investigated by considering their atomic sensitivity. The XPS spectra of undoped zinc oxide shows a quantitative atomic ratio of Zn/O close to that for the stoichiometric zinc oxide [Zou et al., 2004]. For the metal-doped samples, the percentage of dopant on surface of gallium-, copper- and aluminium-doped zinc oxide is increased as the content of is dopant increased from 0 to 12.5 at.%, except for gallium- and aluminium-doped zinc oxide at 5 and 10 at.%, respectively. On the contrary, the percentage of magnesium on magnesium-doped zinc oxide is decreased by an increase in the dopant content. It should be noted that magnesium-doped zinc oxide evidently indicates very large quantity of Mg deposited on the surface of the product. According to Figure 4.17 and 4.18, the binding energies of both zinc and oxygen are changed by the presence of dopant in the sample, which indicates the interaction of zinc and oxygen with dopant atoms and confirms that dopant atoms are incorporated into zinc oxide structure.

Table 4.1 Composition of metal-doped zinc oxide characterized by XPS analysis.

<i>Dopant</i>	<i>XPS spectra</i>	<i>Elemental composition of samples doped with metal in various contents (%)</i>					
		<i>0.5 at.%</i>	<i>2.5 at.%</i>	<i>5 at.%</i>	<i>7.5 at.%</i>	<i>10 at.%</i>	<i>12.5 at.%</i>
Ga	Ga 2p	0.51	1.70	1.35	3.80	4.69	6.93
	Zn 2p	22.46	29.34	11.85	15.42	15.74	17.27
	O 1s	77.03	68.96	86.80	80.78	79.57	75.80
Cu	Cu 2p	1.39	0.97	1.04	1.59	1.94	1.95
	Zn 2p	40.68	22.57	19.68	28.52	18.76	15.85
	O 1s	57.93	76.47	79.28	69.89	79.30	82.20
Al	Al 2p	1.55	1.94	3.72	4.89	3.49	5.33
	Zn 2p	32.25	29.94	25.03	23.25	24.00	24.92
	O 1s	66.20	68.12	71.24	71.86	72.51	69.75
Mg	Mg 2s	65.71	63.88	62.96	61.42	57.94	54.08
	Zn 2p	11.66	11.85	10.72	9.42	8.07	6.70
	O 1s	22.63	24.26	26.32	29.17	33.99	39.22

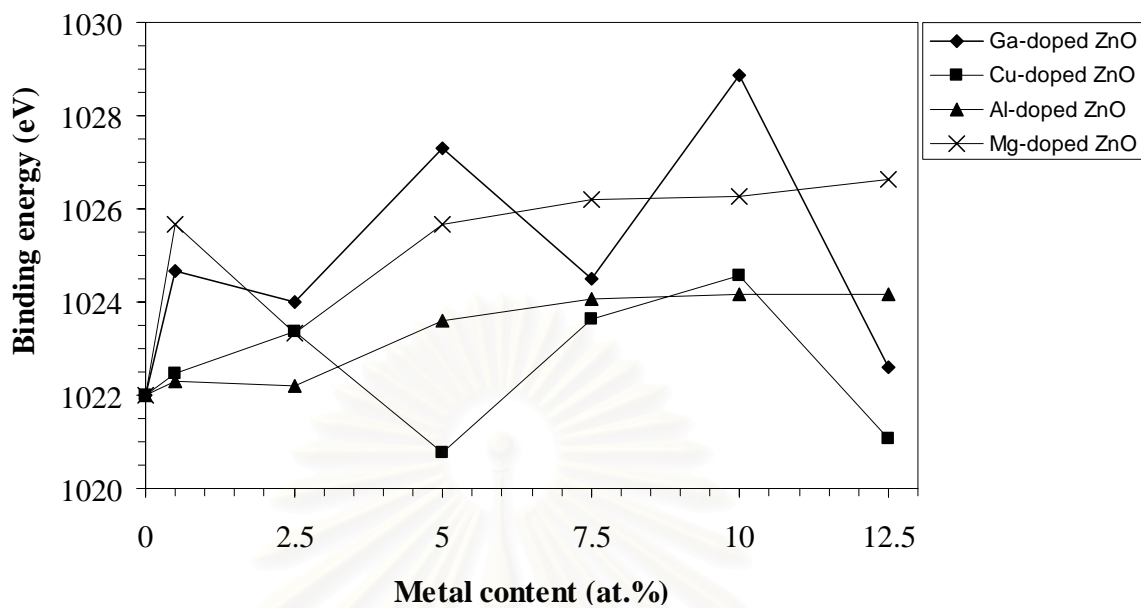


Figure 4.17 The Zn 2p binding energy of metal-doped zinc oxide at various metal contents.

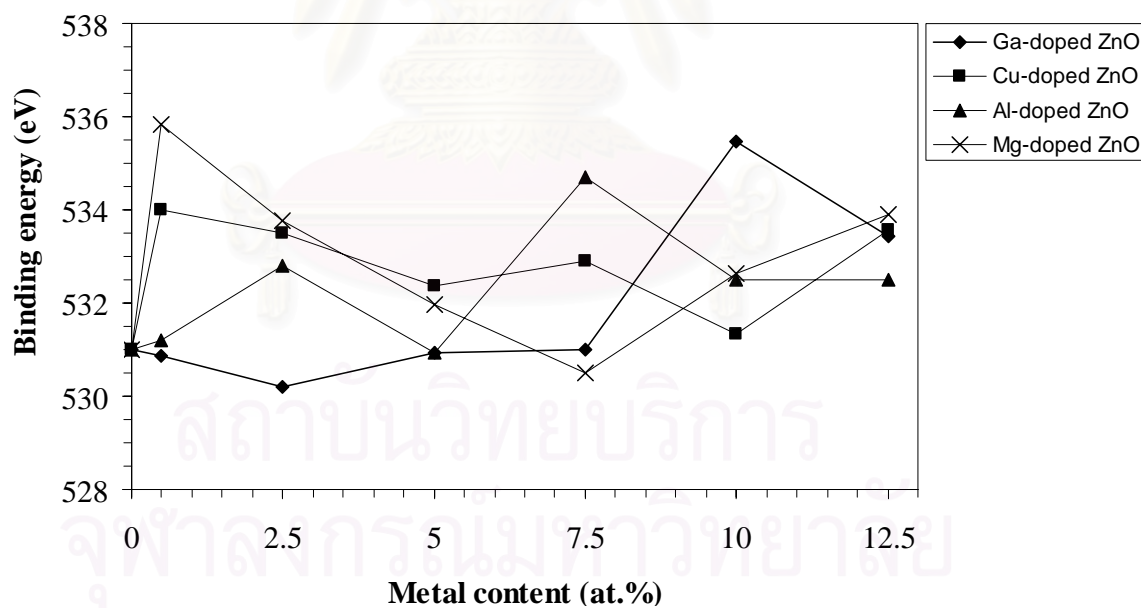


Figure 4.18 The O 1s binding energy of metal-doped zinc oxide at various metal contents.

4.1.5 Optical properties of metal-doped zinc oxide

The band gap energy of undoped and metal-doped zinc oxide was studied from absorption wavelength data from UV-Visible spectroscopy. In the literatures, it has been reported that the variability of the band gap can be rationalized on the basis of the presence of dopants [Roth et al., 1981; Srikant et al., 1997]. Figure 4.19 – 4.22 show the absorption spectra of undoped and metal-doped zinc oxide with metal content between 0 to 12.5 at.%. The undoped zinc oxide shows substantial absorption at wavelength below 380 nm, which is in the range of UV-A (315 – 380 nm). For wavelength higher than 400 nm, no significant absorption is observed. Samples with metal doping also show similar behavior, except for zinc oxide doped with high content of copper, which shows equivalently high absorption wavelength above 720 nm, in addition to the absorption behavior of undoped zinc oxide. This additional absorption is suggested to be the result from metallic copper which has absorption wavelength in the range of 700 – 1000 nm [Nogami et al., 1995]. The presence of metallic copper has already been confirmed by XRD analysis, as discussed in the previous section. The earlier research has also reported that the existence of small amount of Cu and Cu₂O can be observed in copper-doped zinc oxide [Gong et al., 2005]. The shifting in absorption spectra could be the result from the change in morphology of metallic copper as well as metal content. According to literatures, which studied UV-Vis spectra of spherical and rod-shaped copper nanoparticles, absorption at 740 nm was observed for rod-shaped, not for spherical particles [Panigrahi et al., 2006]. It should be noted that the absorption edge at wavelength around 380 nm of the copper-doped samples does not change with copper content. On the contrary, the absorption edges for the gallium- and aluminium-doped zinc oxide shift toward the lower wavelength, when the doping content is increased. This observed blue-shift indicates an increase in the band gap energy, which is attributed to the Burstein-Moss effect [Li et al., 2003; Liu et al., 2003]. At high doping concentrations, Fermi level is raised into the conduction band. Consequently, due to the filling of the conduction band, absorption transitions occur between valence band and Fermi level in the conduction band, instead of valence band and the bottom of the conduction band. This change in the transition levels shift the absorption edge to higher energies (blue shift) and

leads to the energy band broadening [Lee et al., 2004]. Furthermore, small ionic radius of gallium and aluminium causes the decrease in the lattice parameters of pure zinc oxide. So, the crystal structures are compressed and results in increased the band gap energy [Pankove, 1971].

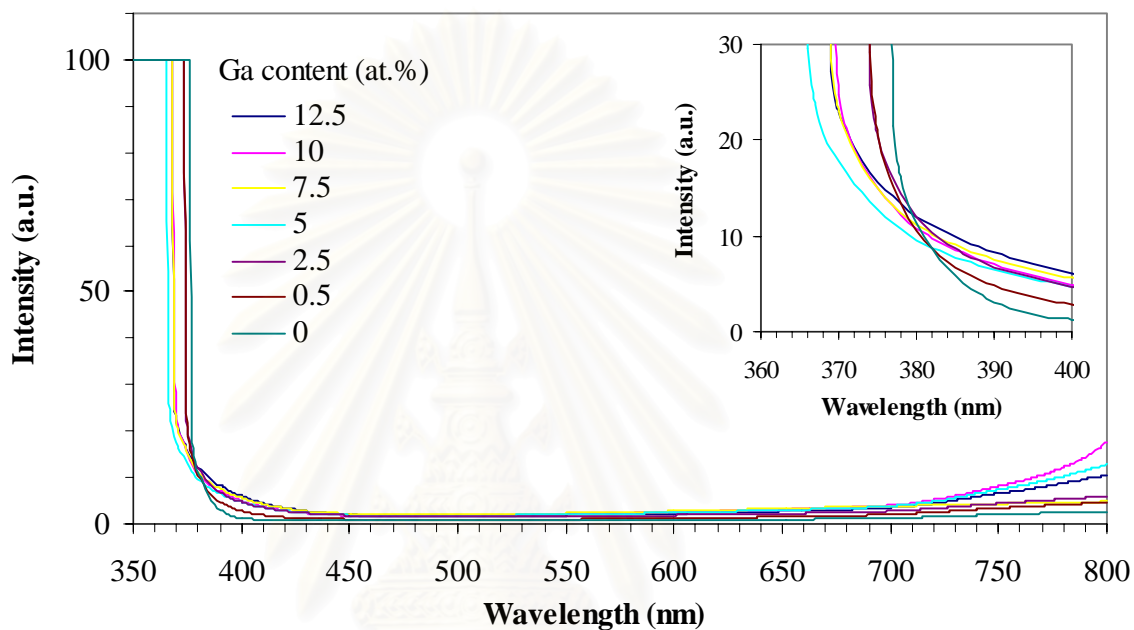


Figure 4.19 The absorption spectra of gallium-doped zinc oxide at metal content 0 to 12.5 at.%.

สถาบันวิทยบริการ
จุฬาลงกรณ์มหาวิทยาลัย

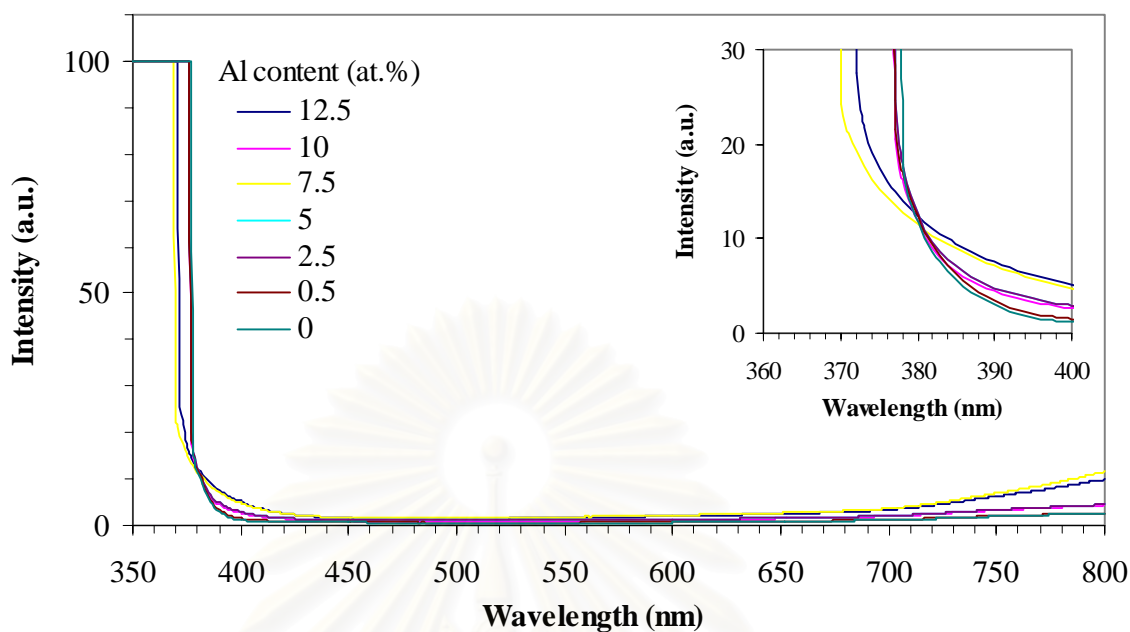


Figure 4.20 The absorption spectra of aluminium-doped zinc oxide at metal content 0 to 12.5 at.%.

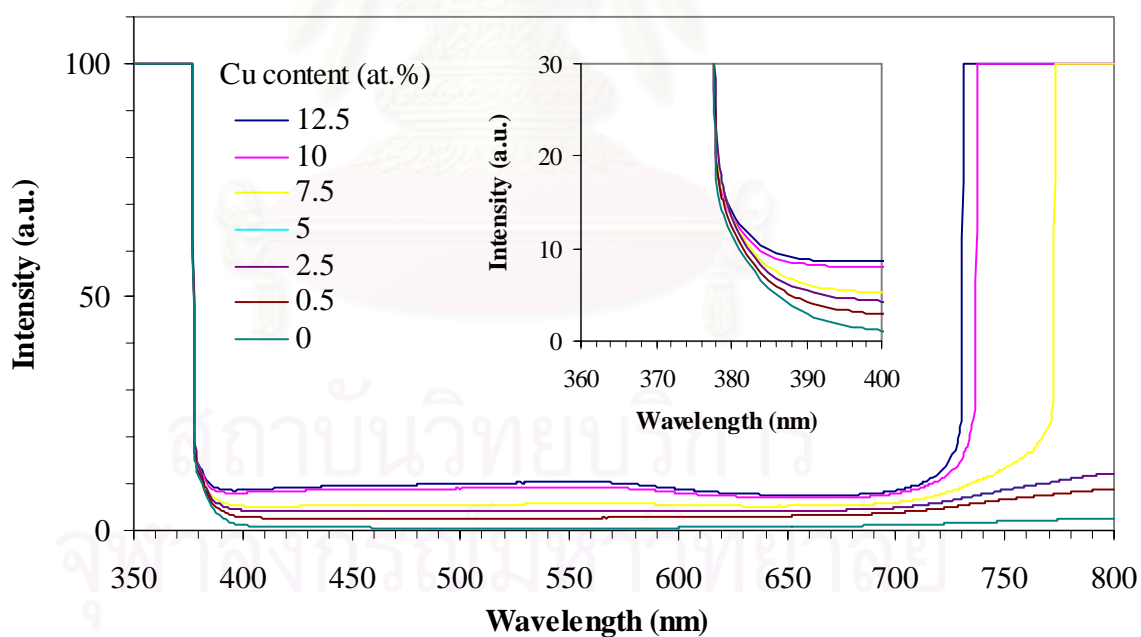


Figure 4.21 The absorption spectra of copper-doped zinc oxide at metal content 0 to 12.5 at.%.

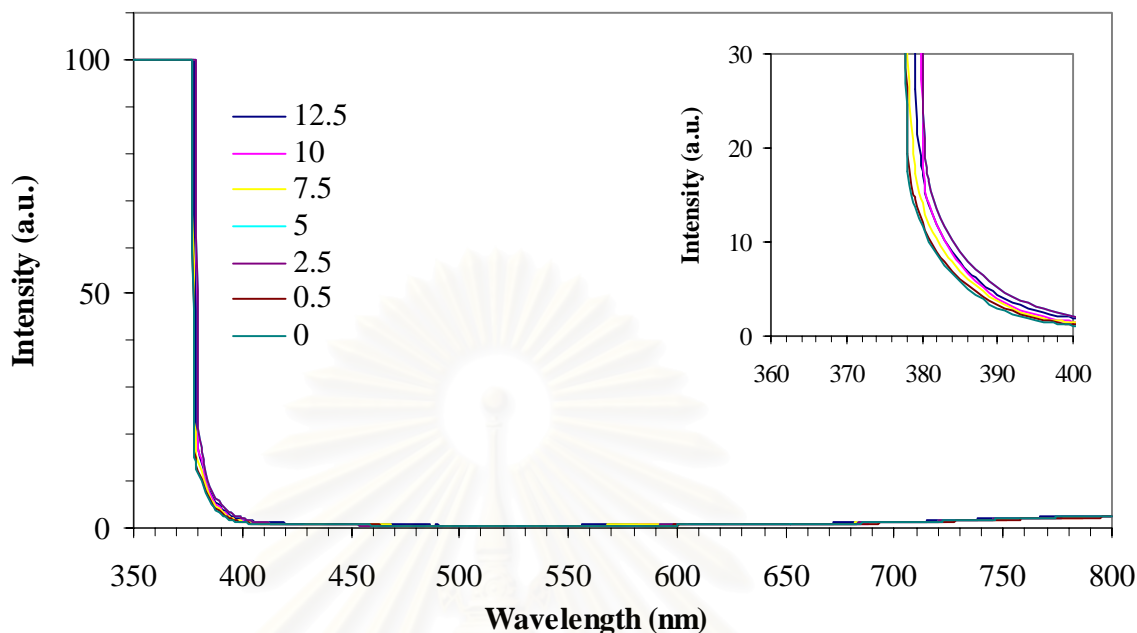


Figure 4.22 The absorption spectra of magnesium-doped zinc oxide at metal content 0 to 12.5 at.%.

The band gap energy of zinc oxide nanoparticles was estimated by using the relation $\nu = E_g/h$ where h is Planck constant (4.135×10^{-15} eV.s), ν is the frequency of photon at the absorption edge and E_g is the band gap energy [Omar, 1975]. The frequency, ν , is related with wavelength by the relationship $\nu = c/\lambda$ where c is the speed of light (3×10^{17} nm.sec⁻¹). To find the absorption edge, the wavelength where the absorbance becomes 50% of the maximum absorbance is selected and called $\lambda_{1/2}$. Then, $\lambda_{1/2}$ is replaced into the aforementioned equations to calculate the band gap energy. This method gives the result comparable to other studies and can reduce errors from the spectra with broad absorption edge [Madler et al., 2002]. The band gap energy of undoped and metal-doped zinc oxide are shown in Figure 4.23.

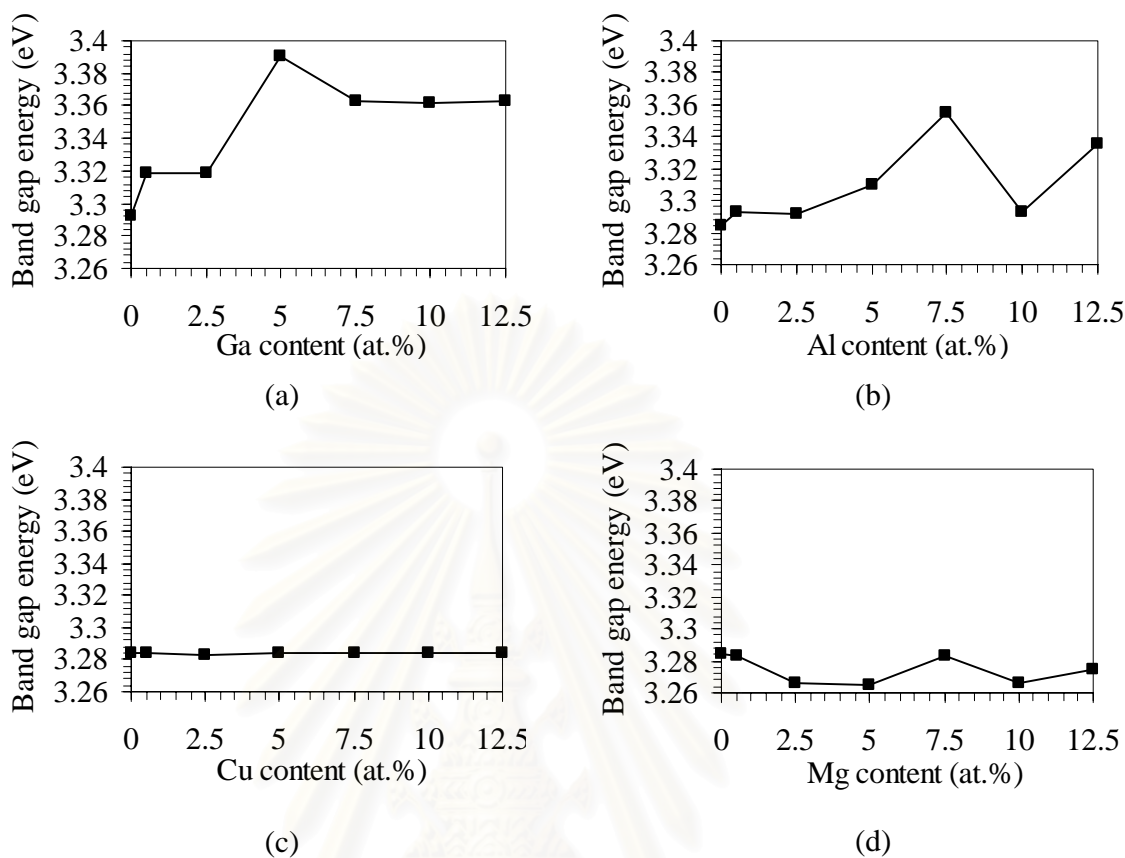


Figure 4.23 The band gap energy of (a) gallium-, (b) aluminium-, (c) copper- and (d) magnesium-doped zinc oxide with metal content in the range of 0 to 12.5 at.%

The band gap energy of undoped zinc oxide sample is 3.28 eV, which is close to the value reported in literature [Srikant et al., 1998]. After doping with gallium or aluminium, the band gap of the sample is increased. The band gap energy of gallium- and aluminium-doped zinc oxide samples are generally increased by increasing of the doping content and seems to level-off after the gallium and aluminium content is greater than 5 and 7.5 at.%, whereas the maximum band gap energy is 3.39 and 3.35 eV, respectively. According to XRD and morphology analyses, the samples with the largest band gap show poor crystallinity, but the particles are the most uniform in morphology. This result is in agreement with the earlier report that high crystallinity of the particles can cause the decrease in band gap energy [Weng et al., 2005].

For copper-doped zinc oxide, no change in the band gap energy was observed, regardless of the content of copper doping. From both of the lattice parameters and optical properties results, it can be concluded that, for the synthesis of copper-doped zinc oxide, small amount of copper ions are incorporated into zinc oxide structure, but it is not significant to affect the band gap energy. The exceeding copper ions are formed as metallic copper and copper (II) oxide outside zinc oxide particles. The results from inductively coupled plasma (ICP) analysis revealed that copper content in the remaining solvent after synthesis of 12.5 at.% copper-doped zinc oxide was very small (~7 mg) comparing to amount of copper in the precursor (765 mg).

The band gap energy of magnesium-doped zinc oxide is slightly decreased, comparing to that of undoped zinc oxide. Nevertheless, the change in band gap energy does not generally depend on the content of magnesium. This result opposes the finding in literature [Shan et al., 2004]. It is possible that the solvothermal method is not appropriate for synthesizing copper- and magnesium-doped zinc oxide. It has been reported that properties of zinc oxide including UV spectra, visible fluorescence spectra and band gap energy are sensitive to the preparation process [Zou et al., 2004]. Hsu et al. reported the synthesis of aluminium-, gallium- and indium-doped zinc oxide films by pulsed laser deposition method and found that gallium and indium doping were successful in increasing the band gap energy. However aluminium doping in zinc oxide seemed to be less effective in causing a blue shift in the band gap energy. Instead, a slight red shift is observed [Hsu et al., 2005].

4.2 Effect of Calcination Temperature

4.2.1 XRD analysis

This section investigates properties of the undoped and metal-doped zinc oxide, which was calcined at 300, 500 and 900°C in air flow. In this section, the content of doping for each metal was kept constant. For gallium and aluminium doping, the metal content of 5 at.% and 7.5 at.%, respectively, were selected because they resulted in the largest deviation in band gap energy from that of the undoped zinc oxide. For copper and magnesium doped zinc oxide, whereas the band gap energy does not significantly depend on doping content, the metal content of 7.5 at.% is also selected. Figure 4.24 – 4.27 show the XRD patterns of undoped and metal-doped zinc oxide after calcinations at various temperatures.

The diffraction peaks of all products can still be indexed to hexagonal structure of zinc oxide (JCPDS 36-1451). Nevertheless, the diffraction peaks of the calcined samples are slightly shifted from these of the as-prepared sample. For gallium- and aluminium-doped samples, although the as-synthesized samples show no sign of impurity in the XRD patterns (Figure 4.24a and 4.25a, respectively), signals for other crystalline phases are observed in the samples calcined at 900°C. They can be indexed as zinc gallate (ZnGa_2O_3) (JCPDS 38-1240) [Goncalves et al., 2006], for gallium-doped zinc oxide and zinc aluminate (ZnAl_2O_4) (JCPDS 03-1161) for aluminium-doped sample, respectively. The diffraction peaks of zinc aluminate can be clearly seen in the enlarged XRD pattern as shown in Figure 4.24b and 4.25b. The low intensity indicates the small amount of impurity. According to the literature, calcination of zinc oxide mixed with aluminium oxide at high temperature or gallium oxide can result in zinc gallate and zinc aluminate [Sampath et al., 1998].

In case of copper doping, since small amount of metallic copper is contaminated with zinc oxide even before the calcinations experiment. The intensity of copper decreases when the calcination temperature is increased. At calcination temperature of

500°C, the additional diffraction peaks can be observed at 2-Theta of 35.2° and 38.5° which can be indexed to $\bar{1}11$ and (111) plane of copper (II) oxide (CuO) (JCPDS 44-0706). The intensity of CuO increases with the calcination temperature, which is the result from oxidation of the contaminated copper. For magnesium-doped zinc oxide, no other crystalline phase was detected at all calcination temperatures.



สถาบันวิทยบริการ
จุฬาลงกรณ์มหาวิทยาลัย

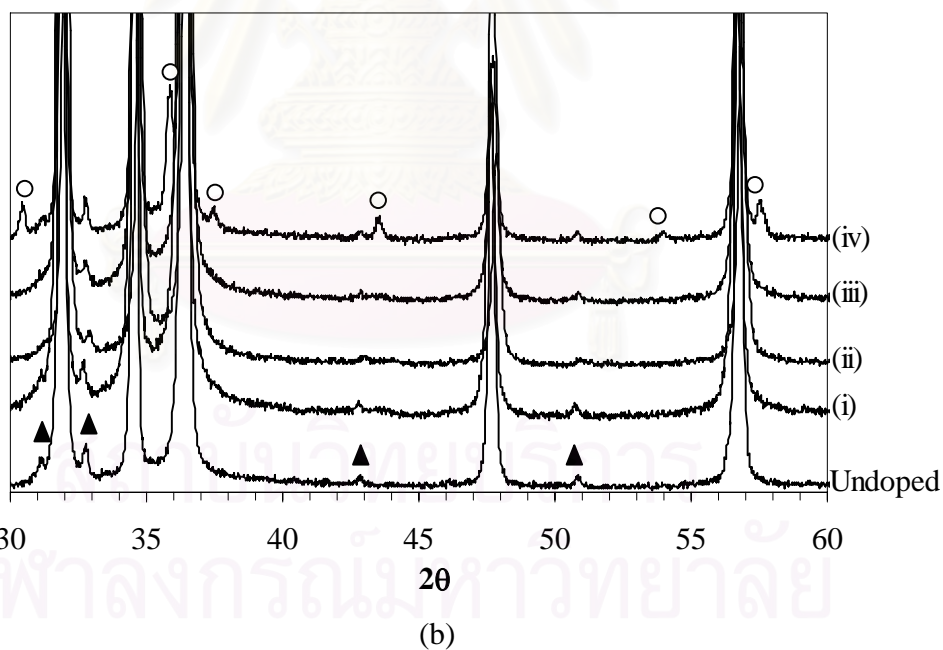
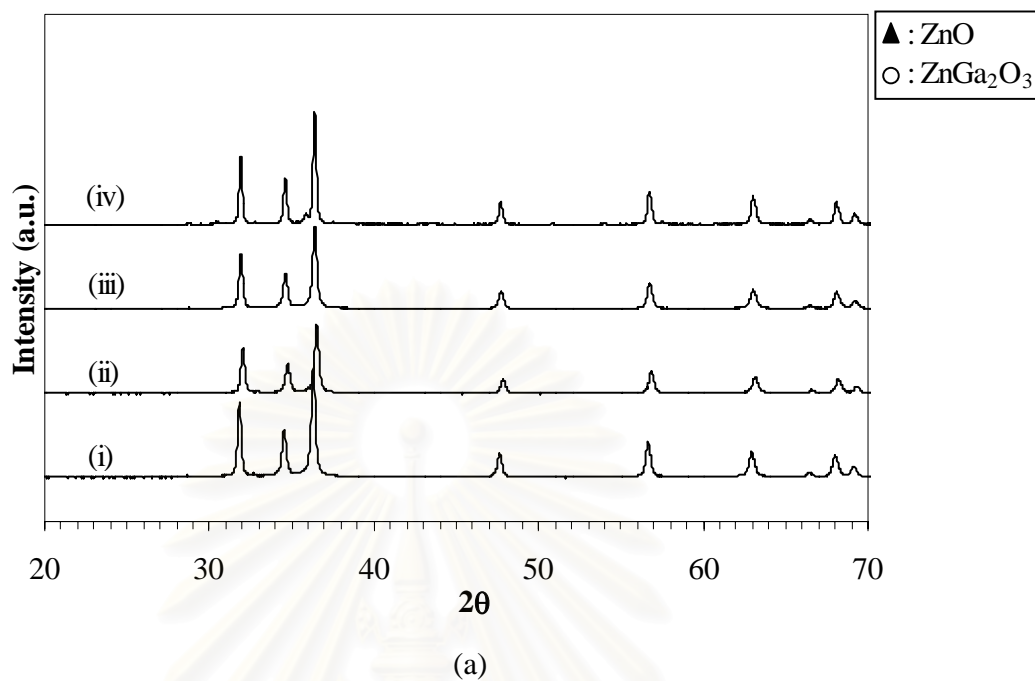
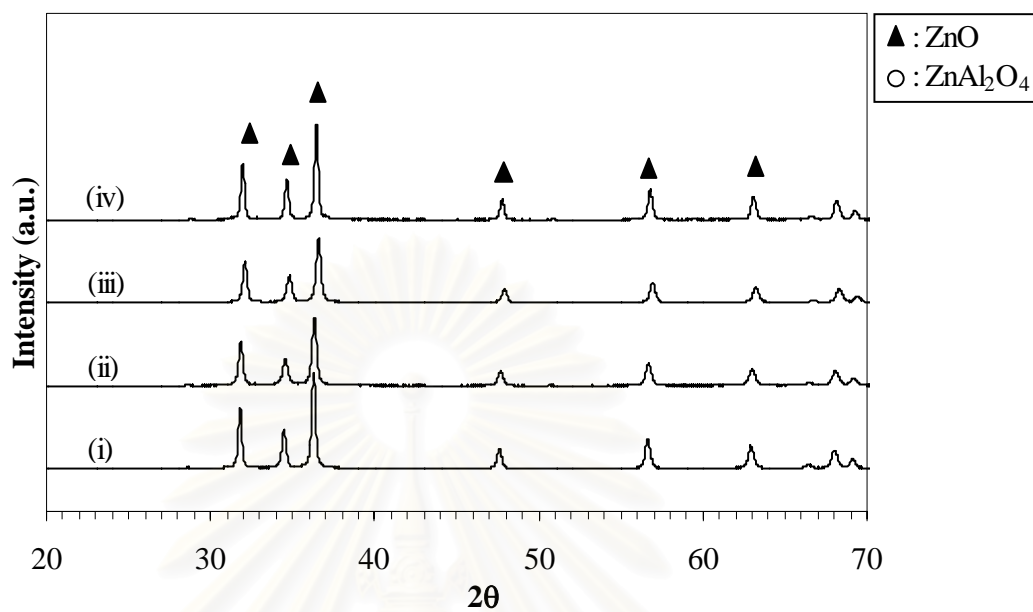
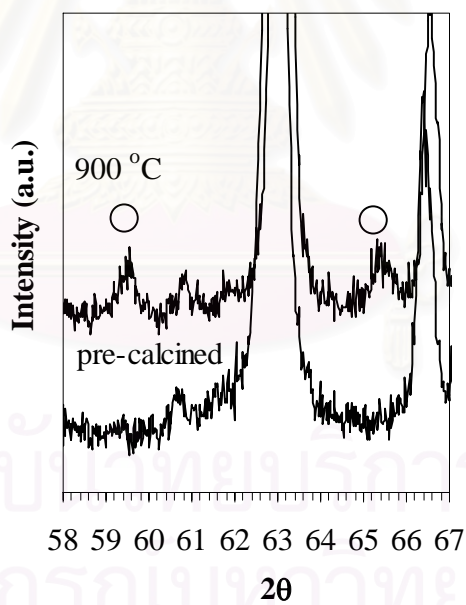


Figure 4.24 (a) The XRD patterns of 5 at.% gallium-doped zinc oxide:
 (i) pre-calcined and calcined at (ii) 300°C, (iii) 500°C and (iv) 900°C.
 (b) The enlarged XRD pattern of gallium-doped zinc oxide.



(a)



(b)

Figure 4.25 (a) The XRD patterns of 7.5 at.% aluminium-doped zinc oxide:
(i) pre-calcined and calcined at (ii) 300°C, (iii) 500°C and (iv) 900°C.
(b) The enlarged XRD pattern of aluminium-doped zinc oxide.

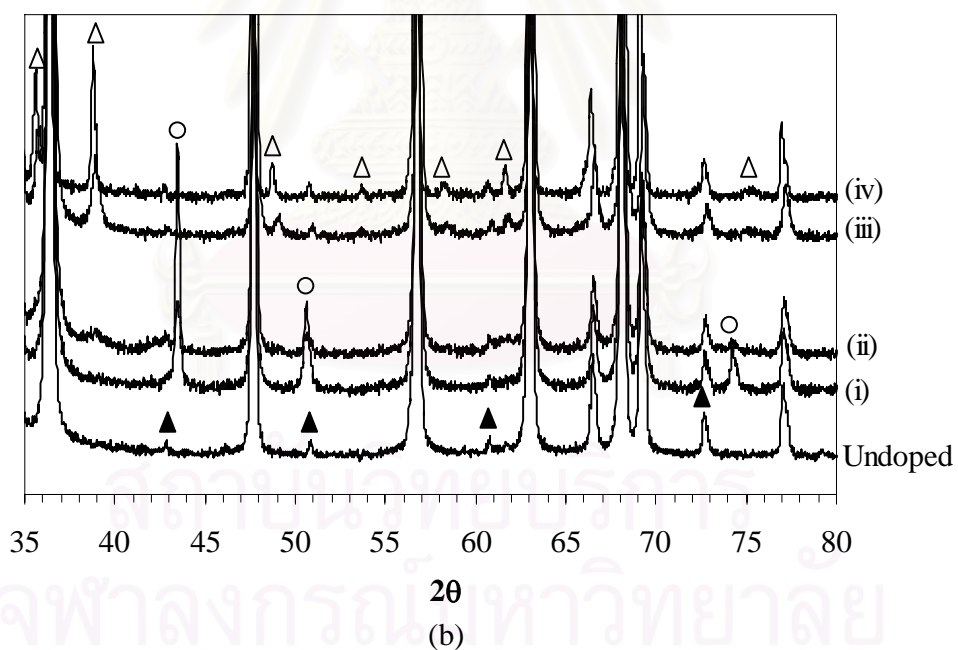
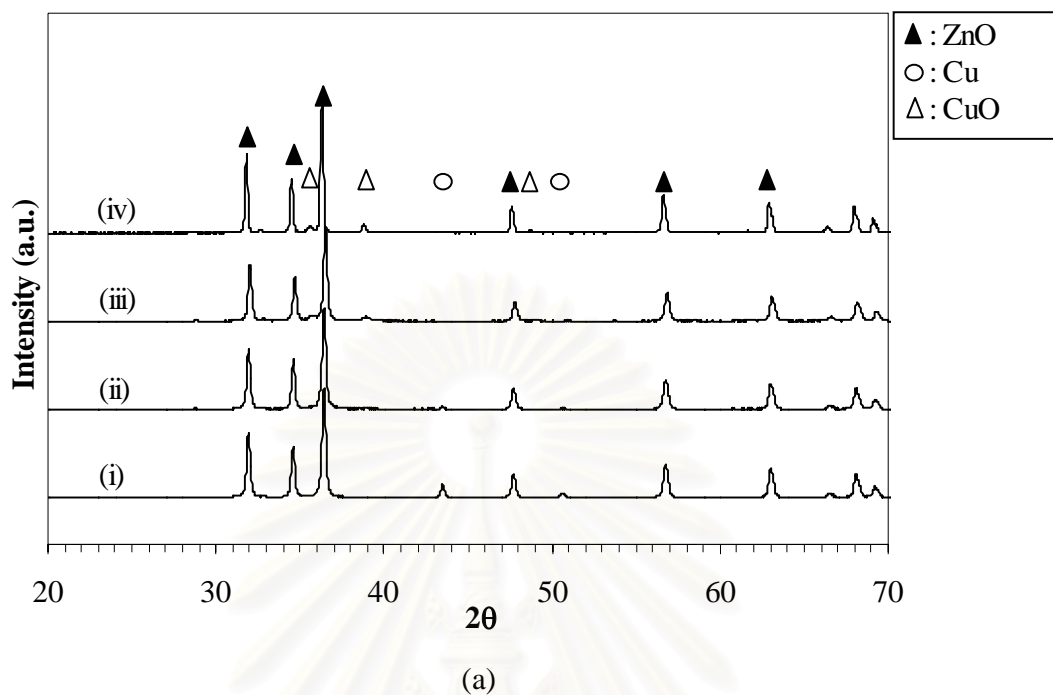


Figure 4.26 (a) The XRD patterns of 7.5 at.% copper-doped zinc oxide:
 (i) pre-calcined and calcined at (ii) 300°C, (iii) 500°C and (iv) 900°C.
 (b) The enlarged XRD pattern of copper-doped zinc oxide.

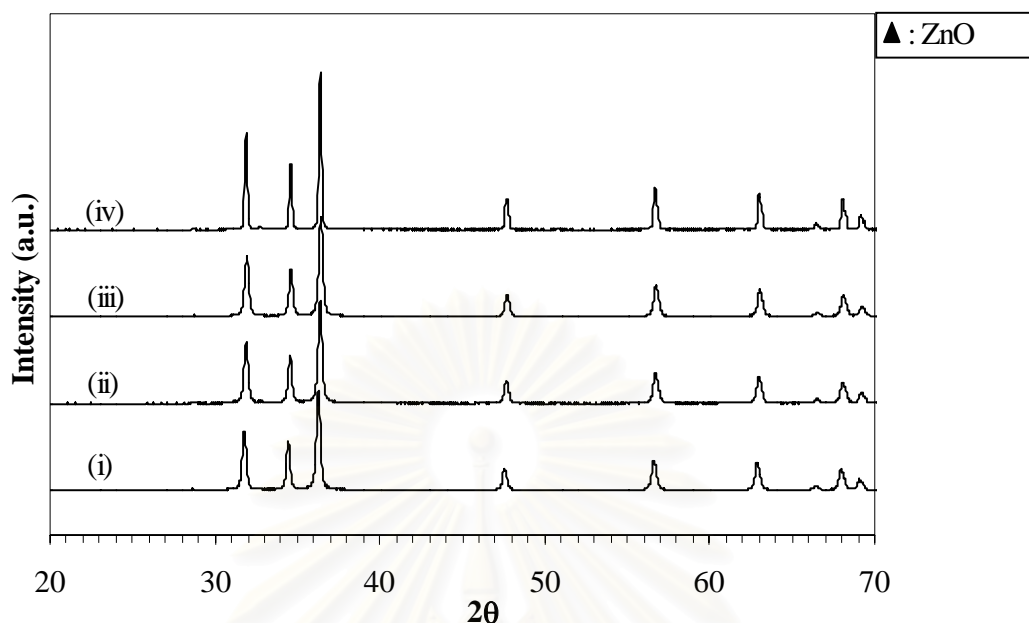


Figure 4.27 (a) The XRD patterns of 7.5 at.% magnesium-doped zinc oxide:
 (i) pre-calcined and calcined at (ii) 300°C , (iii) 500°C and (iv) 900°C .

4.2.2 Lattice parameters of calcined product

The effects of the calcination on lattice parameters are shown in Figure 4.28. It should be noted that the horizontal line in the Figure represents lattice constants, a and c , for undoped ($a = 3.2368 \text{ \AA}$ and $c = 5.201 \text{ \AA}$). All samples show slightly decrease in the lattice parameters when the calcination temperature is increased up to 500°C . Then, the lattice parameters are increased when the calcination temperature is higher than 500°C . For undoped zinc oxide, calcination in oxygen or ambient atmosphere provides oxygen to the sample resulting in the reduction of native point defects and the increases in lattice parameters after the calcination at high temperature has been reported in the literature [Phungphadung, 2001]. For metal-doped zinc oxide, calcination can drive the impurity ions into lattice sites [Georgobiani et al., 2004], resulting in the distortion of crystal structure.

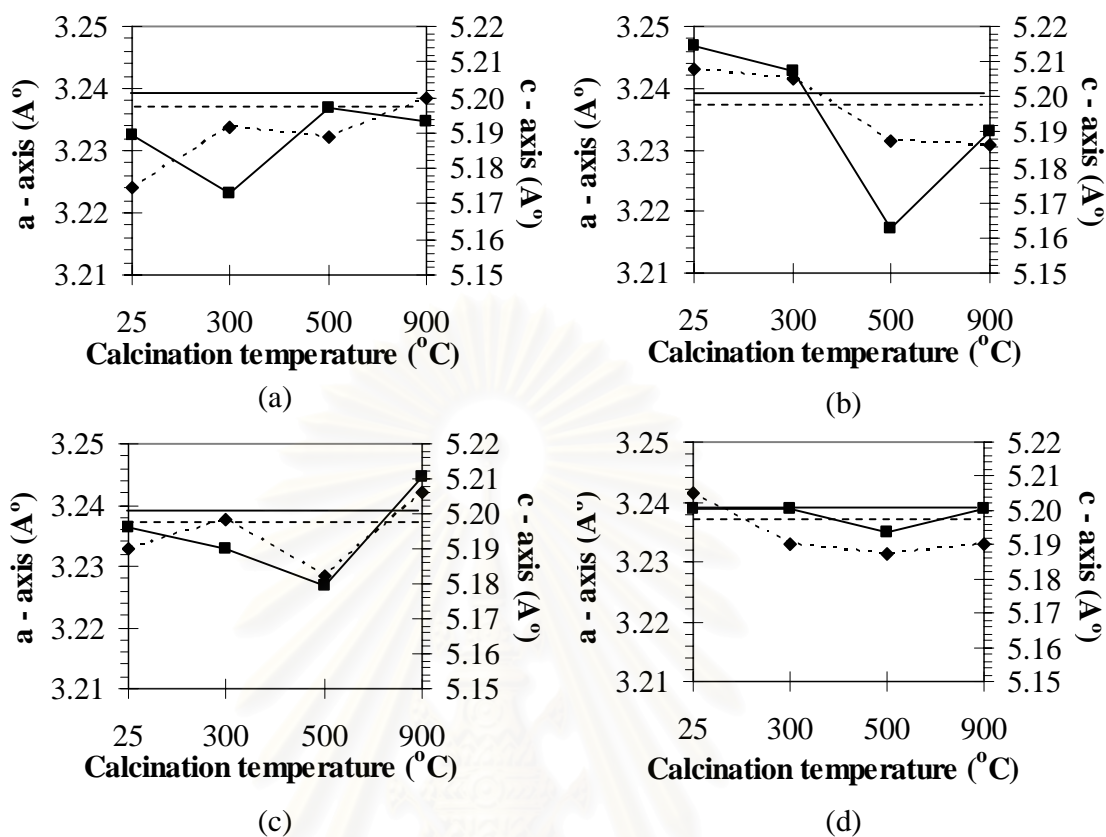


Figure 4.28 The lattice constants of (a) 5 at.% gallium-, (b) 7.5 at.% aluminium, (c) 7.5 at.% copper- and (d) 7.5 at.% magnesium-doped zinc oxide after calcination at various temperatures.: (—) a – axis, (---) c – axis.

4.2.3 Morphology of calcined product

The effects of the calcination on morphology are shown in Figure 4.29 – 4.32. After calcination at temperature of 300 and 500°C, morphology of all samples does not significantly change from the as-synthesized samples. When the calcination temperature is increased to 900°C, size of copper- and magnesium-doped zinc oxide particles increases dramatically. The same behavior has been reported for pure zinc oxide [Phungphadung, 2001]. On the other hand, the morphology of gallium- and aluminium-doped zinc oxide remains unchanged after calcination at high temperature because zinc

gallate and zinc aluminate have high thermal stability and can prevent sintering the particles [Aguilar-Ros et al., 1992].

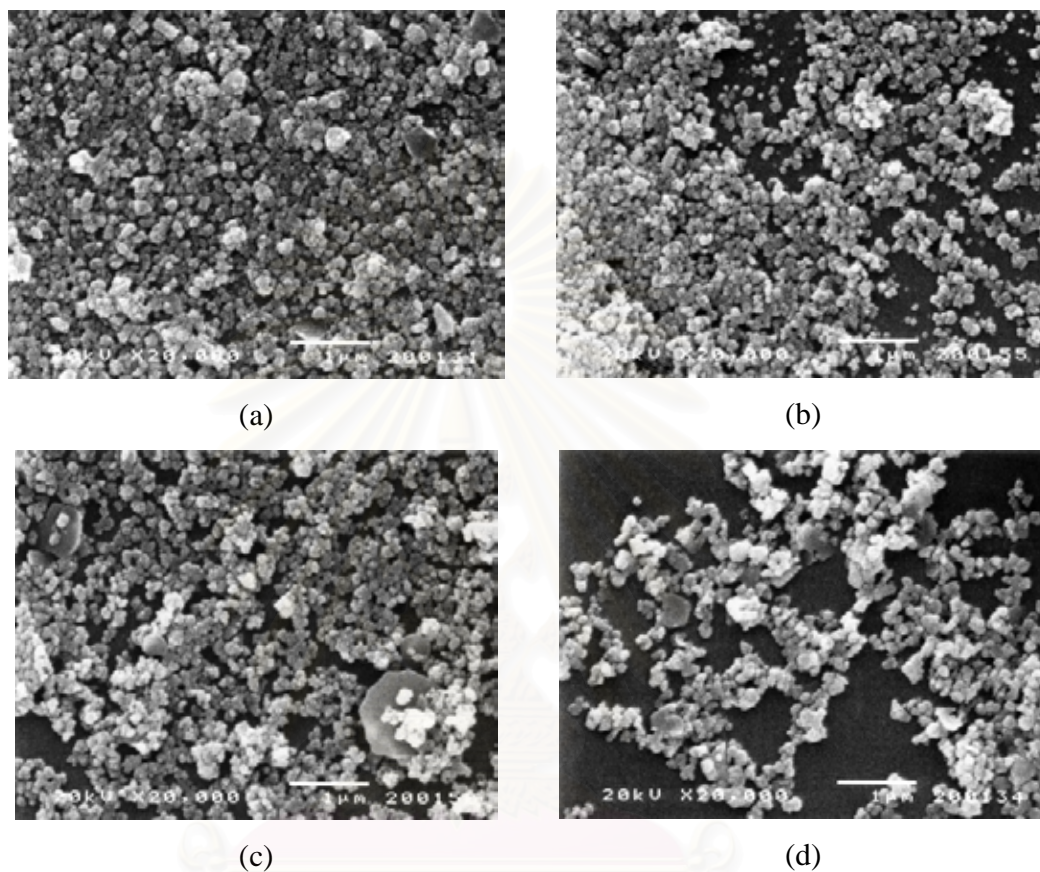


Figure 4.29 SEM micrographs of 5 at.% gallium-doped zinc oxide :
(a) pre-calcined and calcined at (b) 300°C, (c) 500 °C and (d) 900 °C.

สถาบันวิทยบริการ
จุฬาลงกรณ์มหาวิทยาลัย

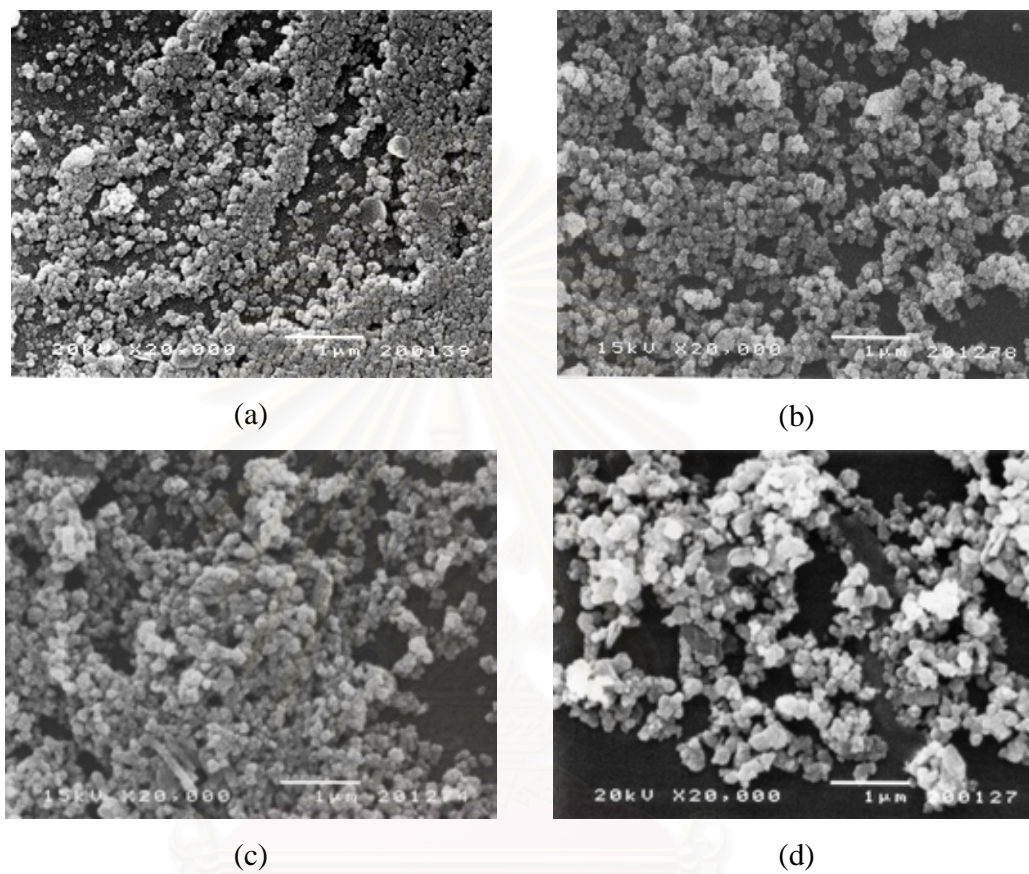


Figure 4.30 SEM micrographs of 7.5 at.% aluminium-doped zinc oxide :
(a) pre-calcined and calcined at (b) 300°C, (c) 500°C and (d) 900 °C.

สถาบันวิทยบริการ
จุฬาลงกรณ์มหาวิทยาลัย

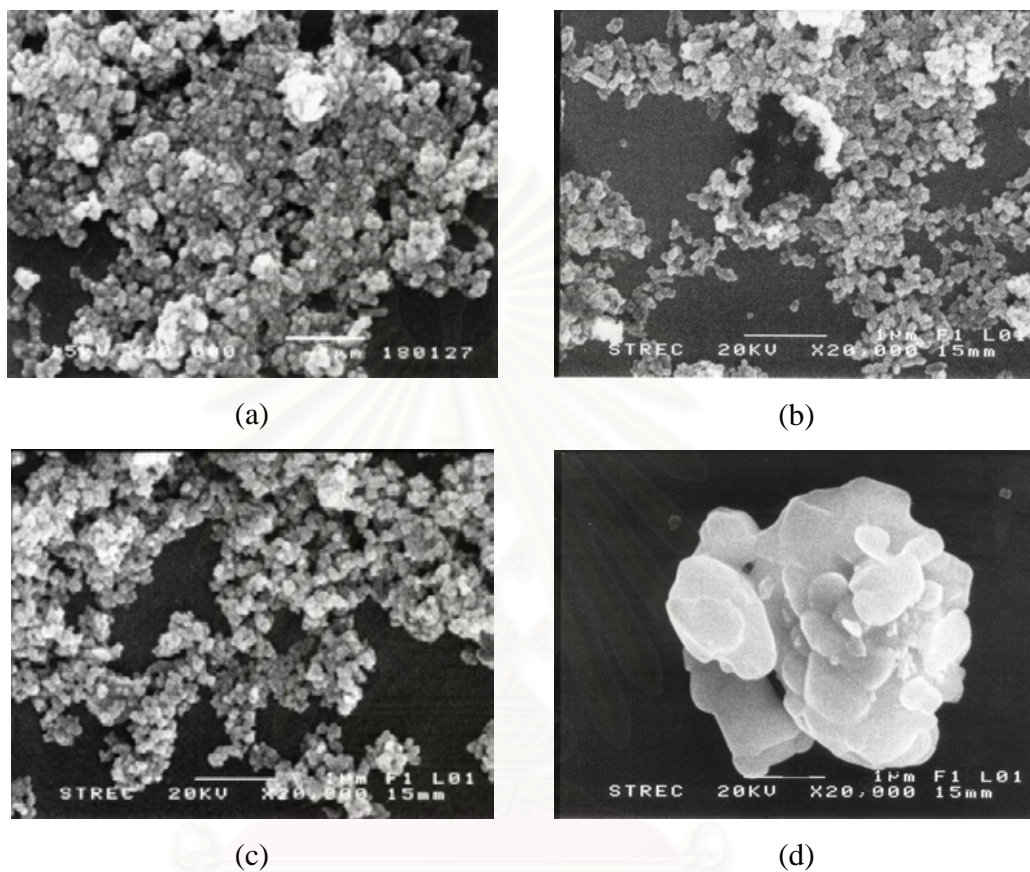


Figure 4.31 SEM micrographs of 7.5 at.% copper-doped zinc oxide :
(a) pre-calcined and calcined at (b) 300°C, (c) 500 °C and (d) 900 °C.

สถาบันวิทยบริการ
จุฬาลงกรณ์มหาวิทยาลัย

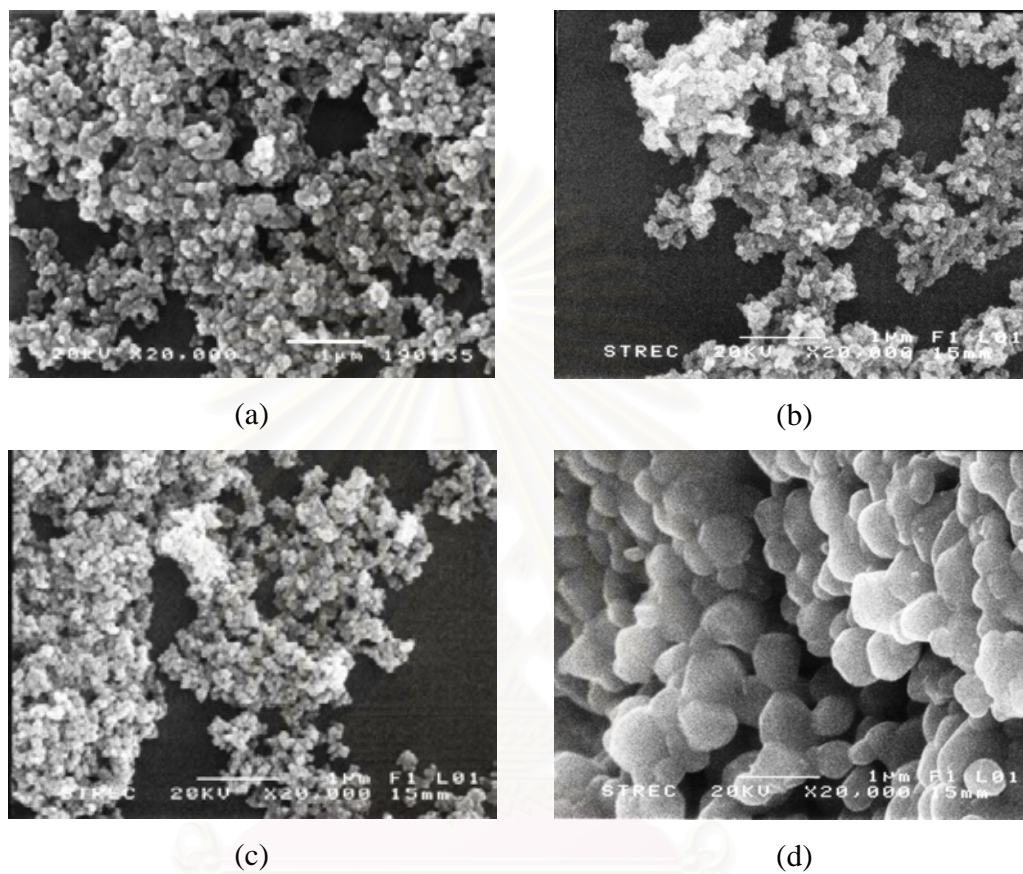


Figure 4.32 SEM micrographs of 7.5 at.% magnesium-doped zinc oxide :
(a) pre-calcined and calcined at (b) 300°C, (c) 500 °C and (d) 900 °C.

สถาบันวิทยบริการ
จุฬาลงกรณ์มหาวิทยาลัย

4.2.4 Optical properties of calcined product

Figure 4.33 - 4.36 show the absorption spectra of some metal-doped samples used in section 4.2.1 – 4.2.3. The absorption edges of gallium- and aluminium-doped zinc oxide show red shifts after the samples are calcined at 300 and 500°C and show slightly blue shifts after calcined at 900°C. For copper-doped zinc oxide, the absorption edges of zinc oxide do not change until the calcination temperature is higher than 500°C. The absorption in the range below 580 nm has been reported to correspond to the absorption of copper (I) oxide (Cu_2O) (~2.1 eV) [Richardson et al., 2003]. The XRD analysis can not detect the diffraction peak of copper (I) oxide because the amount of copper (I) oxide is much less than that of zinc oxide, metallic copper and copper (II) oxide. Moreover, the main diffraction peak for (111) plane of copper (I) oxide locates at 36.5° (JCPDS 03-0892), which is in the proximity of (101) diffraction peak of zinc oxide. For magnesium, interestingly, the samples doped with magnesium show blue shift with the increase in the calcination temperature, although magnesium-doping initially results in red shift.

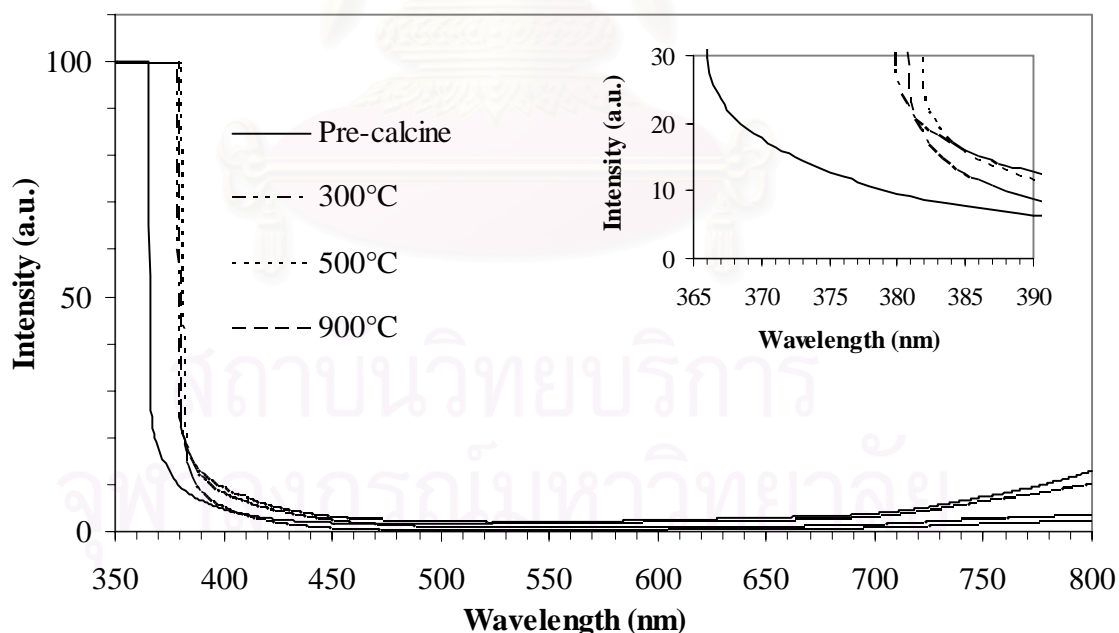


Figure 4.33 The absorption spectra of 5 at.% gallium-doped zinc oxide after calcination at various temperatures.

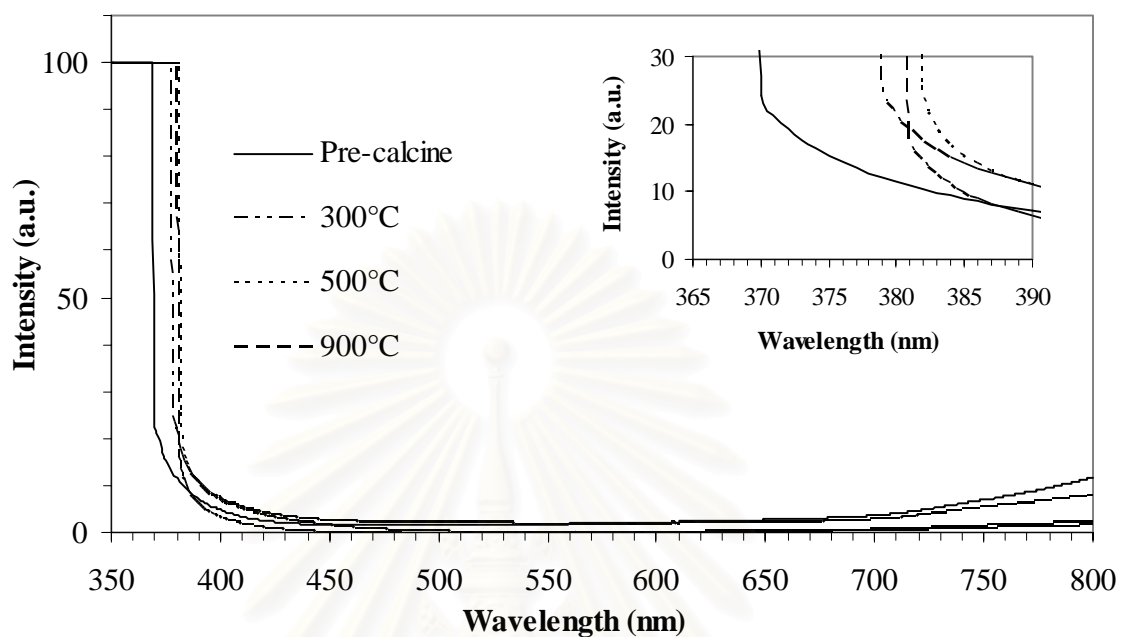


Figure 4.34 The absorption spectra of 7.5 at.% aluminium-doped zinc oxide after calcination at various temperatures.

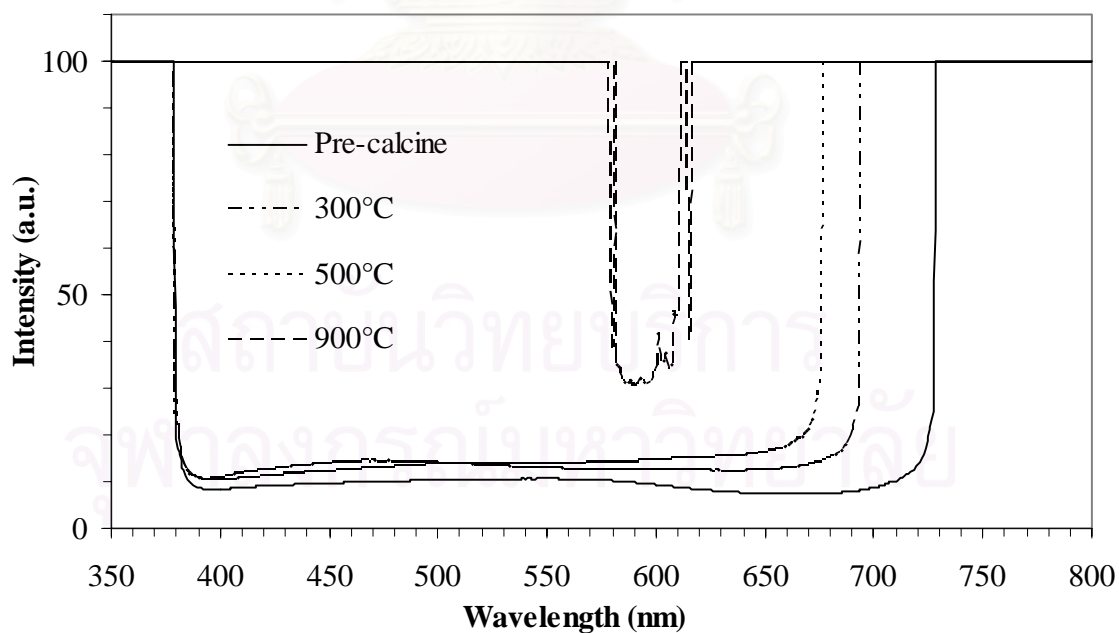


Figure 4.35 The absorption spectra of 7.5 at.% copper-doped zinc oxide after calcination at various temperatures.

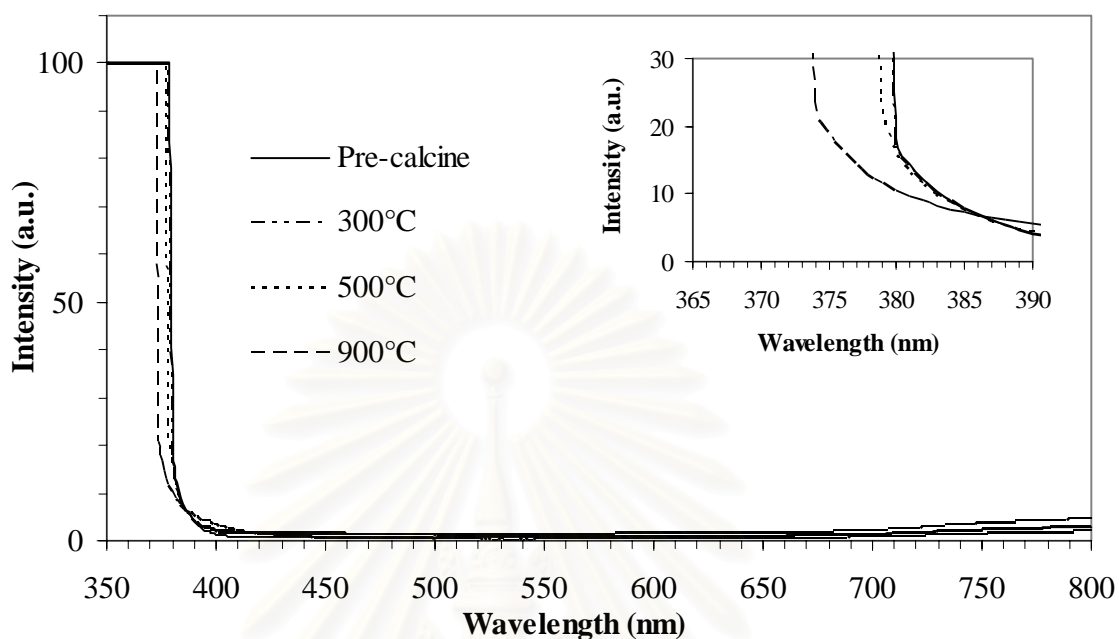


Figure 4.36 The absorption spectra of 7.5 at.% magnesium-doped zinc oxide after calcination at various temperatures.

Figure 4.37 shows the band gap energy of the metal-doped zinc oxide after calcination at various temperatures. The trends of the band gap energy with respect to the change in calcinations temperature for gallium- and aluminium-doped zinc oxide are the same. At calcination temperature lower than 500°C , the band gap energy of both samples decreases with an increase in temperature. The effect of calcination temperature on the band gap energy of gallium- and aluminium-doped zinc oxide becomes insignificant at temperature higher than 500°C . It is possible that the dopant ions in zinc oxide structure could be rearranged during the calcinations at high temperature in air. Lin and coworkers (2004) studied properties of aluminium-doped zinc oxide films before and after annealing in the different atmospheres. They observed that the annealing in air decreased the band gap energy due to the enhanced chemisorption of oxygen, and the formation of AlO_x that reduced the impurity in zinc oxide structure [Lin et al., 2004]. Moreover, from XRD analysis, it can clearly observe that zinc gallate and zinc aluminate are contained in products after calcinations at 900°C . the formation of zinc gallate results in the red-shift

in the emission spectra of gallium-doped zinc oxide [Goncalves et al., 2006]. In the addition, as reported in section 4.1.2, high content of gallium and aluminium doping causes an increase in the lattice parameters. As witnessed from the XRD analysis, high temperature calcinations causes the formation of zinc gallate and zinc aluminate by driving gallium or aluminium atoms into zinc oxide structure. This affects the lattice parameters of the crystal after the reformation. Furthermore, the lacks of dopant ions are the cause of the decreased band gap energy.

For copper-doped zinc oxide, the band gap energy is not changed by calcination. The absorption edge of zinc oxide can be observed as long as long as the calcination temperature below 500°C. At temperature higher than 500°C, the absorption edge of the sample shifts to about ~580 nm that is the absorption wavelength of copper (I) oxide. Therefore, the band gap energy, corresponding to zinc oxide for the sample calcined at 900°C can not be calculated. This result confirms that, even after the calcinations, the synthesis of copper-doped zinc oxide may not be feasible by solvothermal method.

Magnesium-doped zinc oxide is the only sample investigated that shows the increase of the band gap energy with the increase in calcination temperature. The reason for this behavior is that zinc oxide is alloyed with magnesium oxide. Then, the band gap of the ternary alloys, $Mg_xZn_{1-x}O$, can be expanded from 3.3 to 4.20 eV [Minemoto et al., 2000; Narayan et al., 2001; Ohtomo et al., 1999; Sharma et al., 1999]. According to literatures, which studied thermal stability of wurtzite-phase $Mg_xZn_{1-x}O$ alloy and $ZnO/Mg_xZn_{1-x}O$, the thermal diffusion of magnesium across the $Mg_xZn_{1-x}O/ZnO$ interface was observed only after annealing above 700°C [Ohtomo et al., 1999]. Therefore, in this work, $Mg_xZn_{1-x}O$ could be formed by the calcination at 900°C of zinc oxide and magnesium on the zinc oxide surface.

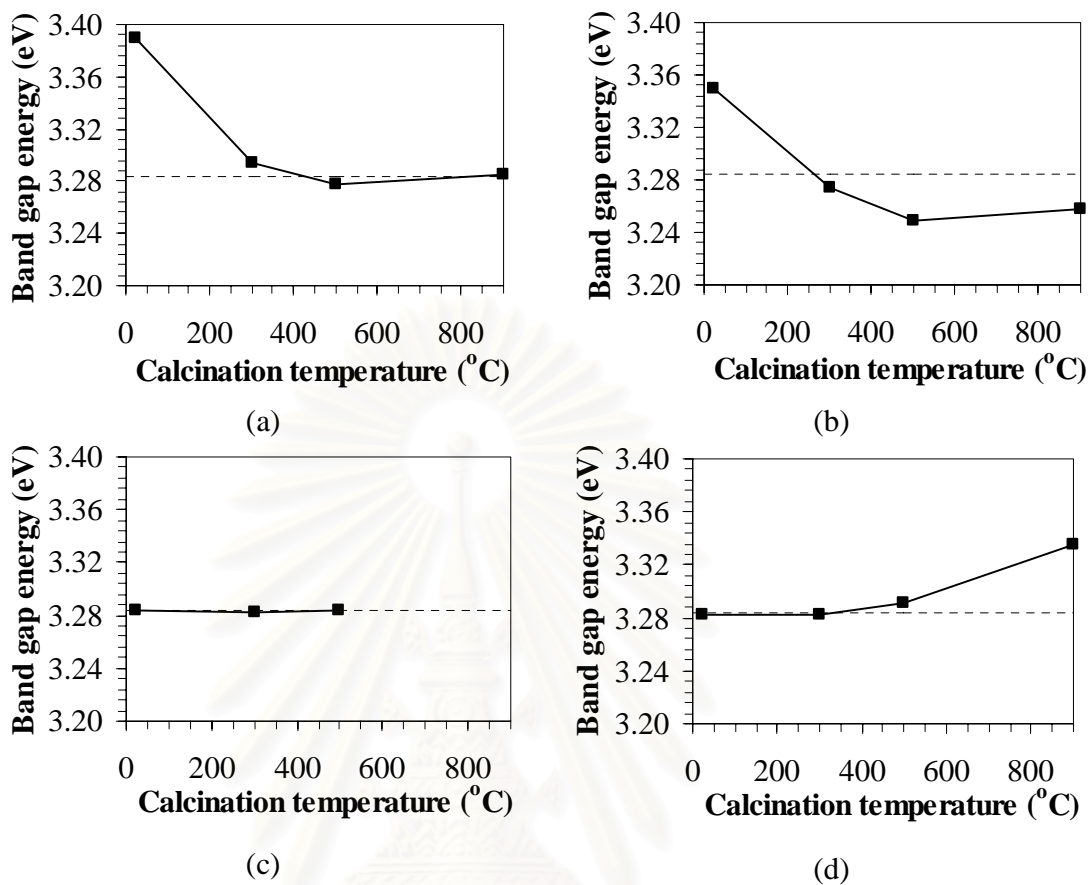


Figure 4.37 The band gap energy of (a) 5 at.% gallium-, (b) 7.5 at.% aluminium-, (c) 7.5 at.% copper-and (d) 7.5 at.% magnesium-doped zinc oxide, calcined at various temperatures.: (---) The band gap energy of undoped zinc oxide.

สถาบันวิทยบริการ
จุฬาลงกรณ์มหาวิทยาลัย

4.3 Photocatalytic Activity

Photocatalytic activity of the synthesized metal-doped zinc oxide was evaluated from the degradation of methylene blue (MB) under UV and solar light irradiation. Activity of undoped and metal-doped zinc oxide particles was investigated in powder form suspending in MB solution. The system was kept in the dark for 1 h to before UV light irradiation minimize the effect of MB absorption. Self degradation of MB without catalysts was also monitored and found that it is much slower than photocatalytic degradation of MB on the synthesized.

The decomposition of MB by using zinc oxide synthesized in this research under UV and solar radiation are shown in Figure 4.38 and 4.39, respectively. The doping content of 5 at.% was selected for gallium, while 7.5 at.% was selected for aluminium, copper and magnesium, because they resulted in maximum deviation in band gap energy from that of undoped zinc oxide. After 6 h, the MB decomposition under UV and solar radiation from undoped zinc oxide was slightly greater than that from the metal-doped zinc oxide. Under UV irradiation, copper-doped zinc oxide showed inferior decomposition, comparing to other samples. Table 4.2 shows BET surface area, band gap energy and absorption edge of zinc oxide used in this experiment, rearranging according to the level of MB decomposition after 6 h. It can be indicated that the surface area is not the major factor affecting the extent of decomposition. High surface area of aluminium- and magnesium-doped zinc oxide is expected to be the results from impurity, e.g. alumina or magnesium oxide, in the sample [Shimada et al., 1988; Xie et al., 1999].

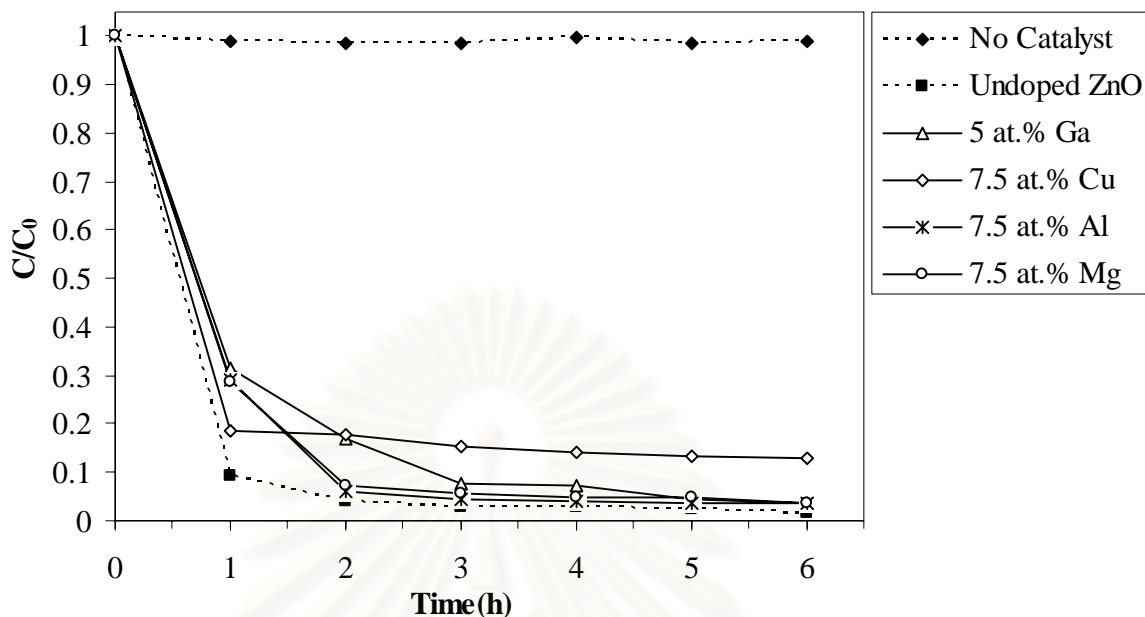


Figure 4.38 Photocatalytic degradation of methylene blue solution, using metal-doped zinc oxide particles under UV irradiation.

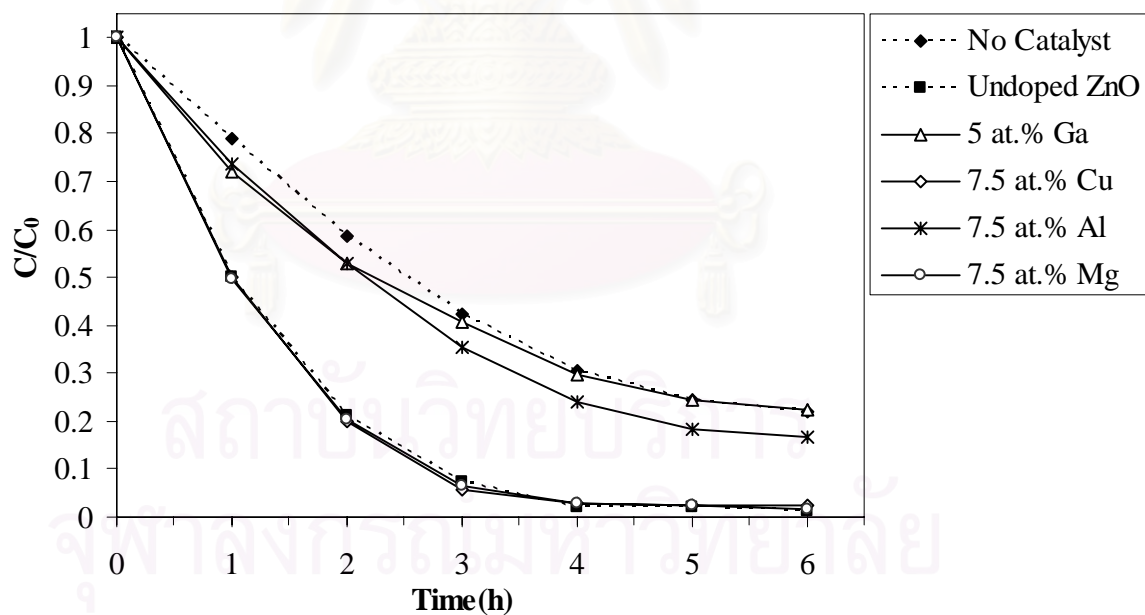


Figure 4.39 Photocatalytic degradation of methylene blue solution, using metal-doped zinc oxide particles under solar irradiation.

Table 4.2 Properties of photocatalysts employed in the photocatalytic degradation experiments.

<i>C/C_o for 6 h MB decomposition</i>		<i>Photocatalyst</i>	<i>BET surface area (m²/g)</i>	<i>E_g (eV)</i>	<i>Absorption edge (nm)</i>
<i>UV</i>	<i>Solar</i>				
0.0163	0.0124	Undoped zinc oxide	5.58	3.28	378
0.0346	0.0146	7.5 at%. Mg-doped ZnO	15.0569	3.28	378
0.1310	0.0244	7.5 at%. Cu-doped ZnO	5.4135	3.28	378
0.0379	0.1676	7.5 at%. Al-doped ZnO	16.7711	3.35	370
0.0382	0.2225	5 at%. Ga-doped ZnO	7.0901	3.39	366

It can be observed from Table 4.2 that the extent of MB decomposition depends upon the band gap energy. Undoped, copper- and magnesium-doped zinc oxide, which have the same band gap energy, show relatively the same photocatalytic activity. For aluminium- and gallium-doped zinc oxide, their increased band gap energy results in lower photocatalytic activity than other samples. This behavior could be discussed by the energy absorption. According to the relationship between intensity and wavelength of emitted light of the UV lamps (Philip, TL'D 15w/05) as shown in Figure 4.40, the lamps emit radiation between 300 to 460 nm with maximum peak at 360 nm. It is known that zinc oxide is the photocatalyst that can absorb light with wavelength equal to or shorter than the absorption edge. The metal doping resulted in the increased band gap energy or decreased absorption edge. Therefore, under the same spectrum of incident light, the fraction of light absorbed by the wide-band gap energy material should be less than that absorbed by the narrow-band gap energy material. Lin and coworkers (2005) explained the key for improved photocatalytic efficiency for many practical applications that photocatalyst such as zinc oxide should absorb not only UV but also visible light due to the fact that visible light accounts for 45% of energy in the solar radiation while UV light accounts for less than 10%. In order to absorb visible light, band gap of zinc oxide has to be narrowed [Lin et al., 2005]. Dash lines in Figure 4.40 represent the absorption spectra

of undoped and metal-doped zinc oxide. It is observed that high fraction of light absorbed leads to high activity in MB decomposition, as shown in Table 4.2.

For the photocatalytic reaction with copper-doped zinc oxide under UV irradiation, the low activity may be the results from impurities, i.e. metallic copper, mixed with the copper-doped zinc oxide. Since metallic copper is not the photocatalyst, it retards the overall photocatalytic activity of the catalyst and causes poor decomposition of MB.

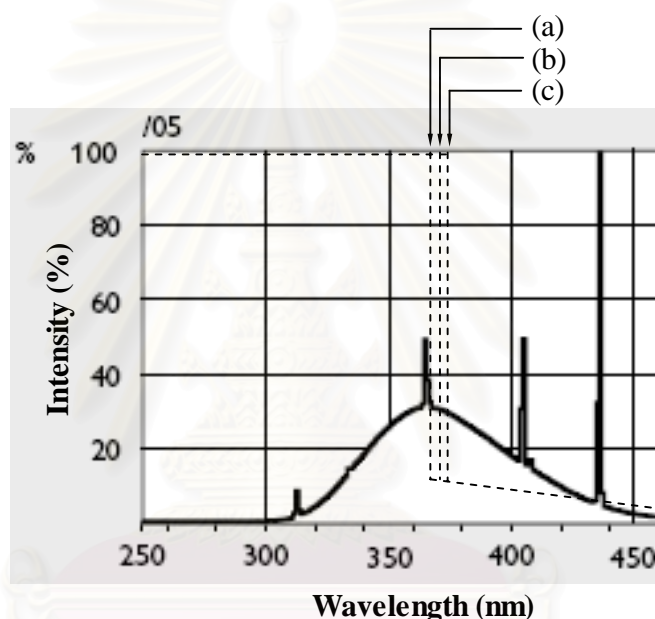


Figure 4.40 Spectral power distribution of the UV lamps employed in this research and absorption spectra of: (a) 5 at.% gallium-doped zinc oxide, (b) 7.5 at.% aluminium-doped zinc oxide and (c) undoped, 7.5 at.% copper-doped and 7.5 at.% magnesium-doped zinc oxide.

The MB decomposition under UV and solar radiation, using gallium-doped zinc oxide with various gallium contents, are shown in Figure 4.41 and 4.42, respectively. According to the prior section, the band gap energy of undoped, 0.5, 5 and 12.5 at.% gallium-doped zinc oxide are 3.28, 3.318, 3.39 and 3.362 eV, respectively. After 6 h of the reaction under UV light, the levels of decomposition from undoped, 0.5 at.% doped and 5 at.% doped zinc oxide were roughly the same. On the other hand, the

decomposition rate achieved from 12.5 at.% gallium-doped zinc oxide was very poor because the excess gallium on the surface of zinc oxide obstructed the reaction. For undoped, 0.5 and 5 at.% gallium-doped zinc oxide, the trend in the extent of MB decomposition followed the trend in the band gap energy as discussed in the previous paragraph.

Similar trend was also observed when solar radiation was employed as energy source. Nevertheless, the decomposition rate of 5 at.% gallium-doped zinc oxide was very close to the self-oxidation of MB. This result indicated the low intensity of ultraviolet radiation at the wavelength below 365 nm. This observation was supported by the fact that the rate of photocatalytic decomposition on undoped zinc oxide under solar radiation was also slower than that under the UV lamps.

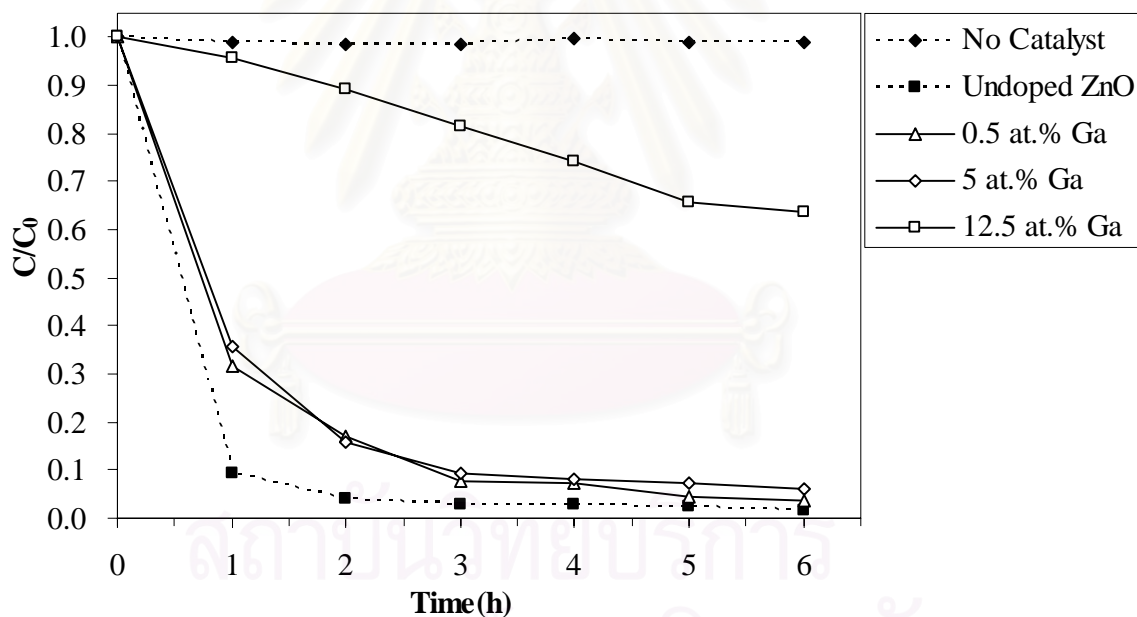


Figure 4.41 Photocatalytic degradation of methylene blue solution on zinc oxide doped with various contents of gallium under UV irradiation.

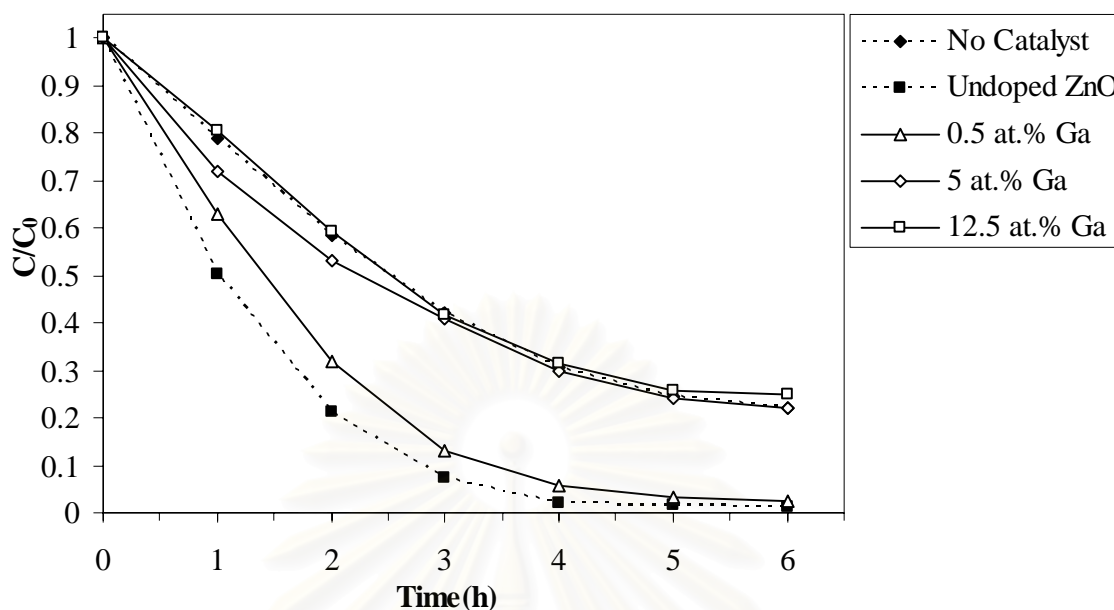


Figure 4.42 Photocatalytic degradation of methylene blue solution on zinc oxide doped with various contents of gallium under solar irradiation.

The effects of calcination on the MB decomposition of gallium-doped zinc oxide, under UV and solar radiation are shown in Figure 4.43 and 4.44, respectively. In this part of the experiment, the content of gallium in zinc oxide was fixed at 5 at.%. It should be noted that the band gap energy of gallium-doped zinc oxide before calcined and after calcined at 300, 500 and 900°C are 3.39, 3.29, 3.27 and 3.28 eV, respectively. After calcination, the photocatalytic activity of gallium-doped zinc oxide decreased dramatically (as seen from Figure 4.43). This behavior can not be explained in this work. However, the activity was improved by increasing the calcinations temperature. Since high temperature calcination can improve crystallinity of zinc oxide, it consequently improve the activity of the catalyst because high crystallinity can reduce the recombination of photogenerated electron-hole pairs [Klongdee et al., 2005].

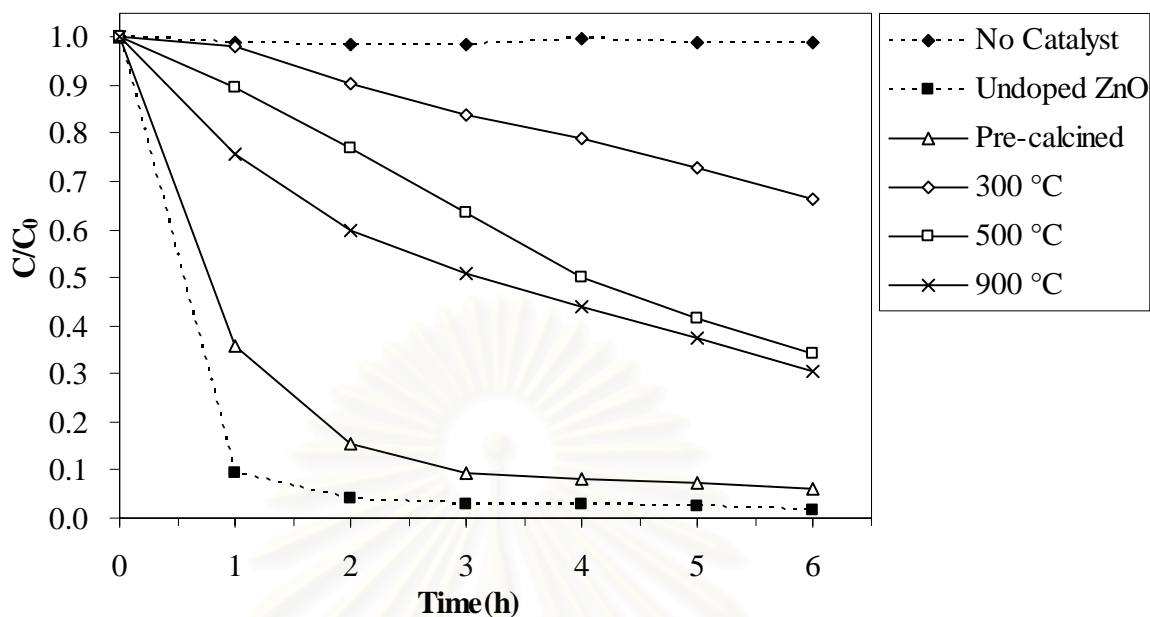


Figure 4.43 Photocatalytic degradation of methylene blue solution under UV irradiation on undoped and gallium-doped zinc oxide that has been calcined at various temperatures.

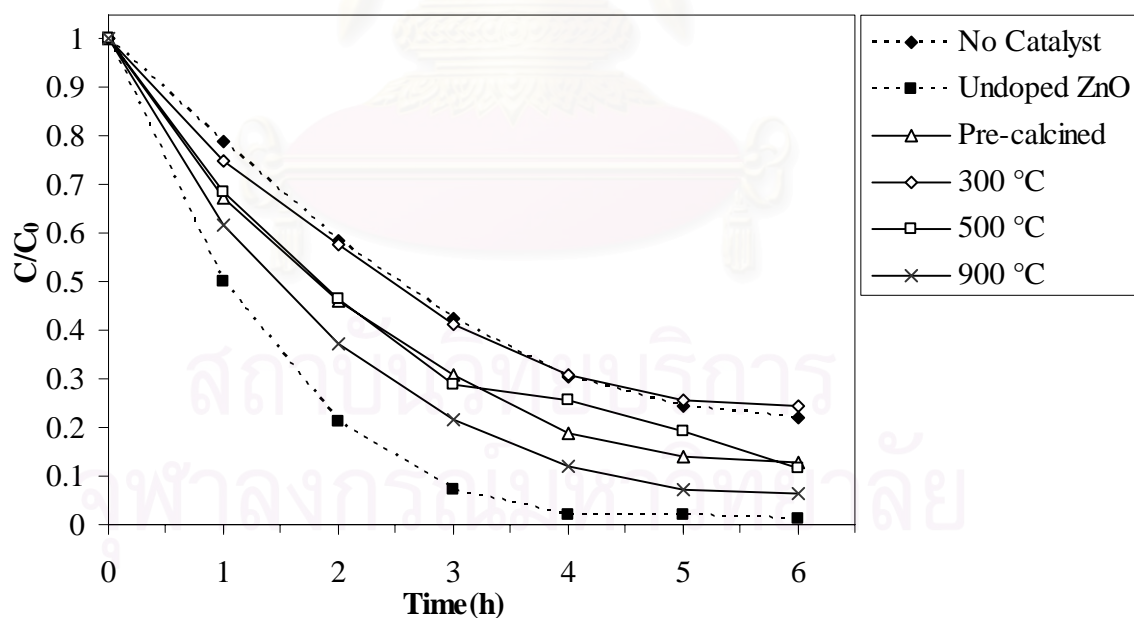


Figure 4.44 Photocatalytic degradation of methylene blue solution under solar irradiation on undoped and gallium-doped zinc oxide that has been calcined at various temperatures.

4.4 Photoluminescence Analysis

In the previous section, the band gap energy was determined from excitation energy. On the contrary, this section studied the band gap energy from emission of photons from the excited zinc oxide. The same metal contents as these in the previous section were also selected in this section. Table 2 compares the band gap energy determined from UV-Vis spectroscopy and Photoluminescence spectroscopy. Figure 4.38 and 4.39 show photoluminescence spectrum of undoped and metal-doped zinc oxide plotted in term wavelength (nm) and energy (eV), respectively. Undoped zinc oxide exhibited sharp UV emission peak at 387 nm which is commonly attributed to the radiative annihilation of excitons. Several weak emission peaks indicated the presence of structural defects in the crystal [Zu et al., 1997; Bagnall et al., 1998]. For instance, the peaks in green region (480-530 nm) have been reported to be the result from oxygen vacancy in zinc oxide [Wang et al., 2006].

The UV emission ($\lambda = 387$) of undoped zinc oxide was shifted by gallium and magnesium doping. Gallium- and magnesium-doped zinc oxide showed blue-shift and red-shift, respectively. Table 2 shows that the band gap energy determined from excitation (UV-Vis) and from emission (Photoluminescence), for undoped, gallium- and magnesium-doped samples, are relatively close together. Therefore, the UV emission is attributed to the near band edge emission from the recombination of excitons. No UV emission was observed for aluminium- and copper-doped zinc oxide. It is known that the emission intensity is determined by radiative and nonradiative transitions. It is also known that the nonradiative transition is induced by crystal imperfections, such as point defects, dislocations and grain boundaries [Al Asmar et al., 2005]. Therefore, copper- and aluminium-doping may cause lattice and surface defects which reduces the UV emission intensity of copper- and aluminium-doped zinc oxide.

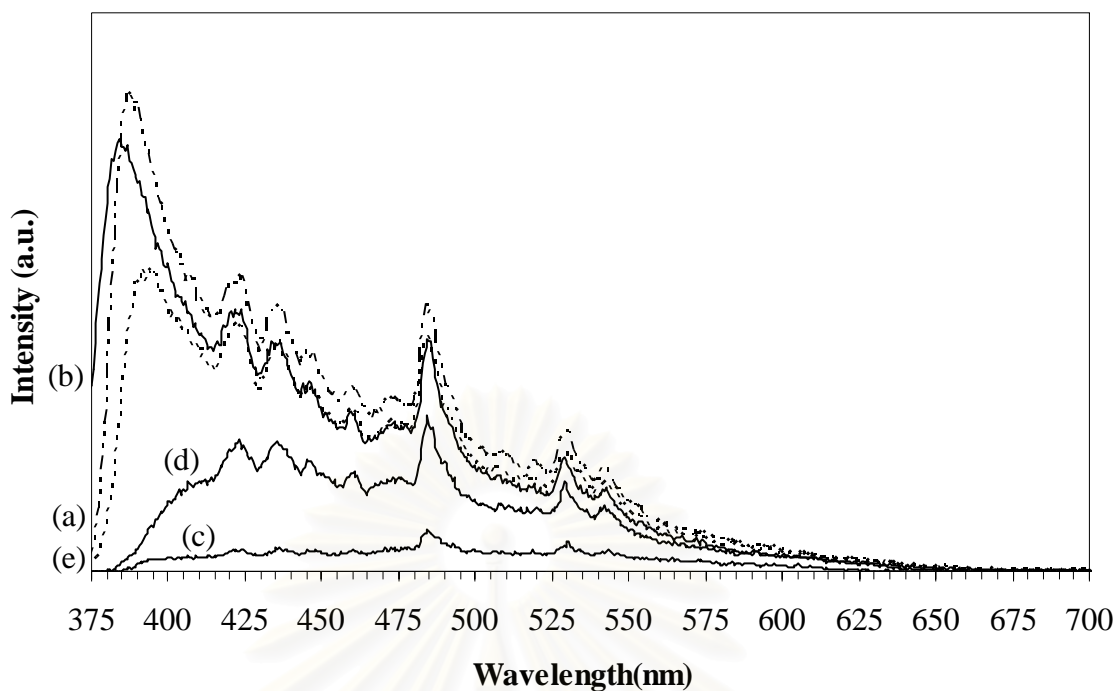


Figure 4.45 Photoluminescence of undoped and metal-doped zinc oxide in form of wavelength: (a) undoped zinc oxide, (b) 5 at.% gallium-, (c) 7.5 at.% copper, (d) 7.5 at.% aluminium- and (e) 7.5 at.% magnesium-doped zinc oxide.

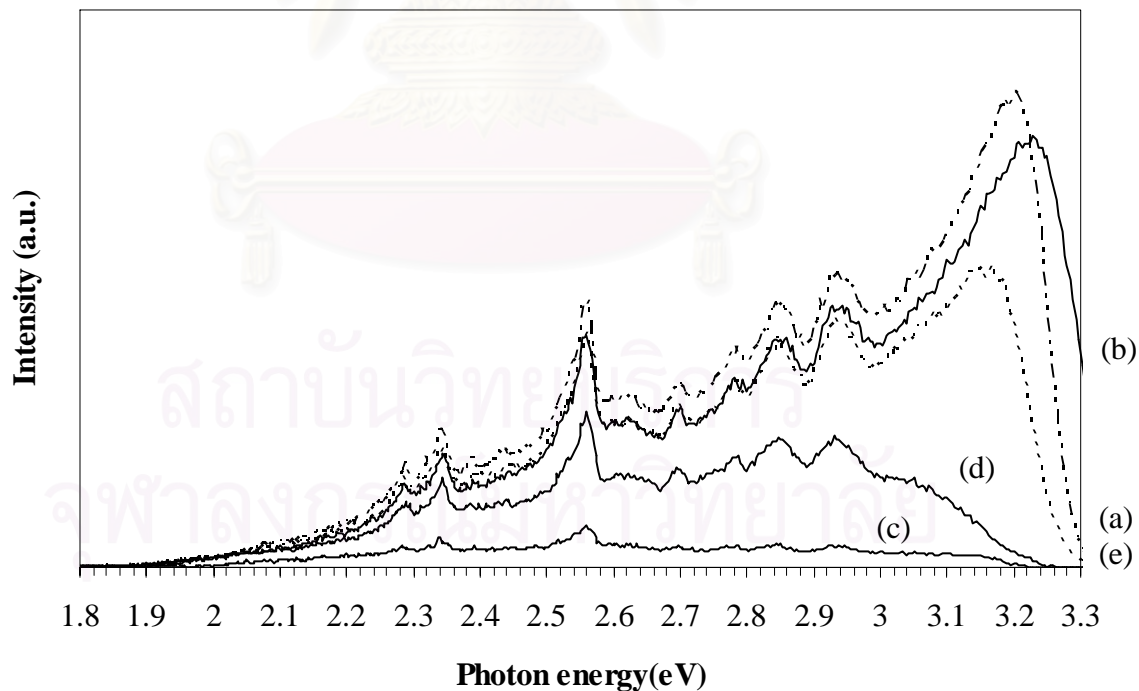


Figure 4.46 Photoluminescence of undoped and metal-doped zinc oxide in form of energy: (a) undoped zinc oxide, (b) 5 at.% gallium-, (c) 7.5 at.% copper, (d) 7.5 at.% aluminium- and (e) 7.5 at.% magnesium-doped zinc oxide..

Table 4.3 The band gap energy of zinc oxide samples determined from the UV-Vis spectroscopy and from photoluminescence.

<i>Sample</i>	<i>Band gap energy (eV)</i>	
	<i>UV-Vis</i>	<i>Photoluminescence</i>
Undoped zinc oxide	3.28	3.20
5 at.% gallium-doped zinc oxide	3.39	3.23
7.5 at.% copper-doped zinc oxide	3.28	-
7.5 at.% aluminium-doped zinc oxide	3.35	-
7.5 at.% magnesium-doped zinc oxide	3.28	3.17



สถาบันวิทยบริการ
จุฬาลงกรณ์มหาวิทยาลัย

CHAPTER V

CONCLUSIONS AND RECOMMENDATIONS

5.1 Conclusions

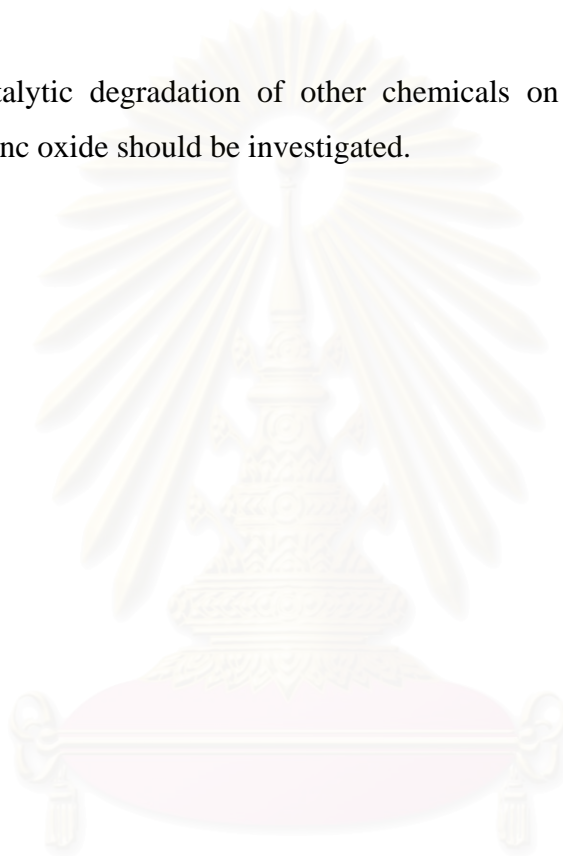
In this thesis, properties of metal-doped zinc oxide synthesized via solvothermal method are investigated. The conclusions of the study are summarized as follow:

1. Gallium- and aluminium-doped zinc oxide was successfully fabricated via solvothermal method. The metal content affect the band gap energy whereas the highest band gap energy is achieved from 5 and 7.5 at.% doping of gallium and aluminium, respectively.
2. The metal content affects the morphology, average diameter, average length and aspect ratio of zinc oxide particles.
3. The incorporation of metal into crystal structure of zinc oxide depends on the synthesis method and preparation procedures.
4. The photocatalytic activity of the synthesized zinc oxide depends upon the band gap energy of photocatalyst and light source (i.e. UV and solar radiation). The photocatalyst with low band gap energy is more effective for practical applications

5.2 Recommendation for Future Studies

From the previous conclusions, the following recommendations for future studies are proposed.

1. Properties of metal-doped zinc oxide synthesized by other method should be investigated.
2. Photocatalytic degradation of other chemicals on the undoped and metal-doped zinc oxide should be investigated.



สถาบันวิทยบริการ
จุฬาลงกรณ์มหาวิทยาลัย

REFERENCES

- Aguilar-Ros, G., M. A. Valenzuela, H. Armendariz, P. Salas, J. M. Dominguez, D.R.Acosta and I. Schifter (1992). "Metal-support effects and catalytic properties of platinum supported on zinc aluminate." Applied Catalysis A: General **90**: 25-34.
- Al Asmar, R., S. Juillaguet, M. Ramonda, A. Giani, P. Combette, A. Khoury and A. Foucaran (2005). "Fabrication and characterization of high quality undoped and Ga₂O₃-doped ZnO thin films by reactive electron beam co-evaporation technique." Journal of Crystal Growth **275**(3-4): 512-520.
- Bagnall, D. M., Y. F. Chen, M. Y. Shen, Z. Zhu, T. Goto and T. Yao (1998). "Room temperature excitonic stimulated emission from zinc oxide epilayers grown by plasma-assisted MBE " Journal of Crystal Growth **184**: 605-609.
- Bahsi, Z. B. and A. Y. Oral (2006). "Effects of Mn and Cu doping on the microstructures and optical properties of sol-gel derived ZnO thin films." Optical Materials (in press).
- Bhattacharya, P., R. R. Das and R. S. Katiyar (2004). "Comparative study of Mg doped ZnO and multilayer ZnO/MgO thin films." Thin Solid Films **447-448** 564-567.
- Blatt, F. J. (1968). Physics of Electronic Conduction in Solids New York, Mc Graw-Hill.
- Cao, H. T., Z. L. Pei, J. Gong, C. Sun, R. F. Huang and L. S. Wen (2004). "Preparation and characterization of Al and Mn doped ZnO (ZnO : (Al, Mn)) transparent conducting oxide films." Journal of Solid State Chemistry **177** (4-5): 1480-1487.
- Chen, P. L. and I. W. Chen (1993). "Reative cerium (IV) oxidase powders by the homogeneous precipitation method." Journal of American Ceramic Society **76**: 1577.
- Chen, S.-J., L.-H. Li, X.-T. Chen, Z. Xue, J.-M. Hong and X.-Z. You (2003). "Preparation and characterization of nanocrystalline zinc oxide by a novel solvothermal oxidation route." Journal of Crystal Growth **252**: 184-189.

- Cheong, K. Y., N. Muti and S. R. Ramanan (2002). "Electrical and optical studies of ZnO:Ga thin films fabricated via the sol-gel technique." Thin Solid Films **410**: 142-146.
- Davolos, M. R., S. Feliciano, A. M. Pires, R. F. C. Marques and J. Miguel Jafelicci (2003). "Solvothermal method to obtain europium-doped yttrium oxide." Journal of Solid State Chemistry **171**: 268-272.
- Georgobiani, A., A. Gruzintsev, V. Volkov, M. O. Vorob'ev and V. A. Dravin (2004). "ZnO thin films with hole conduction produced by N⁺ ion implantation and oxygen-radical annealing." Russian Microelectronics **33**: 165-168.
- Gomez, H., A. Maldonado, M. de la L. Olvera and D.R. Acosta (2005). "Gallium-doped ZnO thin films deposited by chemical spray." Solar Energy Materials & Solar Cells **87**: 107-116.
- Goncalves, A. d. S., S. A. M. d. Lima, M. R. Davolos, S. G. Antonio and C. d. O. Paiva-Santos (2006). "The effects of ZnGa₂O₄ formation on structural and optical properties of ZnO:Ga powders." Journal of Solid State Chemistry **179**: 1286-1290.
- Gong, H., J. Q. Hu, J. H. Wang, C. H. Ong and F. R. Zhu (2005). "Nano-crystalline Cu-doped ZnO thin film gas sensor for CO." Sensors and Actuators B **115**: 247-251.
- Hoffmann, M. R., S. T. Martin, W. Choi and D. W. Bahnemannt (1995). "Environmental applications of semiconductor photocatalysis." Chemical Reviews **95**: 69-96.
- Hsu, L.-S., C. S. Yeh, C. C. Kuo, B. R. Huang and S. Dhar (2005). "Optical and transport properties of undoped and Al-, Ga- and In-doped ZnO thin films." Journal of Optoelectronics and Advanced Materials **7**(6): 3039-3046.
- Inoue, M., H. Kominami and T. Inui (1992). "Thermal transformation of χ -alumina formed by thermal decomposition of aluminum alkoxide in organic media." Journal of the American Ceramic Society **79**: 2597-2598.
- Inoue, M., H. Kominami and T. Inui (1995). "Novel synthesis method for thermally stable monoclinic zirconia: hydrolysis of zirconium alkoxides at high temperatures with a limited amount of water dissolved in inert organic solvent from the gas phase." Applied Catalysis A: General **121**: L1-L5.

- Iwamoto, S., K. Saito, M. Inoue and K. Kagawa (2001). "Preparation of the xerogels of nanocrystalline titanias by the removal of the glycol at the reaction temperature after the glycothermal method and their enhanced photocatalytic activities." Nano Letters **1**: 417-421.
- Jeong, S. H., B. N. Park, S. B. Lee and J.-H. Boo (2005). "Structural and optical properties of silver-doped zinc oxide sputtered films." Surface & Coatings Technology **193**: 340-344.
- John, V. S., T. Mahalingam and J. P. Chu (2005). "Synthesis and characterization of copper doped zinc telluride thin films." Solid-State Electronics **49**: 3-7.
- Kamalasanan, M. N. and S. Chandra (1996). "Sol-gel synthesis of ZnO thin films." Thin Solid Films **288**: 112-115.
- Khranovskyy, V., U. Grossner, V. Lazorenko, G. Lashkarev, B. G. Svensson and R. Yakimova (2006). "PEMOCVD of ZnO thin films, doped by Ga and some of their properties." Superlattices and Microstructures **39**: 275–281.
- Kim, K.-S. and H. W. Kim (2003). "Synthesis of ZnO nanorods on bare Si substrate using metal organic chemical vapor deposition." Physica B **328**: 368-371.
- Kimball, G. E. (1935). "The electronic structure of diamond." Journal of Chemical Physic **3**(9): 560-564.
- Klongdee, J., W. Petchkroh, K. Phuempoonsathaporn, P. Praserttham, A. S. Vangnai and V. Pavarajarn (2005). "Activity of nanosized titania synthesized from thermal decomposition of titanium (IV) n-butoxide for the photocatalytic degradation of diuron." Science and Technology of Advanced Materials **6**: 290-295.
- Lee, H. W., S. P. Laua, Y. G. Wanga, K. Y. Tseb, H. H. Hng and B. K. Taya (2004). "Structural, electrical and optical properties of Al-doped ZnO thin films prepared by filtered cathodic vacuum arc technique." Journal of Crystal Growth **268**: 596-601.
- Li, X. H., A. P. Huang, M. K. Zhu, S. L. Xu, J. Chen, H. Wang, B. Wang and H. Yan (2003). "Influence of substrate temperature on the orientation and optical properties of sputtered ZnO films " Materials Letters **57**: 4655.
- Lin, H.-F., S.-C. Liao and S.-W. Hung (2005). "The dc thermal plasma synthesis of ZnO nanoparticles for visible-light photocatalyst." Journal of Photochemistry and Photobiology A: Chemistry **174**: 82-87.

- Lin, S.-S., J.-L. Huang and P. Sajgalik (2004). "The properties of heavily Al-doped ZnO films before and after annealing in the different atmosphere." Surface & Coatings Technology **185**: 254-263.
- Liu, Z. F., F. K. Shan, Y. X. Li, B. C. Shin and Y. S. Yu (2003). "Epitaxial growth and properties of Ga-doped ZnO films grown by pulsed laser deposition." Journal of Crystal Growth **259**: 130.
- Madler, L., W. J. Stark and S. E. Pratsinis (2002). "Rapid synthesis of stable ZnO quantum dots." Journal of Applied Physics **92**: 6537.
- Mekasuwandumrong, O., P. Praserthdam, M. Inoue, V. Pavrajarn and W. Tanakulrungsank (2004). "Phase transformation behavior of nanocrystalline chi-alumina powder obtained by thermal decomposition of AIP in inert organic solvent." Journal of Materials Science **39**(7): 2417-2421.
- Meulenkamp, E. A. (1998). "Synthesis and Growth of ZnO Nanoparticles." Journal of Physical Chemistry B **102**(29): 5566.
- Minemoto, T., T. Negami, S. Nishiwaki, H. Takakura and Y. Hamakawa (2000). "Preparation of $Zn_{1-x}Mg_xO$ films by radio frequency magnetron sputtering." Thin Solid Films **372**: 173-176.
- Mott, M. F. and E. A. Davis (1979). Electronic Process in Non-Crystalline Materials. Clarendon Press, Oxford.
- Mrowetz, M. and E. Selli (2005). "Photocatalytic degradation of formic and benzoic acids and hydrogen peroxide evolution in TiO_2 and ZnO water suspensions." Journal of Photochemistry and Photobiology A: Chemistry (in press)
- Narayan, J., A. K. Sharma, C. J. A. Kvit, J. F. Muth and O. W. Holland (2001). "Novel cubic $Zn_xMg_{1-x}O$ epitaxial heterostructures on Si (100) substrates." Solid State Communications **121**: 9-13.
- Nishi, M., S. Tanabe, M. Inoue, M. Takahashi, K. Fujita and K. Hirao (2005). "Optical-telecommunication-band fluorescence properties of Er^{3+} -doped YAG nanocrystals synthesized by glycothermal method." Optical Materials **27**: 655-662.
- Nogami, M., Y. Abe and A. Nakamura (1995). "Cu microcrystals in sol-gel derived glasses." Journal of Materials Research **10**(10).
- Ohtomo, A., R. Shiroki, I. Ohkubo, H. Koinuma and M. Kawasaki (1999). "Thermal stability of supersaturated $Mg_xZn_{1-x}O$ alloy films and $Mg_xZn_{1-x}O/ZnO$ heterointerfaces." Applied Physics Letters **75**: 4088.

- Omar, M. A. (1975). Elementary solid state physics: Principles and applications. Lowell technology institute, Addison-wesley publishing company.
- Özgür, Ü., Y. I. Alivov, C. Liu, A. Teke, M. A. Reshchikov, S. Doğan, V. Avrutin, S.-J. Cho and H. Morkoç (2005). "A comprehensive review of ZnO materials and devices." Journal of Applied Physics **98**: 041301.
- Panigrahi, S., S. Kundu, S. K. Ghosh, S. Nath, S. Praharaj, S. Basu and T. Pal (2006). "Selective one-pot synthesis of copper nanorods under surfactantless condition." Polyhedron **25**: 1263-1269.
- Pankove, J. I. (1971). Optical Processes in Semiconductors, Dover Publications, New York.
- Parada, N. J. and J. G. W. Pratt (1969). "New model for vacancy states in PbTe." Physical Review Letters **22**: 180-182.
- Paraguay, F. D., J. Moralesa, W. Estrada L., E. Andrade and M. Miki-Yoshida. (2000). "Influence of Al, In, Cu, Fe and Sn dopants in the microstructure of zinc oxide thin films obtained by spray pyrolysis." Thin Solid Films **366**: 16-27.
- Park, K. C., D. Y. Ma and K. H. Kim (1997). "The physical properties of Al-doped zinc oxide films prepared by RF magnetron sputtering." Thin Solid Films **305** 201-209.
- Payakgul, W., O. Mekasuwandumrong, V. Pavarajarn and P. Prasertdam (2005). "Effects of reaction medium on the synthesis of TiO₂ nanocrystals by thermal decomposition of titanium (IV) n-butoxide." Ceramics International **31**: 391-397.
- Pei, G., C. Xia, S. Cao, J. Zhang, F. Wu and J. Xu (2005). "Synthesis and magnetic properties of Ni-doped zinc oxide powders." Journal of Magnetism and Magnetic Materials (in press).
- Phunghadung, J. (2001). Effect of crystallite size and calcinations temperature on the thermal stability of single nanocrystal of transition metal oxide. Master's Thesis, Chemical engineering Department, Faculty of Engineering, Chulalongkorn University, Thailand.
- Posada, E. d., G. Tobin, E. McGlynn and J. G. Lunney (2003). "Pulsed laser deposition of ZnO and Mn-doped ZnO thin films." Applied Surface Science **208-209**: 589.

- Ren, C.-Y., S.-H. Chiou and C.-S. Hsue (2004). "Ga-doping effects on electronic and structural properties of wurtzite ZnO." Physica B: Condensed Matter **349**(1-4): 136-142.
- Richardson, T. J., J. L. Slack and M. D. Rubin (2003). "The effects of sputtering conditions on the optical transmission and wettability of amorphous copper oxide thin films prepared by magnetron sputtering." Coating materials news **13**(4).
- Rodriguez-Paez, J. E., A. C. Caballero, M. Villegas, C. Moure, P. Duran and J. F. Fernandez (2001). "Controlled precipitation methods: formation mechanism of ZnO nanoparticles." Journal of the European Ceramic Society **21**: 925-930.
- Roth, A. P., J. B. Webb and D. F. Williams (1981). "Absorption edge shift in ZnO thin films at high carrier densities." Solid State Communications **39**: 1269.
- Sakthivel, S., B. Neppolian, B. Arabindoo, M. Palanichamy and V. Murugesan (1999). "Photocatalytic degradation of leather dye, Acid Green 16 using ZnO in the slurry and thin film forms." Indian Journal of Chemical Technology **6**: 161-165.
- Sakthivel, S., B. Neppolian, M. V. Shankar, B. Arabindoo, M. Palanichamy and V. Murugesan (2003). "Solar photocatalytic degradation of azo dye: comparison of photocatalytic efficiency of ZnO and TiO₂." Solar Energy Materials & Solar Cells **77**: 65-82.
- Sampath, S. K. and J. F. Cordaro (1998). "Optical properties of zinc aluminate, zinc gallate, and zinc aluminogallate spinels." Journal of the American Ceramic Society **81**: 649-654.
- Shan, F. K., B. I. Kim, G. X. Liu, Z. F. Liu, J. Y. Sohn, W. J. Lee, B. C. Shin and Y. S. Yu (2004). "Blueshift of near band edge emission in Mg doped ZnO thin films and aging." Journal of Applied Physics **95**: 4772.
- Sharma, A. K., J. Narayan, J. F. Muth and C. W. Teng (1999). "Optical and structural properties of epitaxial Mg_xZn_{1-x}O alloys." Applied Physics Letters **75**: 3327-3329.
- Shimada, H., S. Miyama and H. Kuroda (1988). "Decomposition of nitric oxide over Y—Ba—Cu—O mixed oxide catalysts." Chemistry Letters (1797-1800).
- Shockley, W. and J. Bardeen (1950). "Energy bands and mobilities in monatomic semiconductors." Physical Review **77**: 407-408.

- Srikant, V. and D. R. Clarke (1997). "Anomalous behavior of the optical band gap of nanocrystalline ZnO thin films." Journal of Materials Research **12**: 1425.
- Srikant, V. and D. R. Clarke (1998). "On the optical band gap of zinc oxide." Journal of Applied Physics **83**(10).
- Sue, K., K. Kimura, M. Yamamoto and K. Arai (2004). "Rapid hydrothermal synthesis of ZnO nanorods without organics." Materials Letters **58**: 3350-3352.
- Tonto, P. (2004). Effect of organic solvents on crystal shape and ultraviolet absorption of zinc oxide synthesized via solvothermal method. Master's Thesis, Chemical engineering Department, Faculty of Engineering, Chulalongkorn University, Thailand.
- Wang, S., G. Xia, J. Shao and Z. Fan (2006). "Structure and UV emission of nanocrystal ZnO films by thermal oxidation of ZnS films." Journal of Alloys and Compounds: (in press).
- Wang, Z. L. (2004). "Nanostructures of zinc oxide." Materials today **7**(6): 26-33.
- Weng, J., Y. Zhang, G. Han, Y. Zhang, L. Xu, J. Xu, X. Huang and K. Chen (2005). "Electrochemical deposition and characterization of wide band semiconductor ZnO thin film." Thin Solid Films **478**: 25-29.
- Wu, H. Q. and X. W. Wei (2004). "Synthesis of zinc oxide nanorods using carbon nanotubes as templates." Journal of Crystal Growth **265**: 184-189.
- Xie, S., M. P. Rosynek and J. H. Lunsford (1999). "Catalytic reactions of NO over 0–7 mol% Ba/MgO catalysts: I. The direct decomposition of NO." Journal of Catalysis **188**: 24.
- Xu, Z. Q., H. Deng, Y. Li, Q. H. Guo and Y. R. Li (2006). "Characteristics of Al-doped c-axis orientation ZnO thin films prepared by the sol-gel method." Materials Research Bulletin **41**: 354–358.
- Yang, L. (2005). "Synthesis and photoluminescence of corn-like ZnO nanostructures under solvothermal-assisted heat treatment." Chemical Physics Letters **409**: 337-341.
- Yang, Y. and H. Chen (2004). "Size control of ZnO nanoparticles via thermal decomposition of zinc acetate coated on organic additives." Journal of Crystal Growth **263**: 447-453.

- Yu, Y. S., G. Y. Kim, B. H. Min and S. C. Kim (2004). "Optical characteristics of Ge doped ZnO compound." Journal of the European Ceramic Society **24**: 1865-1868.
- Zhu, P., Y. Masuda and K. Koumoto (2004). "Seedless micropatterning of copper by electroless deposition on self-assembled monolayers." Journal of Materials Chemistry **14**: 976-981.
- Zou, G., D. Yu, D. Wang, W. Zhang, L. Xu, W. Yu and Y. Qian (2004). "Controlled synthesis of ZnO nanocrystals with column-, rosette-and fiber-like morphologies and their photoluminescence property." Materials Chemistry and Physics **88**: 150-154.
- Zu, P., Z. K. Tang, G. K. L. Wong, M. Kawasaki, A. Ohtomo, H. Koinuma and Y. Segawa (1997). "Ultraviolet spontaneous and stimulated emissions from ZnO microcrystallite thin films at room temperature." Solid State Communications **103**(8): 459-463.



สถาบันวิทยบริการ
จุฬาลงกรณ์มหาวิทยาลัย



APPENDICES

สถาบันวิทยบริการ
จุฬาลงกรณ์มหาวิทยาลัย

APPENDIX A

CALCULATION OF LATTICE PARAMETERS

The lattice constants a and c of the wurtzite structure zinc oxide were calculated, according to Bragg's law.

$$2d \sin \theta = n\lambda \quad (\text{A-1})$$

for hexagonal structure, lattice constants a and c are related by

$$\frac{1}{d_{hkl}^2} = \frac{4}{3} \left(\frac{h^2 + hk + k^2}{a^2} \right) + \frac{l^2}{c^2} \quad (\text{A-2})$$

where d_{hkl} is interplanar spacing of (hkl) plane.

with the first order approximation, $n = 1$:

$$\sin^2 \theta = \frac{\lambda^2}{4} \left(\frac{4}{3} \frac{h^2 + hk + k^2}{a^2} \right) + \frac{l^2}{c^2} \quad (\text{A-3})$$

The peak positions of (101) and (001) orientation are selected to calculate the lattice constants a and c . Use data of 0.5 at.% gallium-doped zinc oxide, 2θ of Plane (100) and (101) are 32.22 and 36.72, respectively. Wavelength of X-ray CuK_α radiation are 1.5406 Å.

Substitution 2θ of Plane (100) into equation (A-3).

$$\sin^2\left(\frac{32.22}{2}\right) = \frac{(1.5406)^2}{4} \left(\frac{4}{3} \frac{(1)^2 + (1)(0) + (0)^2}{a^2} \right) + \frac{(0)^2}{c^2}$$

So, we get lattice parameter $a = 3.2055$ Å. Substitution 2θ of Plane (101) and lattice parameter a into equation (A-3).

$$\sin^2\left(\frac{36.72}{2}\right) = \frac{(1.5406)^2}{4} \left(\frac{4(1)^2 + (1)(0) + (0)^2}{3(32.055)^2} \right) + \frac{(1)^2}{c^2}$$

We get lattice parameter $c = 5.1676 \text{ \AA}$, Therefore, the lattice parameters a and c of 0.5 at.% gallium-doped zinc oxide are 3.2055 and 5.1676 \AA , respectively.

Table A-1 Lattice parameters of metal-doped zinc oxide at various metal contents.

at.%. .	<i>Dopant</i>							
	Ga		Cu		Al		Mg	
	a	c	a	c	a	c	a	c
0.5	3.2055	5.1676	3.2427	5.1928	3.2309	5.1970	3.2269	5.1592
2.5	3.2074	5.1933	3.2368	5.1888	3.2467	5.2077	3.2388	5.2010
5	3.2325	5.1755	3.2388	5.2023	3.2427	5.1928	3.2348	5.2023
7.5	3.2230	5.1795	3.2365	5.1902	3.2467	5.2077	3.2388	5.2050
10	3.2447	5.1941	3.2427	5.2050	3.2447	5.1941	3.2348	5.2133
12.5	3.2113	5.1960	3.2348	5.1997	3.2427	5.1928	3.2467	5.1901

Table A-2 Lattice parameters of metal-doped zinc oxide calcined at various temperatures.

Calcination temperature (°C)	<i>Dopant</i>							
	5 at.% Ga		7.5 at.% Cu		7.5 at.% Al		7.5 at.% Mg	
	a	c	a	c	a	c	a	c
25	3.2325	5.1755	3.2365	5.1902	3.2467	5.2077	3.2388	5.2050
300	3.2230	5.1917	3.2328	5.1983	3.2427	5.2050	3.2388	5.1901
500	3.2368	5.1888	3.2269	5.1821	3.2172	5.1877	3.2348	5.1874
900	3.2348	5.1997	3.2447	5.2064	3.2328	5.1861	3.2388	5.1901

APPENDIX B

CALCULATION OF BAND GAP ENERGY

The absorption edge from absorption spectra use to calculate the band gap energy by equation

$$\nu_0 = E_g/h \quad (\text{B-1})$$

Where ν_0 is frequency at absorption edge. Substitution $\nu = \frac{c}{\lambda_{1/2}}$ into equation (B-1).

$$E_g = \frac{c \cdot h}{\lambda_{1/2}} \quad (\text{B-2})$$

Where c = light velocity (3×10^8 m/s)
 h = Planck constant (4.135×10^{-15} eV.s)
 $\lambda_{1/2}$ = wavelength at absorption edge (nm)
 E_g = band gap energy (eV)

The wavelength at half-absorption intensity ($\lambda_{1/2}$) from the UV- Vis absorption spectra of 0.5 at.% gallium-doped zinc oxide are shown in Figure B-1. It can be seen $\lambda_{1/2}$ is about 373.7 nm. Substitution $\lambda_{1/2}=373.7$ nm into equation (B-2).

$$E_g = \frac{(3 \times 10^8 \text{ m/s})(4.135 \text{ eV.s})}{(373.7 \text{ nm})}$$

We get the band gap energy of 0.5 at.% gallium-doped zinc oxide is 3.318 eV. Table B-1 and B-2 shows the band gap energy of metal-doped zinc oxide at various metal content and calcination temperature, respectively.

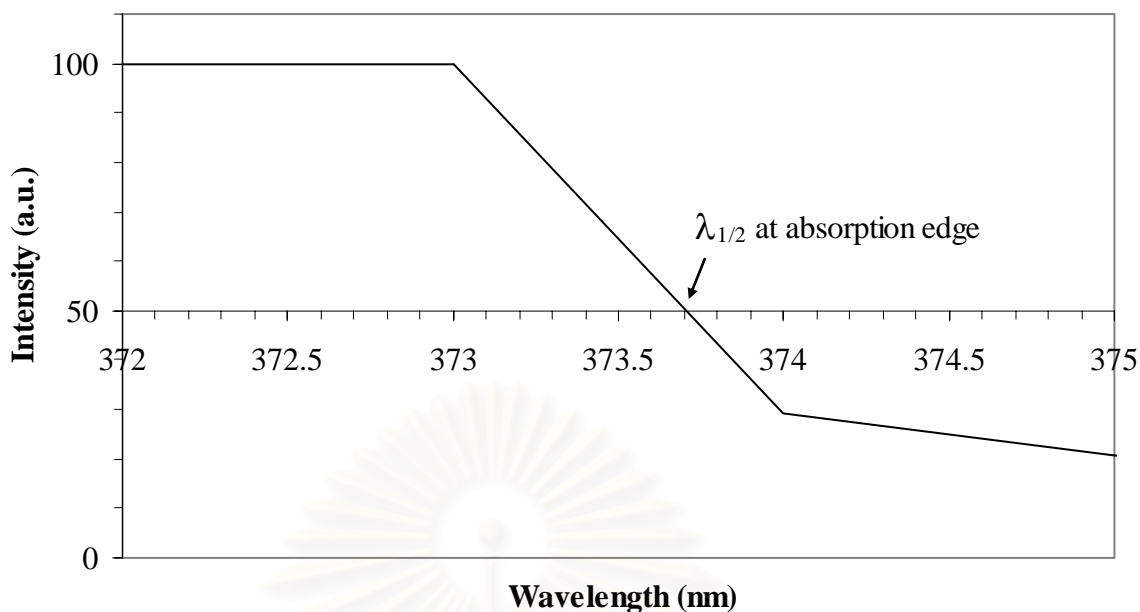


Figure B-1 The UV-Vis absorption spectra of 0.5 at.% gallium-doped zinc oxide. The wavelength at half-absorption intensity ($\lambda_{1/2}$) is the band-gap energy of the material.

Table B-1 The band gap energy of metal-doped zinc oxide at various metal content.

at.%. .	Dopant							
	Ga		Cu		Al		Mg	
	$\lambda_{1/2}$	E_g	$\lambda_{1/2}$	E_g	$\lambda_{1/2}$	E_g	$\lambda_{1/2}$	E_g
0.5	373.70	3.318	377.62	3.284	376.64	3.292	377.62	3.284
2.5	373.68	3.318	377.66	3.283	376.67	3.292	379.65	3.266
5	365.72	3.391	377.64	3.284	374.65	3.310	379.75	3.265
7.5	368.70	3.363	377.64	3.284	369.65	3.355	377.75	3.283
10	368.85	3.362	377.62	3.284	376.63	3.292	379.6	3.267
12.5	368.69	3.363	377.63	3.284	371.70	3.336	378.7	3.274

Table B-2 The band gap energy of metal-doped zinc oxide at various calcine temperature.

Calcination temperature (°C)	<i>Dopant</i>							
	5 at.% Ga		7.5 at.% Cu		7.5 at.% Al		7.5 at.% Mg	
	$\lambda_{1/2}$	E_g	$\lambda_{1/2}$	E_g	$\lambda_{1/2}$	E_g	$\lambda_{1/2}$	E_g
25	365.72	3.391	377.65	3.284	369.65	3.355	377.76	3.283
300	376.47	3.294	377.71	3.283	378.65	3.275	377.76	3.282
500	378.39	3.277	377.63	3.284	381.65	3.249	376.82	3.291
900	377.41	3.286	-	-	380.60	3.258	371.82	3.335

สถาบันวิทยบริการ
จุฬาลงกรณ์มหาวิทยาลัย

APPENDIX C

ANALYSIS OF SOLVENT AFTER SOLVOTHERMAL SYNTHESIS BY INDUCTIVELY COUPLED PLASMA OPTICAL EMISSION

Solvent after synthesis of 12.5 at.% copper-doped zinc oxide are prepared by decrease 1000 time of concentration. The results are shown in Figure C-1.

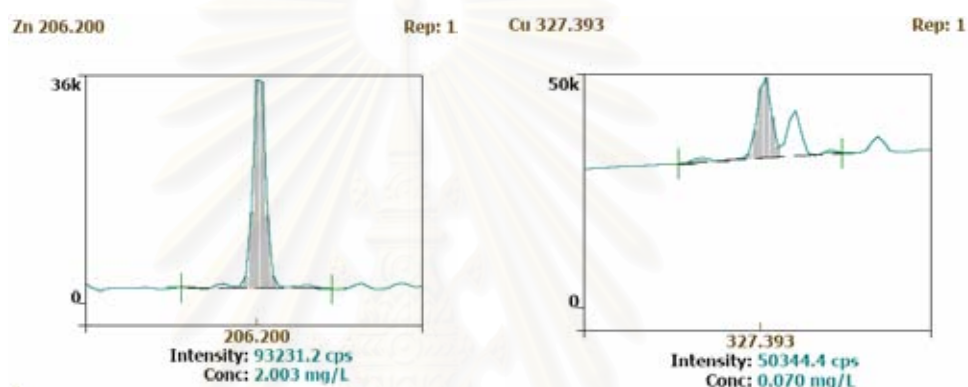


Figure C-1 zinc and cu content into solvent after synthesis of 12.5 at.% copper-doped zinc oxide are prepared.

The results from ICP show zinc and copper content are 2.003 and 0.07 mg/L . So, zinc and copper content into solvent after synthesis are 200.3 and 7 mg into 100 ml of solvent.

Determine copper content into sample

Copper acetylacetonate (MW 261.76 g/mol) are used into sample 3.151 g.

$$\text{So, copper (MW 63.545 g/mol) into sample are } \frac{3.151 \text{ g} \times 63.545 \frac{\text{g}}{\text{mol}}}{261.76 \frac{\text{g}}{\text{mol}}} = 765 \text{ mg.}$$

APPENDIX D

LIST OF PUBLICATION

1. Teerawut Ruangsanam, Okorn Mekasuwandumrong, Piyasan Prasertdam and Varong Pavarajarn (2005) "Physical and Optical Properties of Gallium-Doped Zinc Oxide Nanoparticles Synthesized via Glycothermal Method." Proceedings of the Regional Symposium on Chemical Engineering 2005, Hanoi, Vietnam, Nov. 30 - Dec. 2, 2005, Ref. No. MA26.



สถาบันวิทยบริการ
จุฬาลงกรณ์มหาวิทยาลัย

Physical and Optical Properties of Gallium-Doped Zinc Oxide Nanoparticles Synthesized via Glycothermal Method

Teerawut Ruangsanam^{a),*}, Okorn Mekasuwandumrong^{b)}, Piyasan Praserttham^{a)}
and Varong Pavarajam^{a),†}

^{a)} Center of Excellence on Catalysis and Catalytic Reaction Engineering, Department of Chemical Engineering, Faculty of Engineering, Chulalongkorn University, Bangkok 10330 Thailand.

^{b)} Department of Chemical Engineering, Faculty of Engineering and Industrial Technology, Silpakorn University, Nakorn Pathom 73000, Thailand.

* Presenting author

† Corresponding author (Tel: +66-02-2186890, Fax: +66-02-2186877, Email: fchvprv@eng.chula.ac.th)

Abstract

Zinc oxide is recognized as one of the most promising semiconductor materials due to its good optical, thermal and electrical properties. In this work, nanocrystalline zinc oxide was synthesized by glycothermal process, i.e. thermal decomposition of zinc acetate ($\text{Zn}(\text{CH}_3\text{CO}_2)_2$) in 1,4-butanediol, at 220°C for 2 h under autogeneously high pressure. The physical and optical properties of the product were investigated by X-ray diffraction (XRD), scanning electron microscopy (SEM), X-ray photoelectron spectroscopy (XPS) and UV/Visible spectrometry techniques. It was confirmed that the products after calcination at 300°C for 1 h were zinc oxide crystals with crystallite size in nanometered range. Doping of gallium as the secondary metal into zinc oxide crystals during glycothermal synthesis was also investigated. It was found that gallium incorporated into zinc oxide crystal structure affected properties of zinc oxide nanoparticles. Blue-shift in UV absorption spectrum, which indicates a change in electronic states of the product, was observed in gallium-doped zinc oxide. An increase in the content of gallium doping resulted in further shift in the UV absorption spectrum. Addition of gallium also affected morphology and crystallite size of the synthesized particles. Zinc oxide nanorod was observed from samples doped with gallium in the range of 0.5-2.5 at.%. At higher gallium content, all obtained particles were ellipsoidal.

Keyword

Zinc oxide; Nanoparticle; Gallium; Doping; Glycothermal method.

Introduction

Zinc oxide (ZnO) has been recognized as one of the most promising materials because of its excellence optical and electrical properties. It has large band gap of 3.3 eV as well as free exciton energy of 60 meV at room temperature [1]. Therefore it has been applied for many commercial uses, such as varistor, transparent electrode, solar cell [2, 3] and photocatalyst [4]. According to great function of ZnO, several techniques has been proposed for ZnO nanoparticles synthesis, such as solvothermal synthesis [5], hydrothermal synthesis [6], thermal decomposition [7], sol-gel synthesis [8] and precipitation method [9].

Properties of zinc oxide can be controlled by many techniques. Doping of zinc oxide with various ions is one of the approaches that have been reported earlier in the literatures. Presence of metal such as gallium and germanium in crystal structure of ZnO has proved to affect both optical and electrical properties of ZnO thin film [10, 11]. In this work, the influence of gallium doping on morphology and band gap energy of ZnO nanoparticles synthesized by glycothermal method, which been used to successfully synthesize various types of nanosized metal oxides with large surface area, high crystallinity and high thermal stability [5], was investigated.

Materials and Methods

Zinc oxide was prepared by glycothermal method using zinc acetate as starting material. Gallium acetylacetonate was used as precursors for gallium doping. The mixture of zinc acetate and the gallium acetylacetonate at predetermined ratio was suspended in 100 ml of solvent, i.e. 1,4-butanediol, contained in a test tube. The test tube was then placed in an autoclave. In the gap between the test tube and autoclave wall, 30 ml of the same solvent was added. After the autoclave was completely purged with nitrogen, the autoclave was heated to 220°C at the rate of 2.5°C min⁻¹ and held at that temperature for 2 hours. Pressure in the autoclave reactor gradually increased autogeneously as the temperature was raised and the reaction proceeded. After the holding period, the autoclave was cooled to room temperature. The resulting powder was collected after repeatedly washed with methanol. The product was air-dried and subsequently calcined at 300°C in air for 1 h. The content of gallium in ZnO powder was varied from 0 to 12.5 at.%. All products were analyzed by powder X-ray diffraction (SIEMENS D5000 diffractometer with CuK α radiation), X-ray Photoelectron Spectroscopy (Amicus, using MgK α radiation), Scanning Electron Microscopy (SEM, JEOL JSM6400) and UV/VIS spectroscopy (PerkinElmer Lambda 650, wavelength between 220 and 800). The band gap energy was calculated from the optical absorption data, according to procedures proposed by Madler *et al.* [12].

Results and Discussion

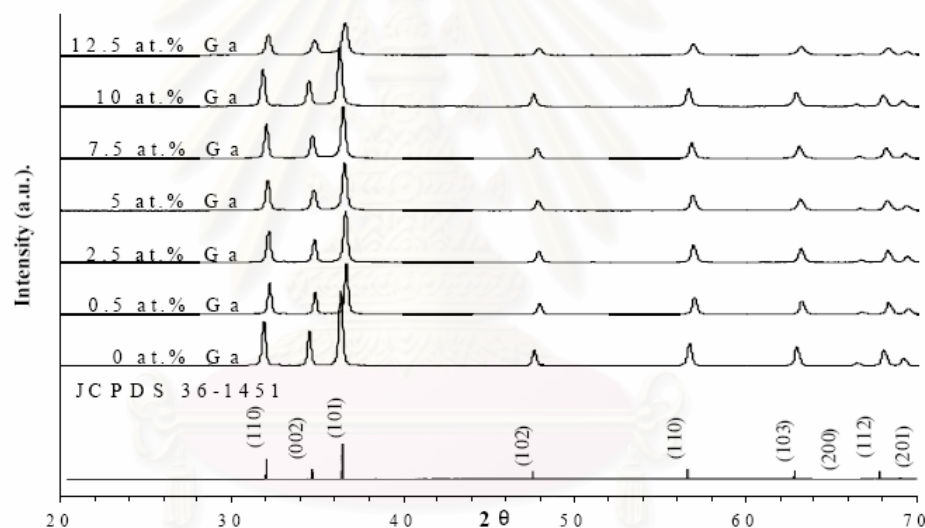


Figure 1- XRD patterns of as-prepared products.

The powder X-ray diffraction (XRD) patterns of as-prepared products are shown in Figure 1. The diffraction peaks of all products can be indexed to hexagonal structure of ZnO (JCPDS 36-1451), regardless of the content of gallium doped in the product. No other crystalline phase is detected. However, detailed investigation indicates that the XRD patterns of the gallium-doped samples are slightly shifted from the pattern of pure ZnO, especially at low value of 2θ .

Figure 2 shows lattice parameters that are calculated from the XRD patterns. It can be clearly seen that the lattice parameters of ZnO are decreased by an addition of 0.5 at.% gallium. Then, the lattice parameters are increased when higher amount of gallium is added to ZnO, up to doping concentration of 10 at.%. At gallium content higher than 10 at.%, the lattice parameters are decreased. It should be noted that the effect of gallium on the *a*-axis of ZnO structure is more pronounced than the *c*-axis. These changes in lattice dimension of ZnO crystal clearly indicate that gallium atoms are incorporated into ZnO crystal, when gallium precursor is added to zinc oxide precursor in the glycothermal synthesis. This result is also confirmed by XPS analysis. According to Table 1, the binding energies of

both zinc and oxygen are shifted by the presence of gallium in the sample, which indicate the interaction of zinc and oxygen with gallium atoms. The more gallium added, the more shifting observed.

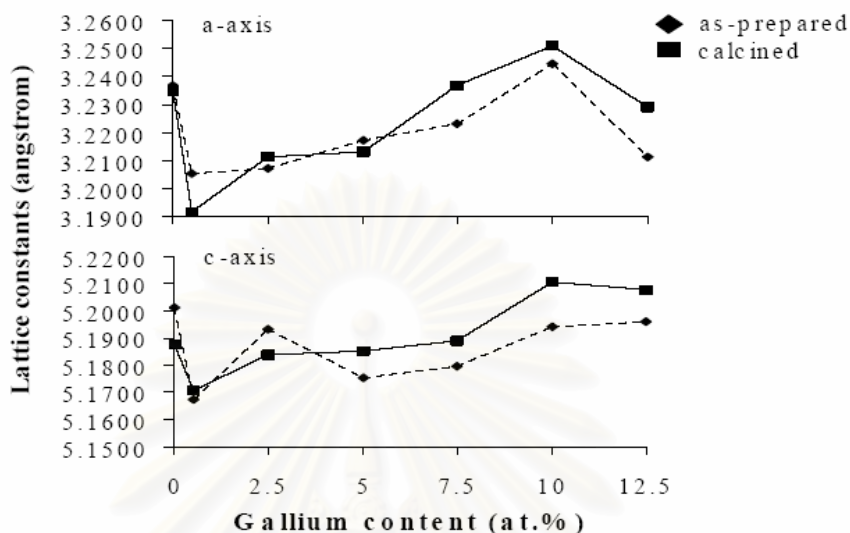


Figure 2- Variation of lattice parameters with the content of gallium doped.

Table 1. XPS analysis of gallium-doped ZnO powder.

Gallium content (at.%)	Binding energy (eV)		
	Zn 2p	O 1s	Ga 2p
0	1022.0	531.0	1117.0
0.5	1022.7	531.3	1119.0
2.5	1024.0	532.5	1120.2
12.5	1025.4	534.2	1121.7

Yu *et al.* have reported similar observation for germanium-doped ZnO [11]. It was suggested that, since ionic radius of germanium (0.53 Å) is smaller than that of zinc (0.74 Å), the inter-atomic distance between germanium atom and oxygen atom is shorter than the length between zinc atom and oxygen atom. Therefore, when germanium atom is present as an interstitial ion, the equilibrium state of the crystal structure is reformed due to the coulombic interaction among Zn^{2+} and O^{2-} ions, resulting in the increased lattice constants. However, when the solid solubility limit is reached, the excess foreign ions no longer exist as interstitial atoms and the lattice is rearranged [11]. In this work, since the ionic radius of gallium (0.61 Å) is also smaller than that of zinc, the similar behavior is expected. It should be noted from Figure 2 that the results from the calcined products also show the same trend in the relationship between gallium content and the lattice parameters, although the values are slightly different than those from as-prepared samples due to structural relaxation during heat treatment.

Figure 3 shows SEM micrographs of the products. It can be seen that the undoped-ZnO particles synthesized by glycothermal technique in 1,4-butandiol appear to be the ellipsoidal (Figure 3a.). When gallium is doped into ZnO at the concentration between 0.5 to 2.5 at.%, however, nanorods mixed with ellipsoidal particles are found. No ZnO nanorod was found at gallium content higher than 2.5 at.%. The results indicate that only low concentration of gallium doping affects the growth mechanism of ZnO particles in glycothermal synthesis.

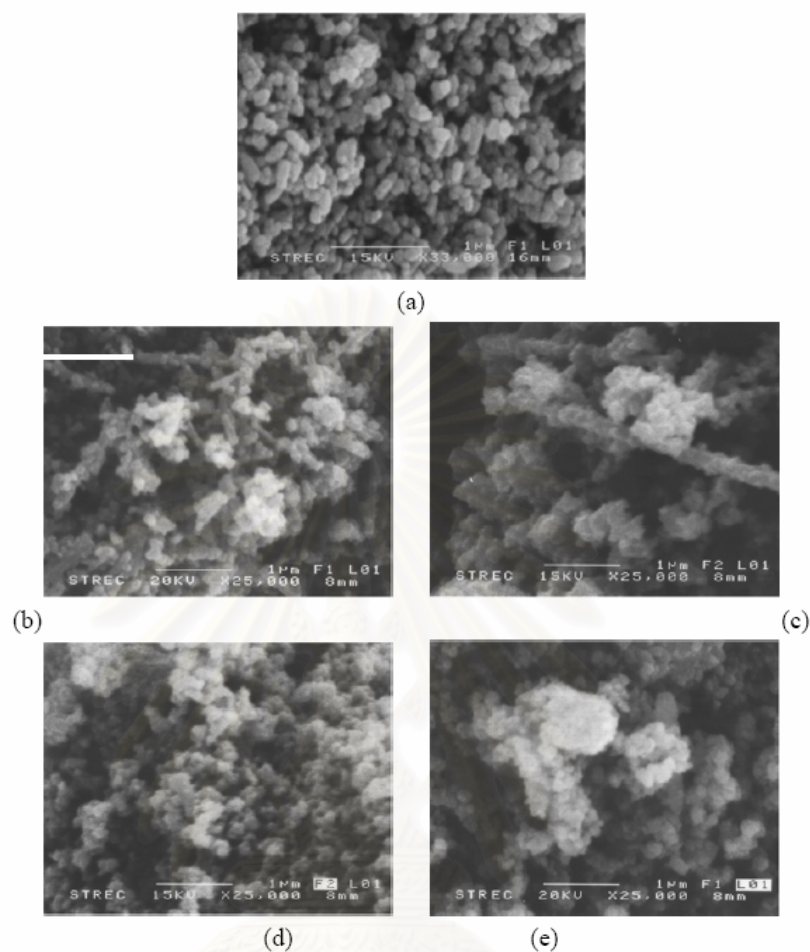


Figure 3- SEM image of (a) Pure zinc oxide and doped with gallium in various amount: (b) 0.5 at.% (c) 2.5 at.% (d) 5 at.% (e) 12.5 at.%.

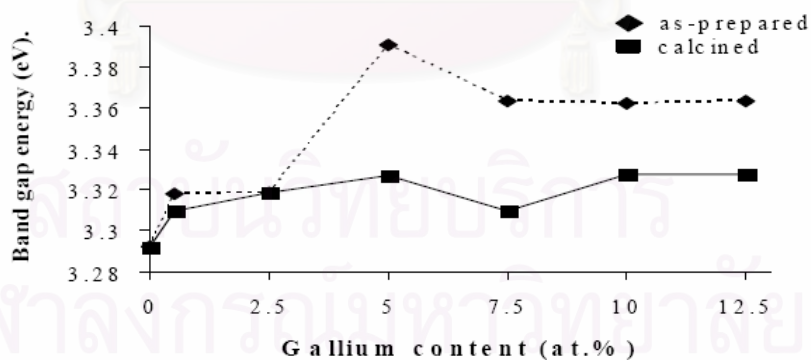


Figure 4- Variation of band gap energy with gallium content in ZnO crystal.

Detailed investigation on light absorption of the synthesized zinc oxide shows that the absorption edge of ZnO nanoparticles is blue-shifted by the gallium doping. Optical transmission curves (not shown) shift toward the shorter wave length when the content of gallium is increased. By using the procedures proposed by Madler *et al.* [12], the band gap energy of all samples can be calculated, as illustrated in Figure 4. It can be seen that the band gap energy of the product is significantly increased by the

incorporation of gallium into ZnO crystal structure. However, the increase in the band gap energy seems to level-off after the content of gallium is higher than 5 at.%. It is also noted that the as-prepared powder shows higher band gap energy than the calcined one. It is possibly due to the presence of hydroxide moiety in the as-prepared product, since zinc hydroxide has been known to have wider band gap than ZnO. These hydroxide groups are eliminated during the calcination. Nevertheless, the results clearly indicate that the electronic states of the ZnO product is altered by the presence of gallium in the crystal.

Conclusion

It has been shown that zinc oxide nanoparticles can be synthesized by glycothermal process without contamination of other phases. Doping of gallium into zinc oxide crystal structure is achievable by simply adding gallium precursor into the reaction system. It is found that the morphology of the synthesized powder is affected by the presence of gallium in the system. Low content of gallium results in the formation of zinc oxide nanorods. Moreover, doping of gallium causes blue-shift in UV absorption spectrum. The band gap energy of zinc oxide can be increased by gallium doping.

Acknowledgements

The authors would like to acknowledge partial support from the Thailand Research Fund (TRF) and the Graduate School, Chulalongkorn University.

References

1. Mang A., Reimann K. and Rubenacke S., **Band-Gaps, Crystal-Field Splitting, Spin-Orbit-Coupling, and Exciton Binding-Energies in ZnO under Hydrostatic-Pressure**, *Solid State Communications* 1995; 94: 251-4.
2. Krunk M. and Melikov E., **Zinc Oxide Thin Films by the Spray Pyrolysis Method**, *Thin Solid Films* 1995; 270: 33-6.
3. Olvera M.D., Maldonado A., Asomoza R., Konagai M. and Asomoza M., **Growth of Textured ZnO-In Thin-Films by Chemical Spray Deposition**, *Thin Solid Films* 1993; 229: 196-200.
4. Jing L.Q., Xin B.F., Yuan F.L., Wang B.Q., Shi K.Y., Cai W.M. and Fu H.G., **Deactivation and Regeneration of ZnO and TiO₂ Nanoparticles in the Gas Phase Photocatalytic Oxidation of n-C₇H₁₆ or SO₂**, *Applied Catalysis A-General* 2004; 275: 49-54.
5. Inoue M., Kominami H. and Inui T., **Thermal Transformation of χ -Alumina Formed by Thermal Decomposition of Aluminum Alkoxide in Organic Media**, *Journal of the American Ceramic Society* 1992; 75: 2597-8.
6. Sue K.W., Kimura K., Yamamoto M. and Arai K., **Rapid Hydrothermal Synthesis of ZnO Nanorods without Organics**, *Materials Letters* 2004; 58: 3350-2.
7. Yang Y., Chen H.L., Zhao B. and Bao X.M., **Size Control of ZnO Nanoparticles Via Thermal Decomposition of Zinc Acetate Coated on Organic Additives**, *Journal of Crystal Growth* 2004; 263: 447-53.
8. Kamalasanan M.N. and Chandra S., **Sol-Gel Synthesis of ZnO Thin Films**, *Thin Solid Films* 1996; 288: 112-5.
9. Rodriguez-Paez J.E., Caballero A.C., Villegas M., Moure C., Duran P. and Fernandez J.F., **Controlled Precipitation Methods: Formation Mechanism of ZnO Nanoparticles**, *Journal of the European Ceramic Society* 2001; 21: 925-30.

10. Cheong K.Y., Muti N. and Ramanan S.R., **Electrical and Optical Studies of ZnO : Ga Thin Films Fabricated via the Sol-Gel Technique**, *Thin Solid Films* 2002; 410: 142-6.
11. Yu Y.S., Kim G.Y., Min B.H. and Kim S.C., **Optical Characteristics of Ge Doped ZnO Compound**, *Journal of the European Ceramic Society* 2004; 24: 1865-8.
12. Madler L., Stark W.J. and Pratsinis S.E., **Rapid Synthesis of Stable ZnO Quantum Dots**, *Journal of Applied Physics* 2002; 92: 6537-40.



สถาบันวิทยบริการ
จุฬาลงกรณ์มหาวิทยาลัย

VITA

Mr. Teerawut Ruangsanam was born on August 27, 1980 in Bangkok, Thailand. He finished in bachelor's degree from Suranaree University of Technology (SUT), Nakhon Ratchasima, in May, 2002. He continued his Master degree in Chemical Engineering at Chulalongkorn University in June, 2006.



สถาบันวิทยบริการ
จุฬาลงกรณ์มหาวิทยาลัย